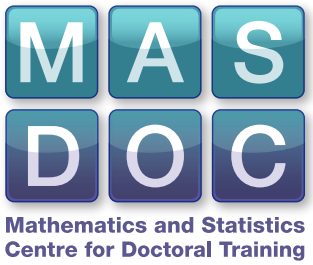

Atomistic modelling of fracture

by

Maciej Buze

Thesis

Submitted for the degree of

Doctor of Philosophy

Mathematics Institute

The University of Warwick

September 2019

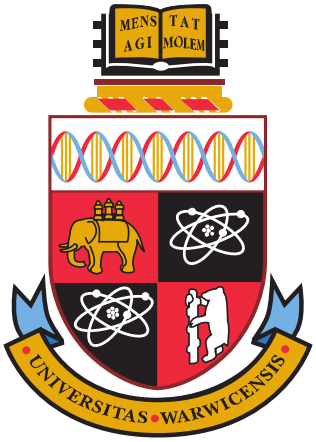

Contents

Acknowledgments

The submission of this thesis marks the conclusion of a crucial formative period in my life. Studying for a PhD is an unorthodox "first adult job" and, for it to be a truly enjoyable and fulfilling experience, a rarely achievable mix of support, luck and resilience is needed.

In my very lucky case, it was indeed deeply gratifying, primarily due to the privilege of working under the supervision of Christoph Ortner and Thomas Hudson, two world-class academics with vast knowledge, true enthusiasm for mathematics and deep sense of empathy towards struggles of often clumsy PhD students. Their joint efforts as PhD advisors were nothing short of exemplary, both in terms of purely mathematical assistance, but also in creating a broader supportive environment. Early on in the PhD this led to a collaboration with Julian Braun, whom I would like thank for his assistance and a lasting influence that fuelled my work on this thesis. Special thanks also go to Patrick van Meurs and Masato Kimura, who enthusiastically embraced our collaboration based on the results of this thesis.

I have been also extremely lucky to be part of MASDOC Doctoral Training Centre and I would like express my gratitude to the directors for giving me this opportunity. I wish to also thank my fellow MASDOC students, in particular Dave, Ifan, Will, Matt, George and Simon. Outside of MASDOC, the Warwick Mathematics Institute and Warwick Statistics provided a thriving environment, resulting in many friendships, including with Natalia, Marisa and Adam.

My good fortune during the last four years was even more profound thanks to my girlfriend Anna, with whom I have been sharing the joys and struggles of living for nearly 7 years now. She remains the cornerstone of my happiness and resilience, particularly thanks to her soothing influence as well as her cheeky-yet-caressing ways of helping me keep my ego in check. I am also forever thankful for her personal sacrifices that meant we could spend the final year together – and what an amazing year it has been!

Declarations

I, Maciej Buze, to the best of my knowledge have presented only my original work and the outcomes of the collaboration with my supervisors, Christoph Ortner and Thomas Hudson, unless specifically referenced or cited in the bibliography. This thesis has not been submitted for another degree or qualification at the University of Warwick or any other higher-education institution.

I also note the following.

- A variant of the model presented in Chapter 2, as well as the results concerning existence, local uniqueness and sharp decay estimates of solutions presented in Chapter 3 can be found in [22]. This publication, recently accepted for publication, also includes results from Chapter 4, that is the construction of a lattice Green's function in the anti-plane crack geometry with suitable decay properties.

- Similarly, the results in Chapter 5 about crack propagation at an atomistic scale employing another variant of the model discussed in Chapter 2 can be found in [23].

Abstract

This thesis is devoted to the mathematical analysis of atomistic modelling of fracture in a crystalline solid. In particular, we focus on a single Mode III crack defect in an infinite two-dimensional square lattice under anti-plane displacements and nearest-neighbour interactions, show that the associated lattice equilibration problem is well-defined over a suitable function space and discuss different regimes of the key parameter known as the (rescaled) stress intensity factor $k \geq 0$, which in continuum fracture mechanics characterises the strength of the stress singularity at the crack tip and more broadly acts as a loading parameter on the crack.

In the first part of the work, we focus on the small-loading regime with k sufficiently small and, under the assumption that interactions across the crack are disregarded, prove existence, local uniqueness and stability of atomistic solutions and further establish their qualitatively sharp far-field decay estimates.

The latter result requires establishing existence and decay estimates for the corresponding lattice Green's function in the anti-plane crack geometry, which constitutes the main technical result of the thesis.

In the final part, we go beyond the small-loading regime and focus on capturing crack propagation in a quasi-static analysis aided by bifurcation theory. We provide evidence that k is a natural bifurcation parameter and that the resulting bifurcation diagram is a periodic "snaking curve". Subsequently we investigate cell size effects in a finite-cell approximation to the infinite problem by proving sharp convergence rates and obtaining a superconvergence result for critical values of k. This enables us to capture the phenomenon of lattice trapping and how it is significantly influenced by the computational domain size.

Chapter 1

Introduction

A crystal is a solid material characterised by a periodic arrangement of its atoms known as a lattice. Such an exactly repeating pattern is prone to being broken by a variety of irregularities, known as defects, which can drastically alter the mechanical, electrical and chemical properties of the underlying material [69]. Typical crystalline defects include point defects, affecting e.g. conductivity of the material [55]; dislocations, known as carriers of plastic, irreversible, deformations [48]; as well as cracks, whose propagation facilitates the process of failure known as fracture [21].

The general aim of static modelling of defects at an atomistic scale is to find an equilibrium configuration of atoms which contains a given defect. This can be achieved via a variational approach, in which such an equilibrium corresponds to a critical point of an associated energy. Our interest lies in first applying this principle to the case of fracture, which in itself presents a number of challenges, and then consider a related quasi-static problem of crack propagation.

The energy in the variational approach is constructed by taking into account interactions between atoms. This procedure is particularly subtle in the case of a crack, which in its essence concerns a situation where, following a successive loss of an *interaction bond* between neighbouring atoms in a crystal, a sharp cut in the material is formed. This process is inherently discrete in nature, hence the modelling of fracture at an atomistic scale holds key to the full understanding of this phenomenon.

Due to the obvious length-scale limitations of an atomistic setup, the classical treatment of this problem, however, employs a continuum approach. Its origins can be traced back to a classic paper by Griffith [44], in which a condition for crack extension, known as *Griffith's criterion*, is derived from the fundamental energy theorems of thermodynamics and mechanics. It postulates existence of some critical

value k_G of the loading parameter known as *stress intensity factor* (SIF), k, beyond which it is energetically feasible for a crack to propagate. The universal insights of this pioneering work gave rise to the well-established theory of fracture mechanics [58], which draws heavily from the more general theory of continuum elasticity [56]. In the more recent mathematical literature, several models generalising the Griffith theory have been proposed [30, 31, 38].

The principal motivation for our work stems from the following limitation of the continuum approaches: Consider a domain $\mathcal{D} \subset \mathbb{R}^2$, representing a cross-section of a three-dimensional elastic body, with a crack set $\Gamma_{\mathcal{D}} \subset \mathcal{D}$. Given a material-specific *strain energy density function* $W : \mathbb{R}^{2\times k} \to \mathbb{R} \cup \{+\infty\}$ (where $k \in \{1, 2, 3\}$ depending on the loading mode), c.f. [56], one can hope to find a non-trivial equilibrium displacement $u : \mathcal{D} \to \mathbb{R}^k$ accommodating the presence of a crack by minimising the continuum energy given by

$$E(u) := \int_{\mathcal{D}\setminus\Gamma_{\mathcal{D}}} W(\nabla u)\, dx,$$

over a suitable function space. In line with continuum linerised elasticity (CLE), one can approximate W by its expansion around zero to second order and obtain the associated equilibrium equation

$$-\mathrm{div}\,(\mathbb{C} : \nabla u) = 0 \quad \text{in } \mathcal{D} \setminus \Gamma_{\mathcal{D}}, \tag{1.0.1}$$

$$(\mathbb{C} : \nabla u)\,\nu = 0 \quad \text{on } \Gamma_{\mathcal{D}}, \tag{1.0.2}$$

supplied with a suitable boundary condition coupling to the bulk [39]. Here $\mathbb{C}$ is the *elasticity tensor* with entries $\mathbb{C}_{i\alpha}^{j\beta} := \partial_{i\alpha j\beta} W(0)$.

It is well-known that regardless of the details of the geometry of $\mathcal{D}$ and $\Gamma_{\mathcal{D}}$, near the crack tip, the gradients of solutions to (1.0.1)-(1.0.2) exhibit a persistent $1/\sqrt{r}$ behaviour, where r is the distance from the crack tip, c.f. [71]. The singularity at the crack tip implies the failure of CLE to accurately describe a small region around it where atomistic (nonlinear and discrete) effects dominate. This near-tip nonlinear zone is argued to exhibit *autonomy* [21, 39], meaning that the state of the system in the vicinity of the singular field is determined uniquely by the stress intensity factor k, and therefore systems with the same SIF but different geometries will behave similarly within the near-tip nonlinear zone.

In order to better understand the microscopic features of this zone, we may exploit the spatial invariance of elasticity and zoom in on the region near the crack tip by performing a spatial rescaling $R\,u(x/R)$, which leads to a simplified geometry of

an infinite domain with a half-infinite straight crack line, as illustrated in Figure 1.1. As we increase the spatial rescaling parameter R we eventually approach the atomic

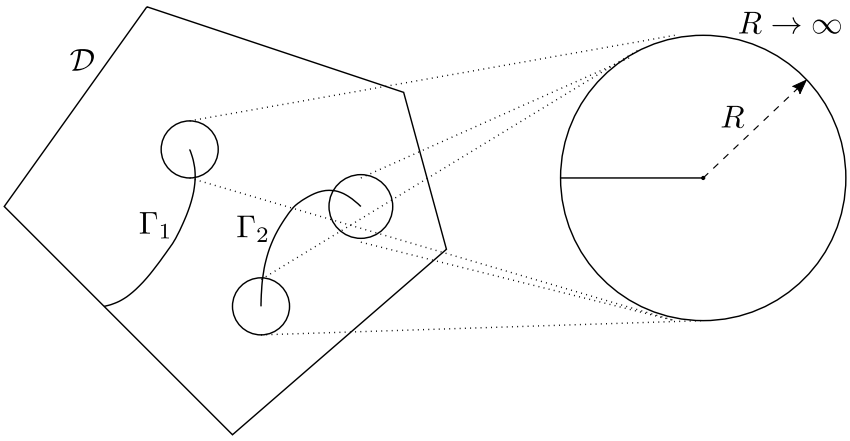

Figure 1.1: A schematic illustration of the setup. A domain $\mathcal{D}$ with the crack set $\Gamma_{\mathcal{D}} = \Gamma_1 \cup \Gamma_2$. The autonomy of the crack implies we can zoom in on each crack tip to obtain a simplified geometry of a ball of radius R. In the limit $R \to \infty$ of the spatial rescaling we obtain a domain $\mathbb{R}^2$ and a half-infinite crack Γ_0.

length-scale at which the hypothesis that the material behaves as a continuum breaks down.

Furthermore, several atomistic studies of fracture revealed phenomena not accounted for in the continuum description. In [24] it has been demonstrated that crack propagation can only occur in certain directions compatible with the crystalline arrangement of atoms. In their seminal paper, Thomson et.al. [82] introduced a simple fracture model exhibiting a phenomenon known as *lattice trapping* in which the lattice keeps the crack *trapped* until the stress intensity factor reaches some k_+ larger than k_G, thus violating Griffith's criterion. This clearly indicates that it is the near-crack-tip zone in which continuum descriptions fail that drives the process of fracture and cannot be disregarded.

In the particular case of a brittle material, in which failure occurs with little prior plastic deformation, fracture processes are key to determining macroscale physical properties of a material. The inherently discrete nature of fracture and the briefly described failure of continuum approaches render the task of creating accurate and efficient simulations of this phenomenon on a large scale particularly difficult [8]. Many of the simulation techniques in operation today rely on simplifying assumptions which are often phenomenological; for example, it is generally unclear under which conditions the standard continuum models of fracture mechanics become invalid, which in practise leads to overly conservative safety measures in engineering

designs [43].

1.1 Recent mathematical results

In the last 25 years, there has been a wealth of interest within the mathematical community devoted to the modelling and analysis of crystalline materials and their defects on an atomistic scale and how it relates to the classical continuum approaches. Our ensuing study of atomistic fracture draws heavily from these efforts and thus in what follows we give a brief account of how this rather versatile research field developed over time, highlight different techniques and approaches employed and discuss the appropriate key results that paved the way for our study.

1.1.1 Atomistic approaches to elasticity and their connection to the continuum counterparts

The key early approach employed in a series of papers starting with [13] centred around the idea of postulating a simple, often one-dimensional model of N equispaced particles interacting via a (nearest-neighbour) pair-potential and employing the framework of Γ-convergence [29] to recover the corresponding continuum integral functional as $N \to \infty$ and thus justifying the continuum theory as an approximation. This approach was subsequently generalised with the help of a broad compactness result in [2], which the authors applied to characterise a class of Γ-limits of discrete energies defined on n-dimensional cubic lattices under pair-interactions with suitable growth and decay assumptions. In this framework, however, the computation of the limiting integral representation is highly non-trivial for cases beyond nearest-neighbour interactions and involves macroscopic homogenisation [10, 64] and relaxation [12].

The further difficulty when working with models beyond nearest-neighbour interactions was laid bare in the pioneering work of Friesecke and Theil [40], who considered a simple two-dimensional linear mass spring model and in particular showed that the inclusion of second-nearest-neighbour interactions creates a nonlinearity of universal geometric nature, which in certain cases can lead to the failure of the so-called Cauchy–Born (CB) rule, which is considered the classical link between atomistic and continuum descriptions.

The study of the validity of the Cauchy–Born rule has been another area of research aimed at understanding connections between atomistic and continuum descriptions. The CB rule, as discussed in [36], or more recently in in a review paper [35] can be summarised in laymen terms as follows: each atom in a deformed material

follows the macroscopic deformation gradient and thus the continuum stored energy function associated to an affine deformation is given by the energy (per unit volume) of a crystal deformed by the same mapping. This has been verified as theorem by Friesecke and Theil in [40] for their model in the small strain regime, but also shown to fail for large displacements as well as for certain not physically feasible choices of interaction parameters. The validity of the CB rule in the small strain regime was later generalised to arbitrary dimensions in [28]. These results were combined in [17] with the aforementioned Γ-convergence methods to further generalise [2] to full finite range many body interatomic potentials and show that in the small strain regime the limiting energy is consistent with the CB rule. Since in our study we make use of the theory of continuum linearised elasticity (CLE) - classically understood to be applicable in the small-strain regime - we further note that it was shown in [15] and subsequently generalised in [76] that one can derive CLE functionals directly from nonlinear discrete models.

In a separate effort motivated by the fact that the machinery of Γ-convergence requires insight into the *global* energy minimisation and is thus inherently incompatible with realistic interatomic potentials such as the Lennard-Jones potential, E and Ming in [32] introduced a different approach. They show that, under suitable stability assumptions, closely related to the fact that elastic deformations are only *local* minimisers of the energy, solutions of certain equations of continuum elasticity are asymptotically approximated by corresponding atomistic equilibrium configurations. In particular, they further discuss that the CB rule holds true for elastically deformed crystals as long as the right unit cell is used in formulating the rule. This approach has been generalised to a large class of interatomic potentials in [68] for a simplified geometry.

1.1.2 Atomistic modelling of point defects and dislocations

The body of work discussed in Section 1.1.1, together with [5], in which authors introduce a framework allowing for a rigorous description of dislocations in an atomistic setting, paved the way for the atomistic study of defects (in particular dislocations) and its even more intricate relation to continuum theories.

The work of Ponsiglione in [70] exploited the machinery of Γ-convergence to obtain the first atomistic-to-continuum results for a simple anti-plane model of screw dislocations as the lattice spacing becomes arbitrarily small. This has been extended in [3] by characterising higher order terms in the asymptotic expansion as well as discussing the associated dislocation dynamics.

The key framework particularly suited for the atomistic study of both point

defects and straight dislocations has been introduced in [34]. In their seminal contribution, Ortner et. al. showed that the decomposition of the atomistic equilibrium $u = \hat{u} + \bar{u}$ into a *far-field predictor* $\hat{u}$, and a *core corrector* $\bar{u}$ can be exploited to gain quantitative insight into the locality of atomistic effects and to further prove rigorous error estimates for finite-domain numerical simulation techniques. The far-field predictor $\hat{u}$ is chosen so that it both enforces the presence of the defect by specifying a suitable boundary condition at infinity and also ensures that the core corrections have finite energy norm. In particular, it is shown that by coupling atomistic and continuum descriptions through the CB rule, the resultant continuum linearised elasticity equation provides such a predictor. In this regard [34] employs the already-mentioned view advanced by E and Ming in [32] that elastic deformations are local minimisers of the energy and hence disregard questions of existence of solutions and simply assume that the existence of a solution with suitable stability property is an inherent feature of the lattice and the interatomic potential. The predictor-corrector approach has also been employed in the preceding study of a model for an anti-plane screw dislocation in [50].

The particular advantage of this approach is that it allows to quantify the strength of atomistic effects by rigorously establishing that, in the case of a straight dislocation, $|D\hat{u}(x)| \sim |x|^{-1}$, while $|D\bar{u}(x)| \leq C|x|^{-2}\log|x|$, where D denotes the discrete gradient operator. The faster decay of $\bar{u}$ encodes the locality of the defect core relative to the far-field and can be used to prove convergence rates for finite-domain approximations, thus allowing for a rigorous numerical analysis of various multi-scale simulation techniques such as [9, 26, 53, 61, 62, 63, 77, 79].

We further note that the theme of locality of defects was subsequently advanced in [19], in which authors introduced and developed techniques to substantially improve the locality of core corrections by prescribing a more accurate far-field predictor. This particular idea proves useful in the context of studying atomistic fracture and is discussed in Chapter 3 in Section 3.6.

For completeness, we conclude by mentioning that this approach was extended to point defects in multilattices in [65] and was also studied in depth in particular case of anti-plane screw dislocations in [50] - a setup which bears a significant resemblance to the anti-plane model of fracture to be introduced in Chapter 2.

1.1.3 Previous approaches to atomistic fracture

Throughout the development of many of the mathematical tools described in this literature review, many of the studies were directly related to fracture and thus we would like to single them out as particular relevant to our study. Already in

the pioneering work of Braides et. al. in [13] the focus was on the phenomena of cleavage fracture, which refers to the tendency of crystalline materials to split along crystal planes. While in the present work we consider a more complex mechanism of fracture, it is worth pointing to the related earlier work by Truskinovsky [83], which to the best of our knowledge is the first article discussing atomistic fracture as a bifurcation phenomenon. An example of a more involved model in the same framework of simple one-dimensional atomistic models is discussed in [14], where the authors consider a general class of suitable interatomic potentials and show that in certain scaling regimes in the Γ-limit some Griffith-type fracture energy can be recovered. Similarly, in [11] authors consider in detail the case of next-to-nearest-neighbour interactions and through a careful consideration of higher-order terms, the authors are able to obtain a localisation result for fracture under the Lennard–Jones potential.

Of particular relevance to the ensuing study of atomistic fracture are the works of Li [59, 60], in which the tools from bifurcation theory in Banach spaces [27] are used to numerically capture crack propagation, which is shown to follow a snaking curve, as will be discussed in Chapter 5 in more detail.

1.2 Main results of the thesis

The primary aim of this work is to lay foundations for a robust mathematical theory of crack propagation at an atomistic scale, which would provide a rigorous grounding for a subsequent study of bottom-up multiscale and coarse-grained models, which are key to bridging the gap between length-scale limitations of purely atomistic approaches and deficiencies of a purely continuum consideration.

As mentioned in Section 1.1.2, a general approach to describe a single localised defect embedded in a homogeneous host crystal has recently been rigorously formalised in [19, 34, 50, 65] for point defects and straight dislocations. This framework, however, has so far explicitly excluded cracks due to two challenges that do not arise for point defects and dislocations. Firstly, as is already evident when comparing continuum linear elasticity approaches to modelling screw dislocations [48] and cracks [58], the latter involves a slower rate of decay of strain away from the defect core, which makes it more difficult to prove that the corresponding atomistic model is even well-defined.

Furthermore, in order to employ an atomistic model in the presence of a crack, one has to consider a domain that is both discrete and inhomogeneous, since the crack breaks translational symmetry even locally. A particularly limiting conse-

quence of this is that before one can establish results about *regularity* of the resulting discrete elastic fields, one first has to prove the existence and decay properties of a *lattice Green's function, $\mathcal{G}$, in the crack geometry.* While the cases of point defects and dislocations permit a spatially homogeneous setup of the reference configuration, allowing us to obtain the lattice Green's function via the semi-discrete Fourier transform, this approach breaks down in the presence of a crack.

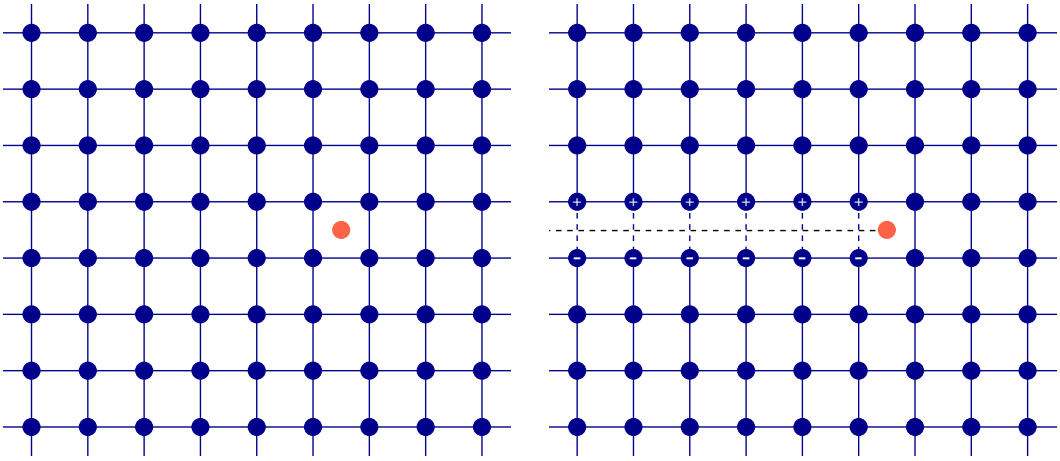

(a) (b)

Figure 1.2: The geometry of the problem with and without the crack present.

1.2.1 Chapter 2

Chapter 2 introduces the general framework, which can be summarised as follows. To simplify the presentation, we restrict the analysis to a mode III fracture on a two-dimensional square lattice $\Lambda := \mathbb{Z}^2 - (1/2, 1/2)$ with anti-plane displacements $u : \Lambda \to \mathbb{R}$. In what follows we always consider an energy difference functional of the form

$$\mathcal{E}(u, k) = \sum_{m \in \Lambda} V\big(D\hat{u}_k(m) + Du(m)\big) - V\big(D\hat{u}_k(m)\big). \tag{1.2.1}$$

Here D denotes the discrete gradient operator, encoding deformed distances between neighbouring lattice sites. Depending on the context, it will be defined in two ways - either with interactions across the crack disregarded or included. This will be discussed in Section 2.1 and is shown in Figure 1.2. Furthermore, V is a suitable C^α interatomic site potential with for $\alpha \geq 5$, as discussed Section 2.3. Finally, with details presented in Section 2.4, the function $\hat{u}_k : \Lambda \to \mathbb{R}$ is the CLE solution to (1.0.1)-(1.0.2) in the anti-plane setup with zero Neumann boundary condition on

the crack and is given in polar coordinates $x = (r\cos\theta, r\sin\theta)$ by

$$\hat{u}_k(x) := k\sqrt{r}\sin\left(\theta/2\right). \tag{1.2.2}$$

The prefactor k is the (rescaled) stress intensity factor, which we can vary and is conventionally set, without loss of generality, to be nonnegative. The function u is an atomistic correction, thus the total displacement is given by $\hat{u}_k + u$. The rigorous details of discrete kinematics and the model are presented in Chapter 2.

1.2.2 Chapter 3

In Chapter 3 we formulate the equilibration problem on a lattice in the presence of a crack as a well-defined variational problem on an appropriate discrete Sobolev space $\dot{\mathcal{H}}^1$.

Theorem 1. *Let the discrete gradient operator D be such that it excludes interactions across the crack. For a fixed k, the energy difference functional $\mathcal{E}(\cdot\,; k)$ in* (1.2.1) *is well-defined on $\dot{\mathcal{H}}^1$ and α-times continuously differentiable.*

We further establish existence, local uniqueness and stability of equilibrium displacements for small loading parameters.

Theorem 2. *Let the discrete gradient operator D be such that it excludes interactions across the crack. For a fixed stress intensity factor k sufficiently small, there exists a locally unique minimiser $\bar{u} \in \dot{\mathcal{H}}^1$ of $\mathcal{E}(\cdot\,; k)$ defined in* (1.2.1) *that depends continuously on ϵ and, under suitable assumptions on V, satisfies strong stability, that is there exists $\lambda > 0$ such that for all $v \in \dot{\mathcal{H}}^1$*

$$\delta^2\mathcal{E}(\bar{u}\,; k)[v, v] \geq \lambda\|v\|^2_{\dot{\mathcal{H}}^1}.$$

Crucially, we also prove qualitatively sharp far-field decay estimates of the atomistic core contribution to the equilibrium fields in order to quantify the "range" of atomistic effects.

Theorem 3. *For any $k \in \mathbb{R}$ fixed, every critical point $\bar{u} \in \dot{\mathcal{H}}^1$ of the energy difference functional $\mathcal{E}(\cdot\,; k)$ in* (1.2.1) *satisfies*

$$|D\bar{u}(l)| \lesssim k|l|^{-3/2+\delta}, \tag{1.2.3}$$

for any $\delta > 0$ and $l \in \Lambda$ with $|l|$ large enough.

1.2.3 Chapter 4

The regularity result (1.2.3) requires a careful characterisation of the lattice Green's function in the crack geometry, which is schematically shown in Figure 1.3 and which we define as follows.

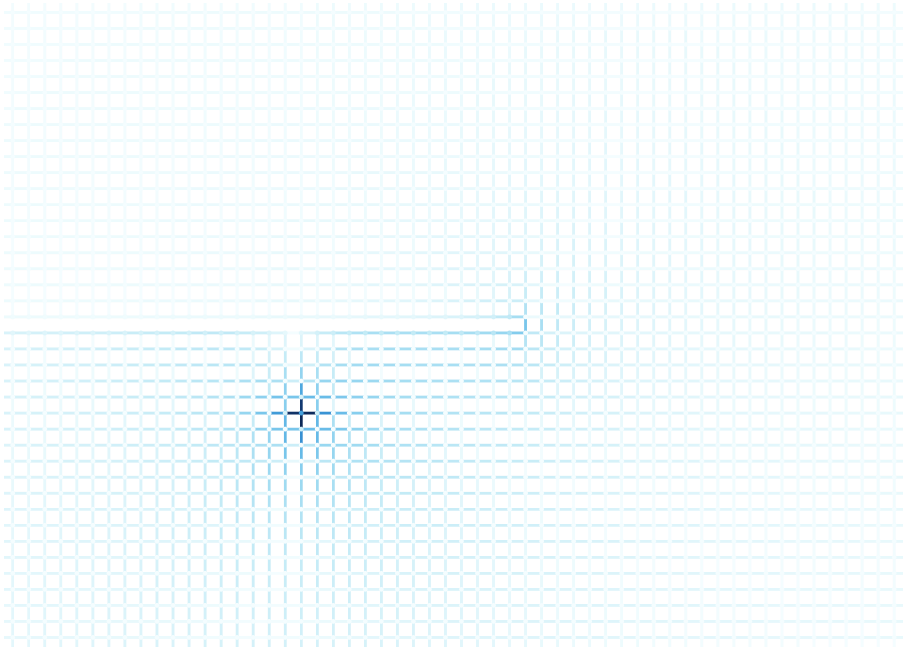

Figure 1.3: A schematic representation of the lattice Green's function in the crack geometry with a point-source s at the centre of the dark blue bonds.

Definition 4. Let the discrete gradient operator D be such that it excludes interactions across the crack and define the Hessian operator H as a discrete divergence of D. A function $\mathcal{G} : \Lambda \times \Lambda \to \mathbb{R}$ is said to be a lattice Green's function $\mathcal{G}$ for the anti-plane crack geometry if for all $m, s \in \Lambda$,

$$\begin{aligned} H\mathcal{G}(m,s) &= \delta_{ms} \\ \mathcal{G}(m,s) &= \mathcal{G}(s,m), \end{aligned}$$

where δ_{ms} denotes the Kronecker delta and H is the Hessian operator applied with respect to first variable.

We note that in our setup the more general notion of the Hessian operator H coincides with the notion of a discrete Laplacian, however in more general setups it is not necessarily the case. This is highlighted in Chapter 4 in (4.1.2).

Chapter 4 is devoted the study of $\mathcal{G}$. We overcome the problem of inhomogeneity of the domain and are able to prove existence and decay estimates for $\mathcal{G}$. The approach employed is centred around the observation that the problem of finding $\mathcal{G}$ can itself be cast as an instance of coupling between continuum and atomistic descriptions, as we prescribe the explicit continuum Green's function G as a boundary condition. This construction ensures the existence of $\mathcal{G}$ and is then followed by a technically involved argument establishing the decay properties of $\mathcal{G}$.

Theorem 5. *There exists a lattice Green's function $\mathcal{G} : \Lambda \times \Lambda \to \mathbb{R}$ such that, for any $\delta > 0$,*

$$|D_1 D_2 \mathcal{G}(l, s)| \lesssim (1 + |\omega(l)||\omega(s)||\omega(l) - \omega(s)|^{2-\delta})^{-1},$$

where D_1 (respectively D_2) is the discrete gradient operator with respect to first (resp. second) variable and ω is the suitably defined complex square root mapping, which will be introduced in Section 2.4.

1.2.4 Chapter 5

In order to capture crack propagation at an atomistic scale, one has to go beyond the small-loading regime of Chapter 3. In Chapter 5, we do this by introducing an extended framework in which atomistic crack propagation can be captured by tracing a continuous curve of critical points of the energy difference introduced in (1.2.1). The mathematical tools we exploit to do so are taken from bifurcation theory in Banach spaces [27]. While this idea has already been explored numerically in [59, 60], a key new conceptual insight is that the stress intensity factor k, which acts as a measure of stability in continuum fracture can be interpreted as the "loading parameter" on the atomistic crack through the far-field boundary condition allowing us to obtain rigorous results about cell size effects.

More specifically, it is clear from (1.2.1) that the SIF enters the model as a scaling parameter multiplying the CLE solution, and so varying it naturally leads to a bifurcation diagram. Moreover, the fact that the CLE crack equilibrium displacement does not belong to the energy space $\dot{\mathcal{H}}^1$ suggests that the bifurcation diagram consists solely of regular points and quadratic fold points, at which the equilibria found transition from being linearly stable to linearly unstable (or vice versa).

This observation and the numerical evidence we obtain together motivate structural assumptions on the bifurcation diagram: we assume (and confirm numerically) that it is a 'snaking curve' [80] with the stability of solutions changing at each bifurcation point. In particular, under our assumptions, a jump from one stable segment to another captures the propagation of the crack through one lattice

cell, with the unstable segment that is crossed in that jump being the collection of corresponding saddle points, which represent the energetic barrier which must be overcome for crack propagation to occur at a given value of the SIF. This allows us to capture the phenomenon of lattice trapping [45, 82], which in this context refers to the idea that in discrete models of fracture there can exist a range of values of SIF for which the crack remains locally stable despite being above or below the critical Griffith stress.

The notable difference in the models considered in Chapters 3 & 5 is that in Chapter 3, in order to prove that the variational problem is well-posed, the interactions crossing the crack were explicitly removed by a suitable definition of the discrete gradient D; by contrast, in Chapter 5 we modify D so that they are included in the interaction range, and instead, the fact that they are effectively broken is encoded in the interatomic potential and in the strain. This gives rise to a physically realistic periodic bifurcation diagram, for which we subsequently prove regularity results both in terms of its smoothness as a submanifold of an appropriate space, as well as uniform spatial regularity of the equilibria along the corresponding solution path. These results can be considered as analogues of Theorems 1 & 3. In contrast, the corresponding result equivalent to Theorem 2 has to be assumed.

Our results for the infinite lattice model naturally lead to an investigation of the numerical approximation of these solutions on a finite-domain. In Chapter 3 we develop the technical tools to establish sharp convergence rates as the domain radius tends to infinity and subsequently use them in Chapter 5 with the notable novelty that there the results apply uniformly to finite segments of the bifurcation diagram.

Theorem 6. *Let the discrete gradient operator be such that it includes the interactions across the crack and R denote the radius of a computational domain $\Lambda_R := \Lambda \cap B_R(0)$. For any $\beta > 0$ there exists R_0 large enough such that for all $R > R_0$, there exists an approximate bifurcation path $\{(\bar{u}_s^R, \bar{k}_s^R) \in \dot{\mathcal{H}}^1 \times \mathbb{R}_+\}$, where $\bar{u}_s^R : \Lambda \to \mathbb{R}$ with $\bar{u}_s^R(m) = 0$ for $m \notin \Lambda_R$ such that*

$$\|\bar{u}_s^R - \bar{u}_s\|_{\dot{\mathcal{H}}^1} + \left|\bar{k}_s^R - \bar{k}_s\right| \lesssim R^{-1/2+\beta} \tag{1.2.4}$$

and

$$\left|\mathcal{E}(\bar{u}_s^R, \bar{k}_s^R) - \mathcal{E}(\bar{u}_s, \bar{k}_s)\right| \lesssim R^{-1+\beta}, \tag{1.2.5}$$

where s denotes the arc-length parameter.

Moreover, in Chapter 5 we establish a superconvergence result for the critical

values of the SIF at which fold point bifurcations occur with estimates of the form

$$\left|\bar{k}_{b^R}^R - \bar{k}_b\right| \lesssim R^{-1+\beta} \quad \text{for any } \beta > 0. \tag{1.2.6}$$

Since the unstable segments of bifurcation diagram correspond to index–1 saddle points of the energy, our work in this regard also extends the convergence results of [16] for saddle point configurations of point defects and suggests possible future extensions to a full transition state analysis [6, 18, 37, 46, 84].

Chapter 2

The atomistic model of anti-plane fracture

In this chapter we introduce the general formulation of the model under consideration. We begin by describing the discrete kinematics, emphasising the subtle role of the interactions across the crack. Subsequently we discuss the function space setup, followed by a detailed discussion about the assumptions on the interatomic potential and how the discrete setup can be coupled with the continuum elasticity via the Cauchy-Born rule. Finally, we provide a rigorous definition of the atomistic energy difference introduced in (1.2.1) in the Introduction.

2.1 Discrete kinematics

Let Λ denote the shifted two dimensional square lattice defined by

$$\Lambda := \left\{ l - (\tfrac{1}{2}, \tfrac{1}{2}) \,\middle|\, l \in \mathbb{Z}^2 \right\}.$$

We consider a crack opening along

$$\Gamma_0 := \{(x_1, 0) \,|\, x_1 \leq 0\} \tag{2.1.1}$$

and distinguish the collection of lattice points directly above and below Γ_0. These are defined as

$$\Gamma_\pm := \left\{ m = (m_1, m_2) \in \Lambda \,\middle|\, m_1 < 0 \text{ and } m_2 = \pm\tfrac{1}{2} \right\}$$

and we refer to Figure 2.1 for a visualisation of the setup. For the purposes of our

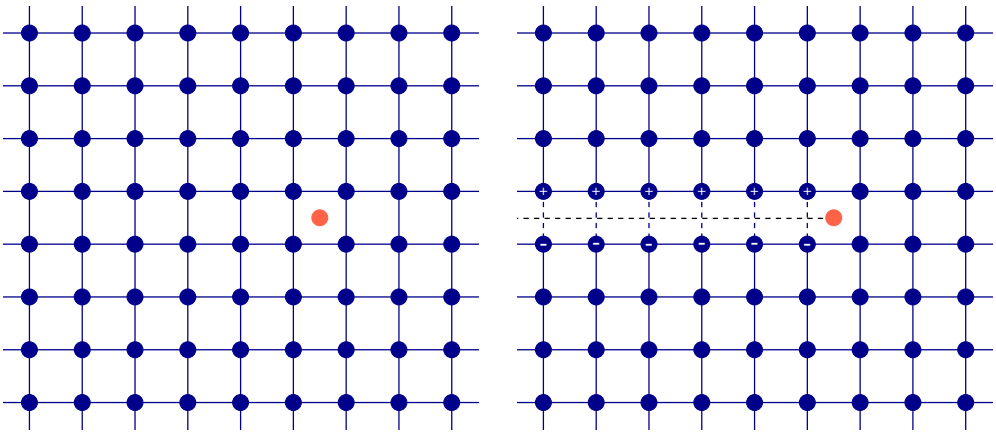

(a) (b)

Figure 2.1: The geometry of the problem with and without the bonds across the crack. The (predicted) crack tip depicted by a red dot. In (b) the crack cut Γ_0 from (2.1.1) is shown as a dashed black line and the lattice points on Γ_+ and Γ_- are highlighted.

analysis, it is helpful to consider two notions of interaction neighbourhood for lattice points. First, the nearest neighbour (NN) directions of the homogeneous square lattice are given by

$$\mathcal{R} = \{e_1, e_2, -e_1, -e_2\}\,.$$

Second, in many cases we may wish to modify these interaction neighbourhoods by disregarding the directions across the crack, as the basic modelling assumption used in treating a crack is that these bonds are effectively broken. For any $m \in \Lambda$, we therefore define

$$\mathcal{R}(m) := \begin{cases} \mathcal{R} & \text{for } m \notin (\Gamma_+ \cup \Gamma_-), \\ \mathcal{R} \setminus \{\mp e_2\} & \text{for } m \in \Gamma_\pm. \end{cases} \tag{2.1.2}$$

For an anti–plane displacement defined on the lattice $u : \Lambda \to \mathbb{R}$, we define the finite difference operator as $D_\rho u(x) := u(x+\rho) - u(x)$ and introduce two notions of the discrete gradient, denoted by $\tilde{D}u(m)$, $Du(m) \in \mathbb{R}^{\mathcal{R}}$ and defined as

$$\big(\tilde{D}u(m)\big)_\rho := D_\rho u(m), \tag{2.1.3a}$$

$$\big(Du(m)\big)_\rho := \begin{cases} D_\rho u(m) & \text{if } \rho \in \mathcal{R}(m), \\ 0 & \text{if } \rho \notin \mathcal{R}(m). \end{cases} \tag{2.1.3b}$$

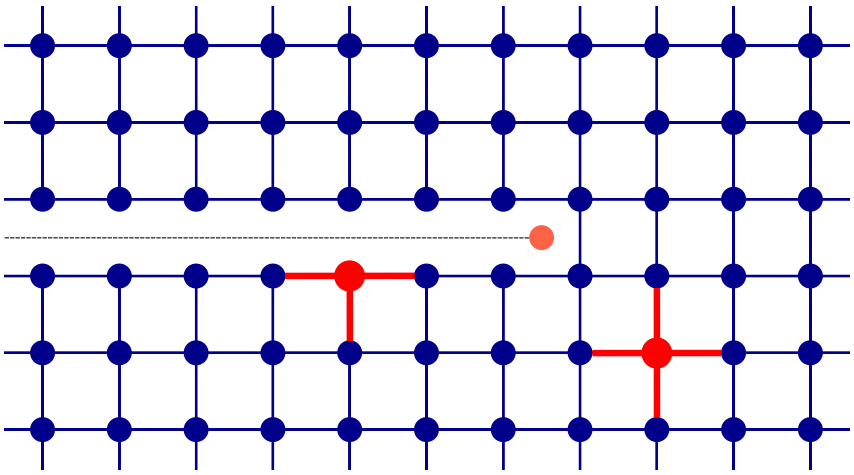

Figure 2.2: The visual representation of $Du(m)$ from (2.1.3).

The discrete gradient $\tilde{D}u$ therefore corresponds to homogeneous NN interactions, whereas Du reflects a defective lattice, as when $m \in \Gamma_{\pm}$, the components of $Du(m)$ which correspond to erased lattice directions are always null. A visualisation is provided in Figure 2.2.

Remark 2.1.1. For future reference, we note that in Chapters 3 & 4 we are only concerned with the formulation of the model with bonds across the crack disregarded. In Chapter 5, however, we will shift our attention to the formulation in which they are included.

2.2 Function space setup

The introduction of the discrete gradient operator D that disregards interactions across the crack allows us to define the appropriate discrete energy space (discrete Sobolev space) for handling arbitrarily large differences in the far–field displacements across the crack,

$$\dot{\mathcal{H}}^1 := \left\{ u : \Lambda \to \mathbb{R} \mid Du \in \ell^2 \text{ and } u(\tfrac{1}{2}, \tfrac{1}{2}) = 0 \right\}, \tag{2.2.1}$$

which has associated norm

$$\|u\|_{\dot{\mathcal{H}}^1} := \|Du\|_{\ell^2} = \left(\sum_{m \in \Lambda} |Du(m)|^2 \right)^{1/2} = \left(\sum_{m \in \Lambda} \sum_{\rho \in \mathcal{R}(m)} (D_\rho u(m))^2 \right)^{1/2}$$

and inner product

$$(u,v)_{\dot{\mathcal{H}}^1} := \sum_{m\in\Lambda} Du(m)\cdot Dv(m) = \sum_{m\in\Lambda}\sum_{\rho\in\mathcal{R}(m)} D_\rho u(m) D_\rho v(m).$$

The choice to restrict $u(\frac{1}{2},\frac{1}{2}) = 0$ ensures that only one constant displacement lies in the space, making $\|\cdot\|_{\dot{\mathcal{H}}^1}$ a norm. This restriction will play a subtle role in the analysis of the lattice Green's function in Chapter 4. We stress that it is the 'crack-aware' discrete gradient D defined in (2.1.3) that is used to define $\dot{\mathcal{H}}^1$, emphasising the fact that arbitrarily large finite differences across the crack are allowed.

For analytical purposes, we also introduce the space of compactly supported displacements,

$$\mathcal{H}^{\mathrm{c}} := \{u : \Lambda \to \mathbb{R} \,|\, \mathrm{supp}(Du) \text{ is compact}\}. \tag{2.2.2}$$

Functions in this space will be employed throughout as test functions

2.3 Assumptions on the interatomic potential

Throughout the thesis, we consider an interatomic potential $V : \mathbb{R}^{\mathcal{R}} \to \mathbb{R}$, which is a material-specific function capturing interactions between atoms. In what follows we assume it to be a nearest-neighbour pair-potential of the form

$$V(Du(m)) = \sum_{\rho\in\mathcal{R}} \phi\big((Du(m))_\rho\big), \tag{2.3.1}$$

with $\phi \in C^\alpha(\mathbb{R})$ for $\alpha \geq 5$ satisfying $\phi(0) = 0$, $\phi(-r) = \phi(r)$ and $\phi''(0) = 1$. The assumption $\phi(0) = 0$ is made without loss of generality since we may always replace $\phi(r) \mapsto \phi(r) - \phi(0)$ without changing the energy difference. The assumption $\phi(-r) = \phi(r)$ is consistent with *anti-plane mirror symmetry* (see also [19, Section 2.2.] and the relevant discussion in Section 3.6). We note it thus follows that $\phi'(0) = \phi'''(0) = 0$. Finally $\phi''(0) = 1$ may be assumed without loss of generality *as long as* $\phi''(0) > 0$ (upon replacing $\phi(r) \mapsto c\phi(r)$). This latter condition is equivalent to lattice stability [32, 34, 50], which is satisfied for virtually all bulk materials.

We further note the condition $\phi(0) = 0$ is compatible with the fact that the 'crack-aware' gradient operator D is used to define the space $\dot{\mathcal{H}}^1$ in (2.2.1). However, as mentioned in Remark 2.1.1, in Chapter 5 we will consider a setup with the interactions across the crack included. This raises the issue that for any $m \in \Gamma_\pm$ and $\rho \notin \tilde{\mathcal{R}}(m)$ crossing the crack surface, we have $D_\rho \hat{u}(m) \sim |m|^{1/2}$. This will be shown in (5.5.11). Thus, in order to avoid summation difficulties, we introduce a

further assumption that the pair-potential satisfies

$$\text{there exists } R_\phi > 0 \text{ such that } \phi'(r) = 0 \quad \forall r \text{ with } |r| \geq R_\phi. \tag{2.3.2}$$

Such an assumption is sufficient for our purposes and simplifies the exposition, but can be easily replaced by an appropriate decay property (e.g. exponential or sufficiently fast algebraic decay).

Remark 2.3.1. For future reference, we note that in Chapter 3 we are only concerned with the setup where bonds across the crack are disregarded, hence (2.3.2) is not assumed there.

2.4 Cauchy-Born rule and continuum linearised elasticity

With V specified, we invoke the Cauchy-Born rule [32, 68], as already discussed in Section 1.1.1, and couple the atomistic potential V with its continuum counterpart $W : \mathbb{R}^2 \to \mathbb{R}$ (the so-called Cauchy-Born strain energy function), via $W(F) := V((F \cdot \rho)_{\rho \in \mathcal{R}})$. Subsequently, we expand W around 0 to second order (compare with the derivation of (1.0.1)-(1.0.2) in the Introduction) to obtain the resulting anti-plane CLE equation

$$\begin{aligned} -\Delta \hat{u} &= 0 \quad \text{in } \mathbb{R}^2 \setminus \Gamma_0, \\ \nabla \hat{u} \cdot \nu &= 0 \quad \text{on } \Gamma_0 \setminus \{0\}, \end{aligned} \tag{2.4.1}$$

with the boundary condition corresponding to a crack at Γ_0. The particularly simple form of the equation is due to the fact that under the Cauchy-Born coupling we have $\delta^2 W(0) = c\mathrm{Id}$, as explicitly calculated in [19].

This equation has infinitely many solutions with the canonical choice being the sole solution (up to rescaling) that ensures local integrability near the crack tip and induces a stress which decays at infinity [78]. This solution can be characterised via the complex square root mapping $\omega : \mathbb{R}^2 \to \mathbb{R}^2$. In polar coordinates, $x = (r_x \cos\theta_x, r_x \sin\theta_x) \in \mathbb{R}^2 \setminus \Gamma_0$, it is given by

$$\omega(x) = (\omega_1(x), \omega_2(x)) = \left(\sqrt{r_x}\cos\left(\tfrac{\theta_x}{2}\right), \sqrt{r_x}\sin\left(\tfrac{\theta_x}{2}\right)\right) \tag{2.4.2}$$

and the canonical solution to (2.4.1) is

$$\hat{u}_k(x) = k\,\omega_2(x). \tag{2.4.3}$$

Here k is the (rescaled) stress intensity factor, which in continuum linear elastic fracture mechanics measures the intensity of the singular field near the crack tip, as discussed in [78, Chapter 3]. In our case, it acts as a loading parameter. Without loss of generality we assume $k \geq 0$, as

$$\hat{u}_{-k}(x) = k\sqrt{r_x}\sin\left(-\tfrac{\theta_x}{2}\right) = \hat{u}_k((x_1, -x_2)).$$

As per Lemma 3.5.1 below, we further note that $|\nabla^j \hat{u}(x)| \lesssim |x|^{1/2-j}$ for any $j \in \mathbb{N}$, $|x| > 0$.

Remark 2.4.1. While in the case of an anti-plane screw dislocation the predictor $\hat{u}_s$ derived from CLE only just fails to be in the discrete energy space $\dot{\mathcal{H}}^1$ (namely $D\hat{u}_{\rm s} \in \ell^{2+\delta}$ for any $\delta > 0$, as described e.g. in [48]), in the case of a crack it is only true that $D\hat{u} \in \ell^{4+\delta}$. This phenomenon is a key reason why the analysis of a general crack defect is more involved. In the anti-plane case one way of circumventing it is to impose the assumption of mirror symmetry, which in our setup is equivalent to $\phi'''(0) = 0$, but in a more general setup it is an open problem. We refer to Section 3.6 for an extended discussion.

Remark 2.4.2. In Chapter 3, we disregard interactions across the crack, thus the (trivial) case $k = 0$ is included and thus in that chapter we assume $k \geq 0$. However, in order to include interactions across the crack in our model, as will be the case in Chapter 5, it is necessary to assume that in fact $k > 0$.

2.5 Definition of energy

Throughout the thesis we consider the energy difference functional $\mathcal{E} : \dot{\mathcal{H}}^1 \times \mathbb{R} \to \mathbb{R}$ given by

$$\mathcal{E}(u, k) = \sum_{m \in \Lambda} V\big(\mathfrak{D}\hat{u}_k(m) + \mathfrak{D}u(m)\big) - V\big(\mathfrak{D}\hat{u}_k(m)\big), \tag{2.5.1}$$

where either $\mathfrak{D} = D$ (in Chapters 3 & 4) or $\mathfrak{D} = \tilde{D}$ (in Chapter 5). Here $V : \mathbb{R}^{\mathcal{R}} \to \mathbb{R}$ is a suitable interatomic site potential as discussed in Section 2.3, and $\hat{u}_k : \Lambda \to \mathbb{R}$ is the CLE predictor, introduced in Section 2.4. The function $u \in \dot{\mathcal{H}}^1$ is a core correction, thus the total displacement is given by $y = \hat{u}_k + u$. The renormalisation in the form of subtracting contributions of the CLE solution is crucial in that it ensures the resulting variational model is well-defined on a Hilbert space $\dot{\mathcal{H}}^1$, even though $y \notin \dot{\mathcal{H}}^1$.

In what follows, we are interested in characterising the set

$$S = \big\{(u,k) \in \dot{\mathcal{H}}^1 \times \mathbb{R} \,\big|\, \delta_u \mathcal{E}(u,k) = 0 \in (\dot{\mathcal{H}}^1)^*\big\},$$

where $\delta_u \mathcal{E} : \dot{\mathcal{H}}^1 \times \mathbb{R} \to (\dot{\mathcal{H}}^1)^*$ is the partial Fréchet derivative of $\mathcal{E}$ with respect to u and will be shown in Chapters 3 and 5 to be given by, for any $v \in \dot{\mathcal{H}}^1$,

$$\langle \delta_u \mathcal{E}(u,k),\, v\rangle = \sum_{m\in\Lambda} \nabla V\big(\mathfrak{D}\hat{u}_k(m) + \mathfrak{D}u(m)\big) \cdot \mathfrak{D}v(m).$$

Importantly, any $(\bar{u}, \bar{k}) \in S$ gives rise to an equilibrium displacement $\bar{y} = \hat{u}_{\bar{k}} + \bar{u}$.

The premise of this formulation is three-fold. Firstly, by treating u as a perturbation of $\hat{u}$, it seeks to validate CLE as an accurate approximation of the atomistic effects away from the defect core in a crack defect setup. On the other hand, it also shows that the CLE solution can serve as an appropriate boundary condition for finite-domain numerical computation in a discrete setup, as tested in numerical tests described in Sections 3.4 & 5.4. Finally, the inclusion of the stress intensity factor k as a variable makes this formulation consistent with the abstract framework of bifurcation theory on Banach spaces.

Remark 2.5.1. For future reference, we note that in Chapter 3 we are only concerned with the small loading regime where k is kept fixed and assumed small enough. In Chapter 5 on the other hand k is varied and is the key to tracing a bifurcation diagram corresponding to crack propagation.

Chapter 3

The small loading regime

In this chapter we rigorously formulate the equilibration problem on a lattice in the presence of the crack for a small enough loading parameter. In particular, we are concerned with proving Theorem 1, Theorem 2 and Theorem 3, which together establish that the underlying variational problem is well-defined, that in the small-loading regime there exists a locally unique stable atomistic equilibrium and that its far-field decay, i.e. the locality of the core corrector, can be sharply estimated.

3.1 Introduction and notation

Throughout this chapter we consider the energy introduced in Section 2.5, in the small loading regime, that is when the stress intensity factor k introduced in Section 2.4 is sufficiently small and the interactions across the crack are excluded, as discussed in Section 2.1.

To be precise, we consider the energy difference functional $\mathcal{E} : \dot{\mathcal{H}}^1 \times \mathbb{R} \to \mathbb{R}$ given by

$$\mathcal{E}(u,k) = \sum_{m\in\Lambda} V(D\hat{u}_k(m) + Du(m)) - V(D\hat{u}_k(m)), \tag{3.1.1}$$

where $\hat{u}_k$ was defined in (2.4.3). We recall that D defined in (2.1.3) is the discrete gradient operator that disregards interactions across the crack, V is the interatomic potential introduced in (2.3.1) (noting that the additional assumption on the pair-potential introduced in (2.3.2) is not assumed in this chapter). Subsequently we set the stress intensity factor k introduced in (2.4.3) to be small enough and in view of the fact that k is fixed throughout, we resort to a minor abuse of notation

$$\mathcal{E}(u) := \mathcal{E}(u\,;k) \tag{3.1.2}$$

to simplify presentation.

Outline of the chapter: In Section 3.2 we state the main results rigorously. In Section 3.3 we consider the finite-domain approximation and prove the small-loading regime equivalent of the convergence rate in (1.2.4). The numerical tests are presented in Section 3.4. The discussion about the model is in Section 3.6. We conclude the treatment of small-loading regime by gathering proofs in Section 3.5.

3.2 Results about the model

Following the theory developed in [19, 34, 50] for point defects and straight dislocations, we formulate the static crack model as a minimisation problem

$$\text{find} \quad \bar{u} \in \arg\min_{\dot{\mathcal{H}}^1} \mathcal{E}, \tag{3.2.1}$$

with the energy difference functional defined in (3.1.2). We proceed to state the main results of this chapter.

Theorem 3.2.1. *The energy difference functional $\mathcal{E}$ in* (3.1.2) *is well-defined on $\dot{\mathcal{H}}^1$ and α-times continuously differentiable. Furthermore, for k sufficiently small, the minimisation problem* (3.2.1) *has a locally unique solution $\bar{u} \in \dot{\mathcal{H}}^1$ that depends continuously on k and satisfies strong stability: there exists $\lambda > 0$ such that for all $v \in \dot{\mathcal{H}}^1$*

$$\delta^2\mathcal{E}(\bar{u})[v, v] \geq \lambda \|v\|^2_{\dot{\mathcal{H}}^1}. \tag{3.2.2}$$

For the proof, see Section 3.5.2.

Theorem 3.2.2. *For any $k \geq 0$, every critical point of the energy difference functional $\mathcal{E}$ in* (2.5.1) *satisfies*

$$|D\bar{u}(l)| \lesssim k|l|^{-3/2+\delta}, \tag{3.2.3}$$

for any $\delta > 0$ and $|l|$ large enough.

For the proof, see Section 3.5.2. The sharpness of this result is tested numerically in Section 3.4. The appearance of arbitrarily small $\delta > 0$ in (3.2.3) is due to the way we construct the lattice Green's function, as will be discussed in Chapter 4 after Theorem 4.2.2.

3.3 Rate of convergence to the thermodynamic limit

In this section we consider a supercell approximation to (3.2.1) on a finite domain confined to a ball of radius R and establish the rate of convergence as $R \to \infty$.

The setup is similar to the one descibed in [19, 34], that is we consider a domain $B_R \cap \Lambda \subset \Omega_R \subset \Lambda$ with the boundary condition $\hat{u}$ on $\Lambda \setminus \Omega_R$ and state it as a Galerkin approximation

$$\text{find } \bar{u}_R \in \arg\min_{\mathcal{H}^0_R} \mathcal{E}, \tag{3.3.1}$$

where

$$\mathcal{H}^0_R := \{v : \Lambda \to \mathbb{R} \,|\, v = 0 \text{ in } \Lambda \setminus \Omega_R\}.$$

We now prove that the finite-domain approximate problem has a solution and how it relates to the solution of the infinite problem.

Theorem 3.3.1. *If $\bar{u}$ is a solution to* (3.2.1) *that is strongly stable in the sense of* (3.2.2)*, then for all $\beta > 0$, there exist $C, R_0 > 0$ such that for all $R > R_0$, there exists a stable solution $\bar{u}_R$ to* (3.3.1) *satisfying*

$$\|\bar{u}_R - \bar{u}\|_{\dot{\mathcal{H}}^1} \le C R^{-1/2+\beta}.$$

The proof of the statement follows almost immediately from the corresponding result in [33, Theorem 3.8], as long as we extend the discrete Poincaré inequality described therein to the domain with a crack. This requires a construction of a suitable interpolation operator that correctly takes into account the region between Γ_0 and $\Gamma_+ \cup \Gamma_-$. This construction shall be carried out as part of the proof of Theorem 3.2.1. For the sake of completeness we present a detailed proof of Theorem 3.3.1 in Section 3.5.3.

3.4 Numerical results

In this section we present results of numerical tests that confirm the rate of decay of $|D\bar{u}|$ established in Theorem 3.2.2 and the convergence rate from Theorem 3.3.1. The setup precisely follows the one described in [19, Section 3], with the pair-potential employed given by

$$\phi(r) = \frac{1}{6}\big(1 - \exp(-3r^2)\big).$$

Theorem 3.2.2 suggests that $|D\bar{u}(x)| \lesssim |x|^{-3/2}$, while Theorem 3.3.1 suggests that in the supercell approximation (3.3.1) we expect $\|\bar{u}_R - \bar{u}\|_{\dot{\mathcal{H}}^1} \sim \mathcal{O}(R^{-1/2})$, where

R is the size of the domain. To compute equilibria we employ a standard Newton scheme, terminating at an ℓ^∞-residual of 10^{-8}.

In Figure 3.1 we plot the decay of $|D\bar{u}|$ rescaled by the value of k used, as well as the convergence rate to the thermodynamic limit, confirming the predictions of Theorems 3.2.2 and 3.3.1.

Remark 3.4.1. We also carried out a similar set of tests for the anti-plane crack problem on a triangular lattice, obtaining qualitatively equivalent results. This indicates that the current restriction to the square lattice has purely technical origins and that it is to be expected that it is possible to extend our results to other Bravais lattices.

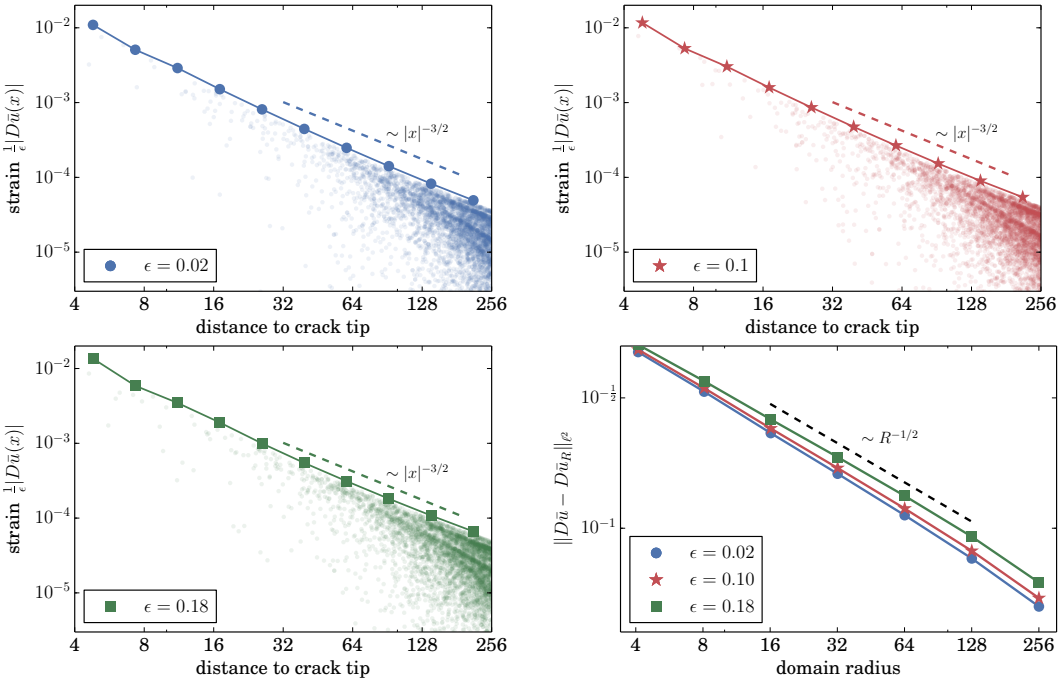

Figure 3.1: The decay of the corrector rescaled by the loading parameter, i.e. $\frac{1}{k}|D\bar{u}|$, for different values of k. Transparent dots denote data points $(|x|, |Du(x)|)$, solid curves their envelopes. We observe the expected rate of $|x|^{-3/2}$ and the linear scaling of $D\bar{u}$ is evident. Bottom right: The rate of convergence of the corresponding supercell approximation. The expected rate $R^{-1/2}$ is observed.

3.5 Proofs

3.5.1 Additional concepts

In this section we introduce the remaining notation and concepts to be used throughout that were left out of the introductory section of this chapter.

Firstly, we define sets

$$\Omega_\Gamma := \left\{ x \in \mathbb{R}^2 \,\middle|\, x_1 \leq \tfrac{1}{2} \text{ and } x_2 \in \left(-\tfrac{1}{2}, \tfrac{1}{2}\right) \right\} \setminus \Gamma_0, \qquad \Gamma := \partial\Omega_\Gamma \setminus \Gamma_0, \tag{3.5.1}$$

with Γ being the line that includes lattice points encompassing Γ_0 and, similarly, Ω_Γ being the space that Γ encompasses, except for Γ_0 itself.

We further comment on the definition of the gradient operator D in (2.1.3) and why we set the contribution of a bond across the crack to zero. This formulation allows us to sum by parts in a convenient way. For instance, for any $u, v : \Lambda \to \mathbb{R}$ with compact support, we have that

$$\sum_{m\in\Lambda} \sum_{\rho\in\mathcal{R}(m)} D_\rho u(m) D_\rho v(m) = \sum_{m\in\Lambda} Du(m) \cdot Dv(m) = \sum_{m\in\Lambda} \left(-\operatorname{Div} Du(m)\right) v(m),$$

where the discrete divergence operator Div is defined as

$$\operatorname{Div} g(m) := -\sum_{\rho\in\mathcal{R}} g_\rho(m-\rho) - g_\rho(m), \quad \text{for } g : \Lambda \to \mathbb{R}^{\mathcal{R}}. \tag{3.5.2}$$

Here we note that $\mathbb{R}^{\mathcal{R}}$ is a standard short-hand notation for $\mathbb{R}^{|\mathcal{R}|}$, where $|\mathcal{R}|$ denotes the number of elements of $\mathcal{R}$, which at the same time introduces ordering with respect to interaction stencils $\rho \in \mathcal{R}$. In our case we have $\mathcal{R} = \{e_1, -e_1, e_2, -e_2\}$, so $|\mathcal{R}| = 4$, which implies $\mathbb{R}^{\mathcal{R}}$ is a four-dimensional space and thus if $g : \Lambda \to \mathbb{R}^{\mathcal{R}}$, then $g(m) = (g_\rho(m))_{\rho\in\mathcal{R}}$.

In the following it is often of interest to only sum over bonds at the crack surface. To this end, for any $m \in \Lambda$ and $\rho \in \mathcal{R}(m)$, we introduce the notation $b(m,\rho) := \{m + t\rho \,|\, t \in [0,1]\}$ and the following short-hand summation notation

$$\sum_{b(m,\rho)\subset\Gamma} \equiv \sum_{\substack{m\in\Lambda, \rho\in\mathcal{R}(m), \\ b(m,\rho)\subset\Gamma}}$$

together with an analogous definition for bonds not on the crack surface. Likewise, it is important to distinguish the following sets corresponding to the unit square centered at the origin

$$\Omega_0 := \Omega_\Gamma \cap [-\tfrac{1}{2}, \tfrac{1}{2}]^2, \quad Q_0 := \Omega_0 \cap \Gamma. \tag{3.5.3}$$

We also introduce a shorthand notation related to the complex square root mapping,

$$\omega_x := \omega(x), \quad \omega_{xs}^- := \omega(x) - \omega(s), \quad \omega_{xs}^+ := \omega(x) + \omega(s) \tag{3.5.4}$$

and quote the following standard result without proof.

Lemma 3.5.1. *For $j \in \mathbb{N}$, the complex square root map ω defined in* (2.4.2) *satisfies*

$$|\nabla^j \omega(x)| \lesssim |x|^{1/2-j}.$$

3.5.2 Proofs for static anti-plane crack model

Proof of Theorem 3.2.1

We separate the proof into two parts, with one devoted to $\mathcal{E}$ defined in (3.1.2) and the other to the solution to (3.2.1).

The energy difference functional $\mathcal{E}$ is well-defined and differentiable: For any $v : \Lambda \to \mathbb{R}$ with compact support we can rewrite the energy difference functional $\mathcal{E}$ as

$$\mathcal{E}(v) = \mathcal{E}_0(v) + \langle \delta\mathcal{E}(0),\, v\rangle, \tag{3.5.5}$$

where

$$\mathcal{E}_0(v) := \sum_{m\in\Lambda} \sum_{\rho\in\mathcal{R}(m)} \Big(\phi(D_\rho \hat{u}(m) + D_\rho v(m)) - \phi(D_\rho \hat{u}(m)) - \phi'(D_\rho \hat{u}(m)) D_\rho v(m)\Big)$$

and

$$\langle \delta\mathcal{E}(0),\, v\rangle = \sum_{m\in\Lambda} \sum_{\rho\in\mathcal{R}(m))} \phi'(D_\rho \hat{u}(m)) D_\rho v(m).$$

Since $\phi \in C^\alpha(\mathbb{R})$ for $\alpha \geq 5$, a simple Taylor expansion argument ensures that $\mathcal{E}_0$ is well-defined on $\dot{\mathcal{H}}^1$ (cf. [34]). Thus the proof relies on showing that $\delta\mathcal{E}(0)$ is a bounded linear functional on $\dot{\mathcal{H}}^1$, as then (3.5.5) holds for any $v \in \dot{\mathcal{H}}^1$. Noting that $\phi'(0) = \phi'''(0) = 0$ and $\phi''(0) = 1$, we Taylor-expand ϕ' around zero to get

$$|\langle \delta\mathcal{E}(0),\, v\rangle| \lesssim \left|\sum_{m\in\Lambda} D\hat{u}(m) \cdot Dv(m)\right| + \left|\sum_{m\in\Lambda} R_\phi(m) \cdot Dv(m)\right|, \tag{3.5.6}$$

where R_ϕ represents the higher-order terms in the Taylor expansion and is given by

$$\big(R_\phi(m)\big)_\rho = \frac{\phi^{(iv)}(0)}{6} D_\rho \hat{u}(m)^3 + \frac{\phi^{(v)}(\xi_m)}{24} D_\rho \hat{u}(m)^4,$$

where $\xi_m \in [0, D_\rho \hat{u}(m)]$. Due to the fact for all $m \in \Lambda$, $|D\hat{u}(m)| \lesssim |m|^{-1/2} \leq C$ and the fact that $\phi \in C^\alpha(\mathbb{R})$ for $\alpha \geq 5$, it is immediate that $\phi^{(v)}(\xi_m)$ is bounded

uniformly and hence

$$|R_\phi(m)| \lesssim |m|^{-3/2} \tag{3.5.7}$$

and hence

$$\left| \sum_{m \in \Lambda} R_\phi(m) \cdot Dv(m) \right| \lesssim \|Dv\|_{\ell^2}.$$

It remains to estimate the first term of the right-hand side of (3.5.6). To this end we shall exploit the fact that $\hat{u}$ solves the equation given by (2.4.1), in particular after constructing a suitable interpolation operator that takes any lattice function to the continuum space. Firstly we tessellate the domain $\mathbb{R}^2 \setminus \Gamma_0$ as follows. We carve the squares in the lattice into two right-angle triangles and introduce a (P1) piecewise linear interpolation operator I over the resulting triangulation (see Figure 3.2).

In order to exploit the boundary condition that $\hat{u}$ satisfies (c.f. (2.4.1)), we also want Iv to be well-defined on Ω_Γ and continuous across Γ. Away from the defect core this is possible by extending it so that it aligns with the the values of $Iv(x)$ for $x \in \Gamma$ and is constant in the normal direction, as shown in Figure 3.2. Additionally, near the origin we create two new interpolation points as shown in Figure 3.2, one at the origin and one in-between points a and d and we denote it by $\widehat{ad}$. We define the interpolation there as $Iu(0) := \frac{1}{4}(u(a) + u(b) + u(c) + u(d))$ and $\lim_{x \downarrow \widehat{ad}} u(x) = u(d)$ whereas $\lim_{x \uparrow \widehat{ad}} u(x) = u(a)$, emphasising the fact that the resulting P1 interpolant does not need to be continuous across Γ_0, but is continuous across the triangle T_3.

We can thus write

$$0 = C_\Lambda \int_{\mathbb{R}^2 \setminus \Gamma_0} (-\Delta \hat{u}(x)) Iv(x)\, dx = C_\Lambda \int_{\mathbb{R}^2 \setminus \Gamma_0} \nabla \hat{u}(x) \cdot \nabla Iv(x)\, dx,$$

where in particular the second equality follows from integration by parts and the boundary term is not there due to the boundary condition in (2.4.1). Hence we in fact aim to estimate

$$\sum_{m \in \Lambda} \langle D\hat{u}(m),\, Dv(m) \rangle - C_\Lambda \int_{\mathbb{R}^2 \setminus (\Omega_\Gamma \cup \Gamma_0)} \nabla \hat{u}(x) \cdot \nabla Iv(x) - C_\Lambda \int_{\Omega_\Gamma} \nabla \hat{u}(x) \cdot \nabla Iv(x).$$

Remark 3.5.2. The constant C_Λ depends on the lattice under consideration. In the case of the square lattice, $C_\Lambda = 2$, but for in instance if we were to consider the triangular lattice with NN interactions, the constant would be $2\sqrt{3}$. The freedom of choice is a consequence of the fact that $\hat{u}$ satisfies Laplace equation with zero Neumann boundary condition. It also justifies why $\hat{u}$ is a valid predictor for any choice of the stress intensity factor k in (2.4.3). This is in contrast with the work in

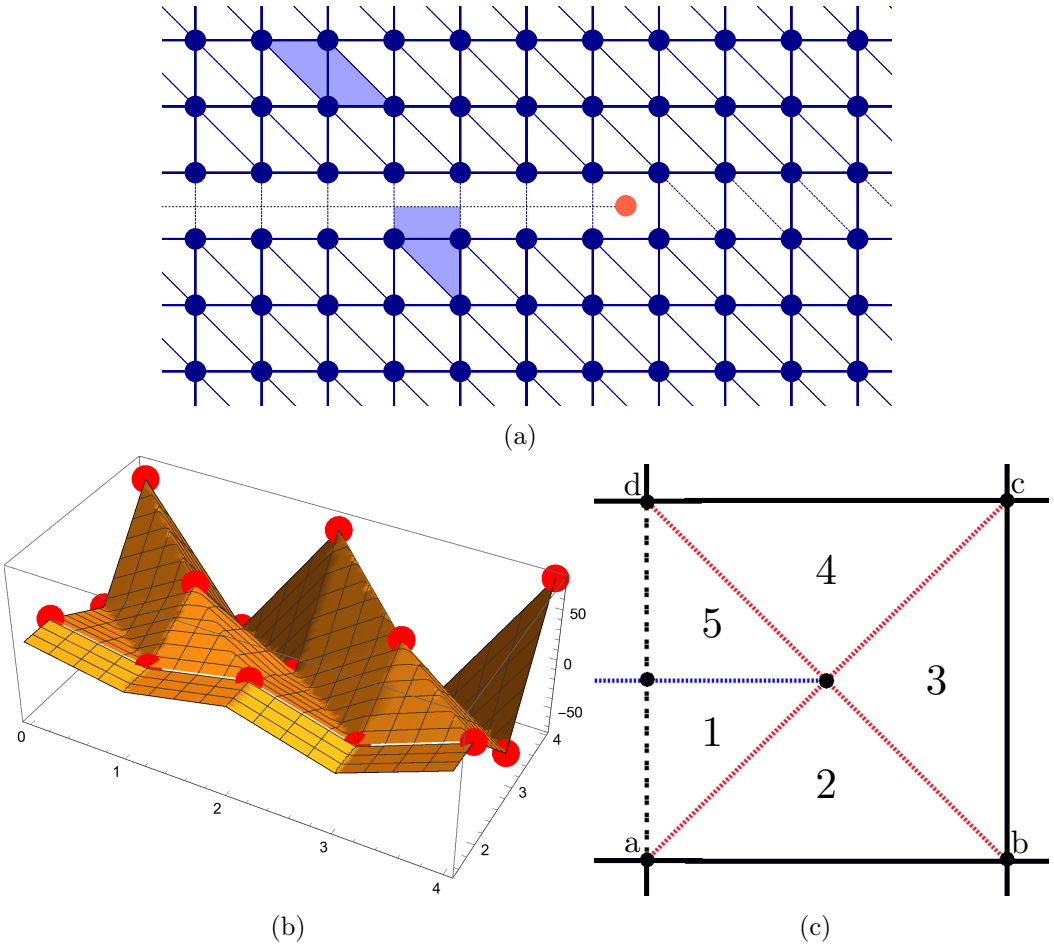

Figure 3.2: (a) The tessellation of the domain $\mathbb{R}^2 \setminus \Gamma_0$, with triangles away from the crack and rectangles at the crack surface. In blue a typical region of integration associated with a bond.
(b) For some lattice function $u : \Lambda \to \mathbb{R}$ each red dot represents the point in the three dimensional space corresponding to $(l_1, l_2, u(l))$ for some lattice point $l \in \Lambda$. The orange region represents the graph of the corresponding interpolant Iu, in particular clearly illustrating its extension to $\Omega_\Gamma \setminus \Gamma_0$ (here looking from above).
(c) Near the origin we create two additional interpolation points, one at the origin and one half-way between lattice points on the crack surface closest to the origin and impose a triangulation as shown. The resulting P1 interpolation introduces a collection triangles $\{T_1, \ldots, T_5\}$ and we stress that Iu is not continuous across the common edge of T_1 and T_5.

Chapter 4 on the lattice Green's function in the anti-plane crack geometry, where in a corresponding argument, to be discussed in Section 4.3, we have to prescribe the correct constant in the equation for the corresponding predictor.

The triangulation of $\mathbb{R}^2 \setminus \Omega_\Gamma$ induced by the P1 interpolation introduces a

collection of triangles $\mathcal{T}$. Inside any given $T \in \mathcal{T}$ both components of ∇Iv are constant and each corresponds to $D_\rho v(l)$ for some bond $b(l,\rho)$ being an edge of T. As a result we can write

$$C_\Lambda \int_{\mathbb{R}^2 \setminus (\Omega_\Gamma \cup \Gamma_0)} \nabla \hat{u}(x) \cdot \nabla Iv(x) = \sum_{m \in \Lambda} \sum_{\rho \in \mathcal{R}(m)} \left(\int_{U_{m\rho}} \nabla_\rho \hat{u}(x)\, dx \right) D_\rho v(m),$$

where $U_{m\rho}$ is the union of triangles for which a given bond $b(m,\rho)$ is an edge (cf. Figure 3.2). The constant $C_\Lambda = 2$ disappears due to the fact that the set of lattice directions under consideration counts each bond twice.

A similar analysis is applicable to the integral over Ω_Γ. Away from Ω_0 (the unit square centred at the origin defined in (3.5.3)), it can be tessellated into a collection of rectangles $\big(Q_{m\rho}\big)$, each associated with one lattice bond $b(m,\rho) \subset \Gamma \setminus Q_0$ (cf. Figure 3.2), where we recall $Q_0 = \Omega_0 \cap \Gamma$. Due to how we construct the interpolant of v, we can thus conclude that

$$C_\Lambda \int_{\Omega_\Gamma \setminus (\Omega_0)} \nabla \hat{u}(x) \cdot \nabla Iv(x)\, dx = \sum_{b(m,\rho) \subset (\Gamma \setminus Q_0)} \left(\int_{Q_{m\rho}} \nabla_\rho \hat{u}(x)\, dx \right) D_\rho v(m).$$

It can also be readily checked that (using the notation from Figure 3.2)

$$\int_{\Omega_0} \nabla \hat{u}(x,s) \cdot \nabla Iv(x) dx = C_{b,a}(v(b) - v(a)) + C_{c,b}(v(c) - v(b)) + C_{d,c}(v(d) - v(c)),$$

where the coefficients are given by

$$C_{b,a} := \frac{1}{2}\Big(3 \int_{T_1} \nabla_{e_1} \hat{u} + 2 \int_{T_2} \nabla_{e_1} \hat{u} + \int_{T_2} \nabla_{e_2} \hat{u} + \int_{T_3} \nabla_{e_1} \hat{u} + \int_{T_4} \nabla_{e_2} \hat{u} - \int_{T_5} \nabla_{e_1} \hat{u}\Big), \tag{3.5.8}$$

$$C_{c,b} := \Big(\int_{T_1} \nabla_{e_1} \hat{u} + \int_{T_2} \nabla_{e_2} \hat{u} + \int_{T_3} \nabla_{e_2} \hat{u} + \int_{T_4} \nabla_{e_2} \hat{u} - \int_{T_5} \nabla_{e_1} \hat{u}\Big), \tag{3.5.9}$$

$$C_{d,c} := \frac{1}{2}\Big(\int_{T_1} \nabla_{e_1} \hat{u} + \int_{T_2} \nabla_{e_2} \hat{u} - \int_{T_3} \nabla_{e_1} \hat{u} - 2 \int_{T_4} \nabla_{e_1} \hat{u} + \int_{T_4} \nabla_{e_2} \hat{u} - 3 \int_{T_5} \nabla_{e_1} \hat{u}\Big). \tag{3.5.10}$$

We note that the directions with respect to which finite differences are taken can be reversed, thus we also define

$$C_{a,b} := -C_{b,a},\ C_{b,c} = -C_{c,b} \text{ and } C_{c,d} := -C_{d,c}. \tag{3.5.11}$$

We can therefore write

$$\sum_{m\in\Lambda} D\hat{u}(m)\cdot Dv(m) = \sum_{b(m,\rho)\not\subset\Gamma}\left(D_\rho\hat{u}(m) - \int_{U_{m\rho}}\nabla_\rho\hat{u}(x)\,dx\right)D_\rho v(m) + \sum_{b(m,\rho)\subset(\Gamma\setminus Q_0)}\left(D_\rho\hat{u}(m) - \int_{U_{m\rho}\cup Q_{m\rho}}\nabla_\rho\hat{u}(x)\,dx\right)D_\rho v(m) + \sum_{b(m,\rho)\subset Q_0}(D_\rho\hat{u}(m) - C_{m+\rho,m})D_\rho v(m),$$

where the coefficients $C_{m+\rho,m}$ are given by (3.5.8)-(3.5.11). Since

$$\int_{B_1(0)\setminus\Gamma_0}|\nabla\hat{u}(x)|dx \lesssim \int_0^1 r^{1/2}dx < \infty,$$

it is clear that for any $b(m,\rho)\subset Q_0$, $(D_\rho\hat{u}(m) - C_{m+\rho,m})$ can be bounded uniformly.

Bearing in mind that $D_\rho\hat{u}(m) = \int_0^1\nabla_\rho\hat{u}(m+t\rho)\,dt$ and observing that for $b(m,\rho)\not\subset\Gamma$, we have $|U_{m\rho}| = 1$, we exploit the fact that both regions of integration share the same mid-point. A Taylor expansion around the mid-point $\hat{m}_\rho := \frac{1}{2}(m+m+\rho)$ yields

$$\begin{aligned} D_\rho\hat{u}(m) =& \nabla_\rho\hat{u}(\hat{m}_\rho)\int_0^1 dt + \int_0^1\nabla\left(\nabla_\rho\hat{u}(\hat{m}_\rho)\right)\cdot(m+t\rho-\hat{m}_\rho)\,dt \\ &+ \int_0^1\nabla^2\left(\nabla_\rho\hat{u}(\xi_1(m))\right)[m+t\rho-\hat{m}_\rho]^2\,dt \end{aligned} \tag{3.5.12}$$

and

$$\begin{aligned} \int_{U_{m\rho}}\nabla_\rho\hat{u}(x)\,dx =& \nabla_\rho\hat{u}(\hat{m}_\rho)\int_{U_{m\rho}}dx \\ &+ \int_0^1\int_{-t}^{1-t}\nabla\left(\nabla_\rho\hat{u}(\hat{m}_\rho)\right)\cdot\left(m+\rho_2\begin{pmatrix}s\\t\end{pmatrix}+\rho_1\begin{pmatrix}t\\s\end{pmatrix}-\hat{m}_\rho\right)ds\,dt \\ &+ \int_{U_{m\rho}}\nabla^2\left(\nabla_\rho\hat{u}(\xi_2(m))\right)[x-\hat{m}_\rho]^2\,dx \end{aligned} \tag{3.5.13}$$

where $\xi_1(m),\xi_2(m)\in\mathbb{R}^2$ depend on m and are such that $|\hat{m}_\rho-\xi_i(m)|\le 1/2$ (the Lagrange form of the remainder). It can then be explicitly calculated that

$$\int_0^1\nabla\left(\nabla_\rho\hat{u}(\hat{m}_\rho)\right)\cdot(m+t\rho-\hat{m}_\rho)\,dt = \nabla\left(\nabla_\rho\hat{u}(\hat{m}_\rho)\right)\cdot\rho\int_0^1(t-1/2)\,dt = 0$$

and similarly it can be verified that, for any $\rho \in \mathcal{R}$,

$$\int_0^1 \int_{-t}^{1-t} \nabla \left(\nabla_\rho \hat{u}(\hat{m}_\rho) \right) \cdot \left(m + \rho_2 \begin{pmatrix} s \\ t \end{pmatrix} + \rho_1 \begin{pmatrix} t \\ s \end{pmatrix} - \hat{m}_\rho \right) ds\, dt = 0.$$

It thus follows that

$$b(m,\rho) \not\subset \Gamma \implies \left| D_\rho \hat{u}(m) - \int_{U_{m\rho}} \nabla_\rho \hat{u}(x)\, dx \right| \lesssim |\nabla^3 \hat{u}(m)|.$$

On the other hand, for $b(m,\rho) \subset \Gamma \setminus Q_0$ there is only one triangle and thus $|U_{m\rho}| = \frac{1}{2}$, but we also have $|Q_{m\rho}| = \frac{1}{2}$. While regions of integration no longer share a mid-point, we still Taylor-expand and realise that the constant terms in (3.5.12) and (3.5.13) still cancel one another out, implying that

$$b(m,\rho) \subset \Gamma \setminus Q_0 \implies \left| D_\rho \hat{u}(m) - \int_{U_{m\rho} \cup Q_{m\rho}} \nabla_\rho \hat{u}(x)\, dx \right| \lesssim |\nabla^2 \hat{u}(m)|.$$

Finally, since Lemma 3.5.1 implies that for both $j = 2, 3$ and $m \in \Lambda$ with $m \approx 0$ we have $|\nabla^j \hat{u}(m)| \sim \mathcal{O}(1)$ (in particular finite since $|m| > \frac{1}{\sqrt{2}}$ as we consider a shifted lattice), we can incorporate any bond $b(m,\rho) \subset Q_0$ into the general conclusion that

$$\left| \sum_{m \in \Lambda} D\hat{u}(m) \cdot Dv(m) \right| \lesssim \sum_{b(m,\rho) \not\subset \Gamma} |\nabla^3 \hat{u}(m)||D_\rho v(m)| + \sum_{b(m,\rho) \subset \Gamma} |\nabla^2 \hat{u}(m)||D_\rho v(m)| \tag{3.5.14}$$

and since $|\nabla^3 \hat{u}(m)| \lesssim |m|^{-5/2}$ and $|\nabla^2 \hat{u}(m)| \lesssim |m|^{-3/2}$, then

$$\left| \sum_{m \in \Lambda} D\hat{u}(m) \cdot Dv(m) \right| \lesssim \|Dv\|_{\ell^2}.$$

Thus we can conclude that for any $v \in \dot{\mathcal{H}}^1$,

$$|\langle \delta\mathcal{E}(0),\, v \rangle| \lesssim \|Dv\|_{\ell^2}.$$

The fact that $\mathcal{E}$ is at least α-times continuously differentiable then naturally follows from $\phi \in C^\alpha(\mathbb{R})$, see [68] for an analogous argument.

This proves the first statement of Theorem 3.2.1.

Existence, local uniqueness, and strong-stability of solutions: We begin by quoting the Implicit Function Theorem, adapted from [57]:

Theorem 3.5.3 (Implicit Function Theorem)**.** *Let X, Y, Z be Banach spaces. Let the mapping $F : X \times Y \to Z$ be continuously Fréchet differentiable with respect to both x and y. If $(x_0, y_0) \in X \times Y$, $F(x_0, y_0) = 0$ and the mapping $x \mapsto DF(x_0, y_0)(x, 0)$ is a Banach space isomorphism from X onto Z, then there exist neighbourhoods U of x_0 and V of y_0 and a Fréchet differentiable function $g : V \to U$ such that $F(g(y), y) = 0$ and $F(x, y) = 0$ if and only if $x = g(y)$, for all $(x, y) \in U \times V$.*

In our setting, we have $X = \dot{\mathcal{H}}^1, Y = \mathbb{R}$ and $Z = (\dot{\mathcal{H}}^1)^*$. Interpreting again the energy difference functional $\mathcal{E}$ as defined on $\dot{\mathcal{H}}^1 \times \mathbb{R}$ we set $F := \delta_u \mathcal{E}$. We notice that for $k = 0$ we have a trivial solution $\bar{u}_0 = 0$, thus giving us the pair $(\bar{u}_0, 0) \in \dot{\mathcal{H}}^1 \times \mathbb{R}$. We further observe that

$$\langle DF(u_0, 0)(v, 0),\, w\rangle = \delta_u^2 \mathcal{E}(u_0, 0)[v, w] = \sum_{m \in \Lambda} \phi''(0) Dv(m) \cdot Dw(m)$$

and since $\phi''(0) = 1$, the mapping $DF(u_0, 0)(\cdot, 0)$ is indeed an isomorphism, as it is in fact the Riesz map from Riesz Representation Theorem for Hilbert spaces (cf. [74]).

Hence all the assumptions of the theorem are fulfilled and we can conclude that in a neighbourhood of $(\bar{u}, 0)$ we have a unique solution path of the form $\{(u(k), k) \,|\, k \in [0, k_{\text{crit}})\}$ with continuous dependence of u on k. The strong-stability (3.2.2) of solutions for k_{crit} small enough follows from the fact that it is trivially satisfied for u_0 with $\lambda = \phi''(0) = 1$ and the continuous dependence of solutions on k, as we can always write

$$\langle \delta_u^2 \mathcal{E}(u(k), k)v,\, v\rangle = \langle \big(\delta_u^2 \mathcal{E}(u(k), k) - \delta_u^2 \mathcal{E}(u_0, 0)\big)\, v,\, v\rangle + \langle \delta_u^2 \mathcal{E}(u_0, 0)v,\, v\rangle$$

and we have

$$|\langle \delta_u^2 \mathcal{E}(u(k), k) - \delta_u^2 \mathcal{E}(u_0, 0)v,\, v\rangle| \lesssim \|u(k) - u_0\|_{\dot{\mathcal{H}}^1} \|v\|_{\dot{\mathcal{H}}^1}^2 \lesssim k \|v\|_{\dot{\mathcal{H}}^1}^2.$$

This concludes the proof of the latter statement of Theorem 3.2.1. □

Proof of Theorem 3.2.2

We begin by stating the definition of a lattice Green's function for an anti-plane crack geometry.

Definition 3.5.4. A function $\mathcal{G} : \Lambda \times \Lambda \to \mathbb{R}$ is said to be a lattice Green's function

$\mathcal{G}$ for the anti-plane crack geometry if for all $m, s \in \Lambda$,

$$H\mathcal{G}(m,s) = \delta_{ms} \tag{3.5.15a}$$

$$\mathcal{G}(m,s) = \mathcal{G}(s,m), \tag{3.5.15b}$$

where δ_{ms} denotes the Kronecker delta and $H := -\operatorname{Div} D$ (recall (3.5.2)) is applied with respect to the first variable.

It will be shown in Chapter 4 in Theorem 4.2.2 that there exists a function satisfying this definition and further satisfying, for any $\delta > 0$,

$$|D_\rho v(m)| \lesssim (1 + |\omega_m||\omega_l||\omega_{ml}^-|^{2-\delta})^{-1},$$

where $v(m) := \mathcal{G}(m, l+\tau) - \mathcal{G}(m,l)$ with $\tau \in \mathcal{R}(l)$.

We can thus write that

$$\begin{aligned} D_\tau \bar{u}(l) &= \sum_{m\in\Lambda} \phi''(0) D\bar{u}(m) \cdot Dv(m) \\ &= \sum_{m\in\Lambda} \sum_{\rho\in\mathcal{R}(m)} \Big(\phi'(D_\rho \hat{u}(m)) + \phi''(0) D_\rho \bar{u}(m) \\ &\qquad - \phi'(D_\rho \hat{u}(m) + D_\rho \bar{u}(m))\Big) D_\rho v(m) \\ &\quad - \sum_{m\in\Lambda} \sum_{\rho\in\mathcal{R}(m)} \phi'(D_\rho \hat{u}(m)) D_\rho v(m) \\ &=: \sum_{m\in\Lambda} A(m) \cdot Dv(m) - B(m) \cdot Dv(m) \end{aligned}$$

where we exploited the fact that $\bar{u}$ is a critical point, that is it satisfies

$$\langle \delta\mathcal{E}(\bar{u}),\, v\rangle = \sum_{m\in\Lambda} \sum_{\rho\in\mathcal{R}(m)} \phi'(D_\rho \hat{u}(m) + D_\rho \bar{u}(m)) D_\rho v(m) = 0 \quad \forall v \in \dot{\mathcal{H}}^1. \tag{3.5.16}$$

A Taylor expansion of ϕ' around zero, followed by application of the standard Young's inequality, yields that

$$|A(m)| \lesssim |D\hat{u}(m)|^4 + |D\bar{u}(m)|^2 \lesssim |\omega_m|^{-4} + |D\bar{u}(m)|^2,$$

where we used $|\nabla \hat{u}(m)| \lesssim |m|^{-1/2} = |\omega_m|^{-1}$. Similarly

$$\left|\sum_{m\in\Lambda} B(m) \cdot Dv(m)\right| \lesssim \left|\sum_{m\in\Lambda} D\hat{u}(m) \cdot Dv(m)\right| + \left|\sum_{m\in\Lambda} R_\phi(m) \cdot Dv(m)\right|,$$

where R_ϕ as in (3.5.7). In light of (3.5.14) we thus obtain

$$\left|\sum_{m\in\Lambda} B(m)\cdot Dv(m)\right| \lesssim \sum_{m\in\Lambda} |\omega_m|^{-3}|Dv(m)|,$$

which, when put together with the decay of v implies that

$$\begin{aligned}|D_\tau \bar{u}(l)| \lesssim & \sum_{m\in\Lambda} |\omega_m|^{-3}(1+|\omega_m||\omega_l||\omega_{ml}^-|^{2-\delta})^{-1} \\ & + \sum_{m\in\Lambda} |D\bar{u}(m)|^2(1+|\omega_m||\omega_l||\omega_{ml}^-|^{2-\delta})^{-1}.\end{aligned} \tag{3.5.17}$$

The first term on the right-hand side of (3.5.17) can be estimated as follows. We define

$$\sum_{m\in\Lambda} f(m) := \sum_{m\in\Lambda} (1+|\omega_m|^3)^{-1}(1+|\omega_m||\omega_l||\omega_{ml}^-|^{2-\delta})^{-1}$$

and observe that away from the sharp spikes at $m=l$ and $m=0$ we can bound this series by the corresponding integral, that is we can say

$$\sum_{m\in\Lambda} f(m) \lesssim f(l)+f(0)+\int_D f dm,$$

where $D := (\mathbb{R}^2\setminus\Gamma_0)\setminus(B_1(l)\cup B_1(0))$. Firstly we note that

$$f(l) = (1+|\omega_l|^3)^{-1} \quad \text{and} \quad f(0) = (1+|\omega_l|^{3-\delta})^{-1}.$$

For the integral term we introduce a change of variables $\xi = \omega_m$, which leads to $\zeta := \omega_l$, and $dm = |\xi|^2 d\xi$. As a result, we have

$$\begin{aligned}\int_D f(x)dx &= \int_{\omega(D)} \frac{|\xi|^2}{(1+|\xi|^3)(1+|\xi||\zeta||\xi-\zeta|)^{2-\delta}} d\xi \\ &\lesssim \int_{\omega(D)} |\zeta|^{-1}|\xi|^{-2}|\xi-\zeta|^{-2+\delta} d\xi =: \int_{\omega(D)} \tilde{f} d\xi.\end{aligned}$$

Bearing in mind that

$$\omega(D) = \mathbb{R}^2_+ \setminus (B_1(0)\cup\omega(B_1(l))),$$

we decompose the region of integration into

$$\Omega_0 := B_{\frac{|\zeta|}{2}}(0)\cap\omega(D), \quad \Omega_\zeta := B_{\frac{|\zeta|}{2}}(\zeta)\cap\omega(D) \quad \text{and} \quad \Omega' := \omega(D)\setminus(\Omega_0\cup\Omega_\zeta)$$

and estimate the integral over each region separately as follows:

$$\int_{\Omega_0} \tilde{f} d\xi \lesssim |\zeta|^{-3+\delta} \int_1^{\frac{|\zeta|}{2}} r^{-1} dr \lesssim |\zeta|^{-3+\delta} \log|\zeta|,$$

$$\int_{\Omega_\zeta} \tilde{f} d\xi \lesssim |\zeta|^{-3} \int_{\frac{1}{|\zeta|}}^{\frac{|\zeta|}{2}} r^{-1+\delta} dr \lesssim |\zeta|^{-3+\delta} + |\zeta|^{-3-\delta} \lesssim |\zeta|^{-3+\delta}, \tag{3.5.18}$$

where,in the second integral, $\frac{1}{|\zeta|}$ appears due to the exclusion of $B_1(l)$ from D which translates in the domain of integration to

$$\xi \in \Omega_\zeta \implies |\xi - \zeta| \geq \frac{1}{|\xi + \zeta|} \geq \frac{1}{|\xi| + |\zeta|} \gtrsim \frac{1}{|\zeta|}. \tag{3.5.19}$$

The last inequality in (3.5.19) follows from $|\xi| \lesssim |\zeta|$. The first inequality in (3.5.19), on the other hand, follows from

$$1 \leq |m - l| = |\omega_{ml}^-||\omega_{ml}^+| = |\xi - \zeta||\xi + \zeta|.$$

The first equality here is a crucial spatial relation that will be discussed in Chapter 4 in (4.3.1). Finally,

$$\int_{\Omega'} \tilde{f} d\xi \lesssim |\zeta|^{-1} \int_{|\zeta|}^{\infty} r^{-3+\delta} dr \lesssim |\zeta|^{-3+\delta}.$$

Since $\zeta = \omega_l$, we can thus conclude that

$$\sum_{m \in \Lambda} |\omega_m|^{-3} (1 + |\omega_m||\omega_l||\omega_{ml}^-|^{2-\delta})^{-1} \lesssim |\omega_l|^{-3+\delta} \log|\omega_l| \lesssim |\omega_l|^{-3+\tilde{\delta}}, \tag{3.5.20}$$

for any $\tilde{\delta} > \delta$.

For the second term on the right-hand side of (3.5.17), we look at three regions separately: $\Omega_1 := B_{\frac{|l|}{2}}(0)$, $\Omega_2 := B_{\frac{|l|}{2}}(l)$ and $\Omega_3 := \Lambda \setminus (\Omega_1 \cup \Omega_2)$. We observe that

$$\sum_{m \in \Omega_1} |D\bar{u}(m)|^2 (1 + |\omega_m||\omega_l||\omega_{ml}^-|^{2-\delta})^{-1} \lesssim |\omega_l|^{-3+\delta} \|D\bar{u}\|_{\ell^2} \lesssim |\omega_l|^{-3+\delta}$$

Similarly, $m \in \Omega_3 \implies |\omega_{ml}^-| \gtrsim |\omega_l|$ and $|\omega_m| \gtrsim |\omega_l|$, hence

$$\sum_{m\in\Omega_3} |D\bar{u}(m)|^2(1+|\omega_m||\omega_l||\omega_{ml}^-|^{2-\delta})^{-1} \lesssim |\omega_l|^{-4} \sum_{m\in\Omega_3} |D\bar{u}(m)|^2 \lesssim |\omega_l|^{-4}\|D\bar{u}\|_{\ell^2}^2 \lesssim |\omega_l|^{-4}.$$

Finally, we can always replace one power of $|D\hat{u}(m)|$ with the ℓ^∞–norm , thus allowing us to apply the Cauchy-Schwarz inequality to obtain

$$\sum_{m\in\Omega_2} |D\bar{u}(m)|^2(1+|\omega_m||\omega_l||\omega_{ml}^-|^{2-\delta})^{-1} \lesssim \|D\bar{u}\|_{\ell^\infty(\Omega_2)}\|D\bar{u}\|_{\ell^2(\Omega_2)} \left(\sum_{m\in\Omega_2}(1+|\omega_m|^2|\omega_l|^2|\omega_{ml}^-|^{4-2\delta})^{-1}\right)^{1/2}$$

Noting that the sum is finite and that $\Omega_2 \subset \Lambda \setminus B_{\frac{|l|}{2}}(0)$ we combine this with (3.5.20) to obtain that there exists a constant $C > 0$ such that for $|l|$ large enough it holds that

$$|D_\tau \bar{u}(l)| \leq C\left(|\omega_l|^{-3+\tilde{\delta}} + \|D\bar{u}\|_{\ell^2(\Lambda\setminus B_{\frac{|l|}{2}}(0))}\|D\bar{u}\|_{\ell^\infty(\Lambda\setminus B_{\frac{|l|}{2}}(0))}\right).$$

Subsequently we define $w(r) := \|D\bar{u}\|_{\ell^\infty(\Lambda\setminus B_r(0))}$ and employ a technical result detailed in [33, Lemma 6.3, Step 2] originating from the regularity theory for systems of elliptic PDEs [42], to conclude that the function

$$v(r) := r^{-3/2+\bar{\delta}} w(r) \tag{3.5.21}$$

is bounded on $\mathbb{R}_+$, where $2\bar{\delta} = \tilde{\delta}$.

To this end, we note that

$$\|D\bar{u}\|_{\ell^2(\Lambda\setminus B_r(0))} \leq \frac{1}{C}2^{-3}$$

for r large enough, since $\|D\bar{u}\|_{\ell^2} < \infty$ and thus $\|D\bar{u}\|_{\ell^2(\Lambda\setminus B_r(0))} \to 0$ as $r \to \infty$. Hence, for $l \in \Lambda$ with $|l| > R$ for some R large enough, it holds that

$$|D_\tau \bar{u}(l)| \leq C|\omega_l|^{-3+\tilde{\delta}} + 2^{-3}\|D\bar{u}\|_{\ell^\infty(\Lambda\setminus B_{\frac{|l|}{2}}(0))}. \tag{3.5.22}$$

We can take the supremum over all $l \in \Lambda$ with $|l| \geq R$ of (3.5.22) to deduce

$$w(r) \leq Cr^{-3/2+\bar{\delta}} + 2^{-3}w\left(\frac{r}{2}\right) \tag{3.5.23}$$

for $r \geq R$, where $2\bar{\delta} = \tilde{\delta}$. Thus

$$r^{3/2-\bar{\delta}} w(r) \leq C + \frac{1}{2}\left(\frac{r}{2}\right)^2 w\left(\frac{r}{2}\right)$$

for $r \geq R$. If further $\frac{r}{2} \geq R$, then we can apply (3.5.23) to $w\left(\frac{r}{2}\right)$ and we continue to iterate this argument, that is: if $\frac{r}{2^n} \geq R$, then

$$r^{3/2-\bar{\delta}} w(r) \leq C\left(1 + \frac{1}{2} + \cdots + \frac{1}{2^n}\right) + \frac{1}{2^{n+1}}\left(\frac{r}{2^{n+1}}\right)^2 w\left(\frac{r}{2^{n+1}}\right).$$

We now note that the n-term sum in the brackets can be bounded above by 2. Furthermore, one can always find $n \in \mathbb{N}$ so that $\frac{r}{2^{n+1}} < R$ and noting that w is monotonically decreasing, we thus obtain that $w\left(\frac{r}{2^{n+1}}\right) \leq w(R)$. We can hence conclude that v defined in (3.5.21) is bounded, since in fact

$$v(r) \lesssim 1 + (2R)^2 w(R).$$

This implies that

$$|D_\tau \bar{u}(l)| \lesssim |\omega_l|^{-3+\tilde{\delta}}.$$

This estimate holds for an arbitrary $\tau \in \mathcal{R}(l)$ and arbitrarily small $\tilde{\delta} > 0$, hence we have established the result. The linear scaling with k is evident from the fact that in the interpolation trick used to obtain (3.5.14), the loading parameter can be taken outside the summation, thus persists linearly. □

3.5.3 Proof of convergence

In this section we shall prove Theorem 3.3.1. In the argument we closely follow the argument in [33, Theorem 3.8]. We begin with the discrete Poincaré inequality on a domain with the crack.

Lemma 3.5.5. *Let $0 < R_1 < R_2$ and set $\mathcal{A} := \Lambda \cap (B_{R_2} \setminus B_{R_1})$. Then there exists a constant $C_P > 0$ such that, whenever $R_2 - R_1 \geq 4$ and $R_1 \geq 6$,*

$$\|u - a\|_{\ell^2(\mathcal{A})} \leq R_2 C_P \|Du\|_{\ell^2(\mathcal{A}')} \quad \forall u : \mathcal{A}' \to \mathbb{R},$$

where $\mathcal{A}' := \Lambda \cap (B_{R_2+3} \setminus B_{R_1-3})$ and $a := \fint_{(B_{R_2} \setminus B_{R_1}) \setminus \Gamma_0} Iu\, dx$ with I being the P1 interpolation operator introduced in the proof of Theorem 3.2.1 in Section 3.5.2.

Proof. We recall from the proof of Theorem 3.2.1 that the aforementioned interpolation operator I is constructed as a P1 interpolation on a triangulation $\mathcal{T}$ of $\mathbb{R}^2 \setminus \Omega_\Gamma$

(with the definition of Ω_Γ given in (3.5.1)) and then extended to the tessellation of $\Omega_\Gamma \setminus \Omega_0$, with Ω_0 defined in (3.5.3) into a collection of rectangles $\mathcal{Q}$.

Let $A := (B_{R_2} \setminus B_{R_1}) \setminus \Gamma_0$ and

$$A' := \left(\bigcup_{\substack{T \in \mathcal{T} \\ T \cap A \neq \emptyset}} T \right) \cup \left(\bigcup_{\substack{Q \in \mathcal{Q} \\ Q \cap A \neq \emptyset}} Q \right)$$

The fact that $R_2 - R_1 \geq 4$ ensures that for any $l \in \mathcal{A}$ there exists $T \in \mathcal{T}$ such that $l \in T$ and $T \subset A$ (and hence the same is true for some $Q \in \mathcal{Q}$). This implies

$$\|u - a\|_{\ell^2(\mathcal{A})} \leq C \|I(u-a)\|_{L^2(A)}.$$

We note that despite the exclusion of Γ_0, the standard continuum Poincaré inequality applies to domain A, since it satisfies the cone property [75] and thus

$$\|u - a\|_{\ell^2(\mathcal{A})} \leq C R_2 \|\nabla u\|_{L^2(A)} \leq C_P R_2 \|\nabla u\|_{L^2(A')} \leq R_2 C_P \|Du\|_{\ell^2(\mathcal{A}')},$$

where the scaling with R_2 in the first inequality is standard and discussed e.g. in [47] and the final inequality follows from the fact that any triangle $T \in \mathcal{T}$ such that $T \subset A'$ and any rectangle $Q \in \mathcal{Q}$ such that $Q \subset A'$, both have their vertices in $\mathcal{A}'$. □

We also require a result about a suitable truncation operator.

Lemma 3.5.6. *There exists a truncation operator $T_R : \dot{\mathcal{H}}^1 \to \mathcal{H}^{\mathrm{c}}$, where $\mathcal{H}^{\mathrm{c}}$ was defined in* (2.2.2)*, such that, for any $u \in \dot{\mathcal{H}}^1$,*

$$\|DT_R u - Du\|_{\ell^2} \lesssim \|Du\|_{\ell^2(\Lambda \setminus B_{R/2})}. \tag{3.5.24}$$

Proof. A possible choice for the truncation operator $T_R : \dot{\mathcal{H}}^1 \to \mathcal{H}^{\mathrm{c}}$ is given by

$$T_R u(l) := \eta(|l|/R)(u(l) - a_R),$$

where the cut-off function $\eta : \mathbb{R} \to \mathbb{R}$ satisfies $\eta(r) = 1$ for $r \leq 4/6$ and $\eta(r) = 0$ for $r \geq 5/6$ and smooth and monotonic in-between, and

$$a_R := \fint_{\left(B_{5R/6} \setminus B_{4R/6}\right) \setminus \Gamma_0} I u \, dx.$$

We note that

$$D_\rho u(l) - D_\rho T_R u(l) = (1 - \eta(l+\rho))D_\rho u(l) - D_\rho \eta(l)\,(u(l) - a_R)$$

and subsequently we take the ℓ^2 norm of both sides. Noting that $|D_\rho \eta(|l|/R)| \lesssim R^{-1}$, we apply the discrete Poincaré inequality from Lemma 3.5.5 to the right-hand side to conclude that indeed

$$\|DT_R u - Du\|_{\ell^2} \lesssim \|Du\|_{\ell^2(\Lambda \setminus B_{R/2})}.$$

□

We can now prove the convergence result.

Proof of Theorem 3.3.1. Recalling that $\bar{u}$ denotes the strongly stable solution to the infinite problem (3.2.1), we note that the inequality in (3.5.24) implies that for the truncation operator T_R from Lemma 3.5.6, it holds that $T_R\bar{u}$ converges strongly to $\bar{u}$ in the $\dot{\mathcal{H}}^1$-norm. Furthermore, Theorem 3.2.1 establishes that $\mathcal{E} \in C^\alpha$ where α is assumed to satisfy $\alpha \geq 5$ (c.f. Section 2.3). It hence follows that $\delta^2\mathcal{E}(T_R\bar{u}) \to \delta^2\mathcal{E}(\bar{u})$ in the operator norm. Recalling (3.2.2), we can thus conclude that for the domain size R large enough, for all $v \in \mathcal{H}^{\mathrm{c}}$,

$$\langle \delta^2\mathcal{E}(T_R\bar{u})v,\, v\rangle \geq \frac{1}{2}\lambda\|v\|^2_{\dot{\mathcal{H}}^1}.$$

Moreover it follows that

$$\langle \delta\mathcal{E}(T_R\bar{u}),\, v\rangle = \langle \delta\mathcal{E}(T_R\bar{u}) - \delta\mathcal{E}(\bar{u}),\, v\rangle \lesssim \|T_R\bar{u} - \bar{u}\|_{\dot{\mathcal{H}}^1}\|v\|_{\dot{\mathcal{H}}^1}.$$

The fact that for R large enough a strongly stable solution $\bar{u}_R$ to (3.3.1) exists thus follows from a standard application of the inverse function theorem [33, Lemma 7.2], which further establishes that

$$\|T_R\bar{u} - \bar{u}_R\|_{\dot{\mathcal{H}}^1} \lesssim \|T_R\bar{u} - \bar{u}\|_{\dot{\mathcal{H}}^1}. \tag{3.5.25}$$

Exploiting (3.5.24) and (3.5.25) as well as the decay estimate (3.2.3), we can conclude

that

$$\|\bar{u}_R - \bar{u}\|_{\dot{\mathcal{H}}^1} = \|\bar{u}_R - T_R\bar{u} + T_R\bar{u} - \bar{u}\|_{\dot{\mathcal{H}}^1} \lesssim \|T_R\bar{u} - \bar{u}\|_{\dot{\mathcal{H}}^1} \lesssim \|Du\|_{\ell^2(\Lambda\setminus B_{R/2})}$$
$$\lesssim \left(\int_{R/2}^{\infty} r\, r^{-3+2\delta}\, dr\right)^{1/2} \lesssim R^{-1/2+\beta},$$

with β arbitrarily small, since δ can be chosen arbitrarily small. □

3.6 Discussion

The results of this chapter extend the mathematical theory of atomistic modelling of crystalline defects studied in [19, 34, 50] to the case of an anti-plane crack defect under nearest-neighbour interactions on a square lattice. This work can be regarded as a first step towards an extension to general atomistic models of fracture, including vectorial models on an arbitrary lattice under an arbitrary interatomic potential.

In this chapter we have laid out many of the steps needed to achieve this, and in what follows we discuss some of the key technical difficulties which must be overcome to extend the present work.

Anti-plane models on an arbitrary Bravais lattice under many-body finite interactions potential: The missing ingredient needed to extend the results to anti-plane models beyond NN interactions on a square lattice is the ability to estimate the lattice Green's function in the crack geometry $\mathcal{G}$, which is discussed in Chapter 4 and is needed to prove Theorem 3.2.2. We refer to the discussion in Section 4.5 for further details.

More general static crack models: Already in the simplified anti-plane setup, the key limiting consequence of the the slow decay of the predictor $\hat{u}$ can be seen by looking at

$$\langle \mathcal{E}(\bar{u}),\, v\rangle = \sum_{m\in\Lambda} \sum_{\rho\in\mathcal{R}(m)} \phi'(D_\rho\hat{u}(m) + D_\rho\bar{u}(m))D_\rho v(m)$$

and Taylor-expanding ϕ' around 0. Crucially, without the further assumption of mirror symmetry, which in the case of a square lattice, as discussed in [19, Section 2.2.], fails if *both* $\phi(-r) \neq \phi(r)$ and the interaction range is such that each nearest-neighbour finite difference is accounted for only in one direction, that is $\tilde{\mathcal{R}} := \{e_1, e_2\}$

(with suitable adjustments in the resulting $\tilde{\mathcal{R}}(m)$ for atoms at the crack surface Γ), the slow decay rate of $\hat{u}$ implies that

$$\left(v \mapsto \frac{\phi'''(0)}{2} \sum_{m\in\Lambda} \sum_{\rho\in\tilde{\mathcal{R}}(m)} (D_\rho \hat{u}(m))^2 D_\rho v(m) \right) \notin (\dot{\mathcal{H}}^1)^*, \tag{3.6.1}$$

unless $\phi'''(0) = 0$, which is usually not true when considering the 2D lattice as a projection of an associated 3D lattice. Note that $\phi(-r) \neq \phi(r)$ is not in itself enough for the mirror symmetry to fail, because for $\mathcal{R}(m)$ defined in (2.1.2), it holds that

$$m \in \Lambda \text{ and } \rho \in \mathcal{R}(m) \implies m + \rho \in \Lambda \text{ and } -\rho \in \mathcal{R}(m+\rho),$$

which renders (3.6.1) (with inner sum over $\mathcal{R}(m)$ and not $\tilde{\mathcal{R}}(m)$) null even if $\phi'''(0) \neq 0$, since the contribution of $(m, m+\rho)$ is cancelled by the contribution of $(m+\rho, m)$.

To extend the theory beyond models with mirror symmetry one has to follow the idea of *development of solutions* introduced in [19], which consists in prescribing a predictor of the form $\hat{u}+\hat{u}_2$, with the additional term arising from the higher-order expansion of the atomistic model and how it can be linked to linear PDEs related to nonlinear elasticity. This ensures that

$$v \mapsto \sum_{m\in\Lambda} \phi''(0) D\hat{u}_2(m) \cdot Dv(m)$$

up to leading order cancels with (3.6.1). The role of $\hat{u}_2$ is especially important for vectorial models, since the concept of mirror symmetry does not translate to models that allow for in-plane displacements, meaning that the vectorial equivalent of (3.6.1) never automatically vanishes.

In-plane static crack models: A further complication related to vectorial models is that as soon as we look beyond nearest-neighbours interactions, we begin to observe surface effects, as for instance investigated in [81]. These effects, induced by the crack surface, do not enter the analysis of vectorial models for dislocations and point defects in [34] and thus pose a major new challenge, as they can potentially lead to surface atoms assuming a different structure compared to the bulk which renders the approximation of CLE invalid. Likewise, this may have an impact on the corresponding lattice Green's function and can potentially make obtaining its decay estimates much more involved.

The role of loading parameter k: It is the appearance of k that ensures we can prove existence of strongly-stable solutions to the problem in (3.2.1), as it allows us to employ the Implicit Function Theorem. This is in contrast with dislocation problems, where, except for specific cases with stringent assumptions as e.g. in [50], we simply assume that a solution exists. The use of IFT also points to a potential bifurcation occurring for some critical k_{crit}, which is a further deviation from the known theory, as in CLE the choice of k is irrelevant. This idea will be discussed in detail in Chapter 5.

Chapter 4

Lattice Green's function in the anti-plane crack geometry

In this chapter we investigate the notion of a lattice Green's function in the anti-plane crack geometry, as discussed in the Introduction in Definition 4, which we already used in the proof of Theorem 3.2.2. We recall from Section 1.2 that this is particularly difficult due to the fact that the crack breaks the translational symmetry of the setup, thus rendering the usual Fourier methods, as employed e.g. in [34], not applicable. However, as is the case in translation-symmetry-preserving setups, the underlying principle that we follow is that in the far-field away from a source point, a discrete Green's function is well-approximated by its continuum counterpart. We exploit it to construct a suitable Green's function with desirable decay properties.

Theorem 5, which characterises the decay properties of such a lattice Green's function in the anti-plane crack geometry, constitutes the main technical result of the thesis upon which all other results rely. In particular, in proving Theorem 5 we ensure that Theorem 3 discussed in Chapter 3 can be proven. Furthermore, the underlying construction and characterisation of a lattice Green's function in this geometry is of independent interest and can be employed, e.g. to study upscaling of screw dislocations [49] in the vicinity of a crack.

4.1 Introduction and notation

In order to ensure clarity, we recall several relevant notions already introduced, starting with the discussion about the discrete kinematics in Section 2.1. In particular we recall the definition of the discrete gradient operator D in (2.1.3), which disregards

interactions across the crack by imposing that for any lattice function $v : \Lambda \to \mathbb{R}$,

$$\text{if } m \in \Gamma_\pm \text{ and } \rho \notin \mathcal{R}(m), \text{ then } (Dv(m))_\rho = 0.$$

This, as discussed in Section 2.2, gives rise to our function space setup, noting that in particular the definition of the Sobolev space $\dot{\mathcal{H}}^1$ in (2.2.1) tells us that

$$v \in \dot{\mathcal{H}}^1 \implies Dv \in \ell^2 \text{ and } v(\tfrac{1}{2}, \tfrac{1}{2}) = 0.$$

We remark that the latter restriction, used to ensure that the associated $\|\cdot\|_{\dot{\mathcal{H}}^1} = \|D\cdot\|_{\ell^2}$ is a norm, plays a subtle role in the way we construct a lattice Green's function for the anti-plane crack geometry. This is discussed below in the concluding part of Section 4.3.1.

We further recall the definition of the discrete divergence operator from (3.5.2):

$$\operatorname{Div} g(m) := -\sum_{\rho \in \mathcal{R}} g_\rho(m-\rho) - g_\rho(m), \quad \text{for } g : \Lambda \to \mathbb{R}^{\mathcal{R}} \tag{4.1.1}$$

and adapt the general formulation of the Hessian operator H from [34] to the case of the pair-potential defined in (2.3.1), in particular noting that $\phi''(0) = 1$, which results in

$$\langle Hu, v\rangle = \sum_{m \in \Lambda} Du(m) \cdot Dv(m) \implies Hu(m) = -\operatorname{Div} Du(m) \quad \forall m \in \Lambda, \tag{4.1.2}$$

with the pointwise formulation following from summation by parts.

In what follows we often work with functions in two variables, thus we introduce a notation for finite differences as follows. If $v : \Lambda \times \Lambda \to \mathbb{R}$, then

$$D_{1\rho} v(m,l) := v(m+\rho, l) - v(m,l) \quad \text{and} \quad D_{2\rho} v(m,l) := v(m, l+\rho) - v(m,l)$$

and for $j \in \{1,2\}$, we have $D_j v(m^1, m^2) \in \mathbb{R}^{\mathcal{R}}$ with

$$\left(D_j v(m)\right)_\rho := \begin{cases} D_{j\rho} v(m^1, m^2) & \text{if } \rho \in \mathcal{R}(m^j), \\ 0 & \text{if } \rho \notin \mathcal{R}(m^j). \end{cases} \tag{4.1.3}$$

Finally, we refer to Section 3.5.1 in which several other technical concepts of relevance to our investigation are introduced, in particular the definition of regions Ω_Γ, Γ, Γ_0, Q_0, the short-hand notation related to the complex square root mapping ω and the short-hand summation notation that we employ throughout.

Outline of the chapter: In Section 4.2 we introduce a rigorous definition of a lattice Green's function in the anti-plane crack geometry and discuss a general strategy to prove its existence and to characterise its decay properties. We also introduce some relevant notation. This is followed by the construction of the Green's function in Section4.3 and the proof of its decay properties in Section 4.4. We conclude with a discussion about possible extensions to more general setups in Section 4.5.

4.2 Main Result

We begin with the definition of a Green's function.

Definition 4.2.1. A function $\mathcal{G} : \Lambda \times \Lambda \to \mathbb{R}$ is said to be a lattice Green's function $\mathcal{G}$ for the anti-plane crack geometry if for all $m, s \in \Lambda$,

$$H\mathcal{G}(m,s) = \delta_{ms} \tag{4.2.1a}$$

$$\mathcal{G}(m,s) = \mathcal{G}(s,m), \tag{4.2.1b}$$

where δ_{ms} denotes the Kronecker delta and H is applied with respect to first variable.

We note that in (4.2.1a) one can view s as a parameter and H as a difference operator applied with respect to the first variable. However, due to (4.2.1b), it is also true that (4.2.1a) holds with H applied with respect to the second variable. Furthermore, $\mathcal{G}$ is not uniquely determined, since any discretely harmonic function can be added, i.e. if $v : \Lambda \to \mathbb{R}$ is such that $Hv = 0$, then $\mathcal{G}(m,s) + v(m) + v(s)$ also satisfies (4.2.1).

For any $\mathcal{G}$ satisfying Definition 4.2.1, any solution $\bar{u}$ to (3.2.1) can be rewritten as

$$D_\tau \bar{u}(l) = \sum_{m \in \Lambda} \left(H(D_{2\tau}\mathcal{G}(m,l))\right) \bar{u}(m) = \sum_{m \in \Lambda} D\bar{u}(m) \cdot D_1 D_{2\tau}\mathcal{G}(m,l),$$

hence highlighting why finding a lattice Green's function that has desired decay properties of its mixed derivative is key to proving Theorem 3.

We establish the following.

Theorem 4.2.2. *There exists a lattice Green's function $\mathcal{G} : \Lambda \times \Lambda \to \mathbb{R}$ satisfying Definition 4.2.1 such that, for any $\delta > 0$, $\rho \in \mathcal{R}(l)$, and $\sigma \in \mathcal{R}(s)$,*

$$|D_{1\rho} D_{2\sigma}\mathcal{G}(l,s)| \lesssim (1 + |\omega_l||\omega_s||\omega_{ls}^-|^{2-\delta})^{-1}, \tag{4.2.2}$$

where ω is the complex square root map defined in (2.4.2) *and we recall the shorthand*

notation introduced in (3.5.4)*, that is*

$$\omega_l := \omega(l), \quad \omega_{ls}^- := \omega(l) - \omega(s), \quad \omega_{ls}^+ := \omega(l) + \omega(s). \tag{4.2.3}$$

4.3 Construction of the Green's function

The approach we employ is based on the observation that finding $\mathcal{G}$, similarly to the crack problem in Chapter 3 can also be cast as a predictor-corrector problem, with the decomposition $\mathcal{G} = \hat{\mathcal{G}} + \bar{\mathcal{G}}$, where $\hat{\mathcal{G}}$ has an explicit expression and $\bar{\mathcal{G}}$ belongs to the energy space $\dot{\mathcal{H}}^1$ in both variables. This idea has already been explored in [34], but was notably aided by the applicability of Fourier methods due to the spatial homogeneity of the reference configuration. The novelty and difficulty of the present setting stem from the fact that the discreteness and inhomogeneity of the domain means that Fourier analysis is no longer applicable. In particular, it renders the task of establishing the decay estimates on $\mathcal{G}$ much more challenging. In our approach we first establish suboptimal estimates on $\bar{\mathcal{G}}$ with the help of the homogeneous lattice Green's function $\mathcal{G}^{\mathrm{hom}}$, which we define in (4.3.10), employed together with suitably chosen cut-offs and a local mapping onto a discrete Riemann surface corresponding to the complex square root. We then use this initial estimate in a boot-strapping argument. The appearance of arbitrarily small $\delta > 0$ in (4.2.2) follows from the fact that this argument saturates at the known decay of $\hat{\mathcal{G}}$.

Remark 4.3.1. While $|\omega_m| = |m|^{1/2}$, in general it is not true that $|\omega_{ms}^-| \sim |m-s|^{-1/2}$, as in fact

$$|m - s| = |\omega_{ms}^-||\omega_{ms}^+|. \tag{4.3.1}$$

The estimate is thus expressed in terms of ω-map, as one can then conveniently resort to a change of variables $\xi = \omega_m$ when estimating sums involving $\omega_m, \omega_s, \omega_{ms}^{\pm}$. See Figure 4.1.

We proceed by first considering two closely related predictor-corrector problems: one to find $\tilde{\mathcal{G}}_1(\cdot, s) \in \dot{\mathcal{H}}^1$ that satisfies (4.2.1a) for a fixed s and the other to find $\tilde{\mathcal{G}}_2(m, \cdot) \in \dot{\mathcal{H}}^1$ that satisfies (4.2.1a) for a fixed m but with H applied to the second variable. To conclude the there exists a Green's function satisfying Definition 4.2.1, one then has to make a suitable adjustment that takes into account how $\dot{\mathcal{H}}^1$ is defined, in particular the restriction that, for

$$\hat{x} := \left(\frac{1}{2}, \frac{1}{2}\right), \tag{4.3.2}$$

we have $\tilde{\mathcal{G}}_1(\hat{x}, s) = \tilde{\mathcal{G}}_2(m, \hat{x}) = 0$ as a result of (2.2.1).

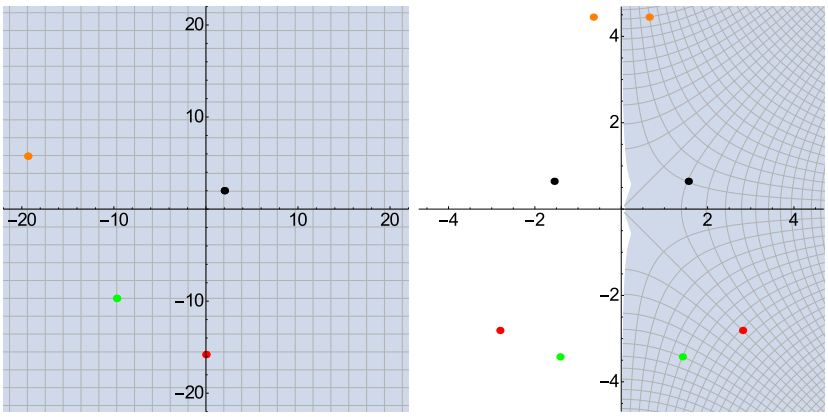

Figure 4.1: The complex square root ω maps the square lattice (left) onto a distorted half-space lattice (right). In particular, the distorted lattice lives in $\mathbb{R}^2_+$, the half-space with positive first coordinate. The dots represent lattice points and their images under ω and also their reflections across y-axis.

Rewriting both problems in variational form, we consider

$$\text{find } \tilde{\mathcal{G}}_i \in \arg\min_{\dot{\mathcal{H}}^1} \tilde{\mathcal{E}}_i, \tag{4.3.3}$$

where

$$\tilde{\mathcal{E}}_1(\mathcal{F}) = \sum_{m\in\Lambda} \left[\frac{1}{2} \left(|D_1\hat{\mathcal{G}}(m,s) + D\mathcal{F}(m)|^2 - |D_1\hat{\mathcal{G}}(m,s)|^2 \right) - \delta_{ms} \left(\hat{\mathcal{G}}(m,s) + \mathcal{F}(m) \right) \right], \tag{4.3.4}$$

and

$$\tilde{\mathcal{E}}_2(\mathcal{F}) = \sum_{s\in\Lambda} \left[\frac{1}{2} \left(|D_2\hat{\mathcal{G}}(m,s) + D\mathcal{F}(s)|^2 - |D_2\hat{\mathcal{G}}(m,s)|^2 \right) - \delta_{ms} \left(\hat{\mathcal{G}}(m,s) + \mathcal{F}(s) \right) \right]. \tag{4.3.5}$$

As in the case of the crack problem itself, the crucial step is the correct choice of the predictor $\hat{\mathcal{G}}$, which ensures the minimisation problems are well-defined. This can be achieved by prescribing $\hat{\mathcal{G}}$ which, away from the point source, is equal to $\hat{G}$ satisfying the corresponding continuum problem, i.e. solving, for $s \in \Lambda$ fixed,

$$\begin{aligned} -C_\Lambda \Delta_x \hat{G}(x,s) &= \delta(x-s) && \text{for } x \in \mathbb{R}^2 \setminus \Gamma_0 \\ \nabla_x \hat{G}(x,s) \cdot \nu &= 0 && \text{for } x \in \Gamma_0, \end{aligned} \tag{4.3.6}$$

and, for $x \in \Lambda$ fixed,

$$\begin{aligned} -C_\Lambda \Delta_s \hat{G}(x,s) &= \delta(x-s) \quad && \text{for } s \in \mathbb{R}^2 \setminus \Gamma_0 \\ \nabla_s \hat{G}(x,s) \cdot \nu &= 0 && \text{for } s \in \Gamma_0. \end{aligned} \tag{4.3.7}$$

Here δ represents the Dirac delta. The constant C_Λ is equal to $C_\Lambda = 2$ in the present case, however generally it depends on the choice of the lattice and the interatomic potential – this is closely related to the discussion in Remark 3.5.2.

Since ω introduced in (2.4.2) is a conformal mapping, it preserves harmonicity [1]. Further, it maps the crack domain to a half-space domain (cf. Figure 4.1), for which a Green's function can be obtained by a reflection argument. It therefore can be verified that (4.3.6) has a solution

$$\hat{G}(x,s) = \frac{-1}{2\pi C_\Lambda} \big[\log(|\omega(x) - \omega(s)|) + \log(|\omega(x) - \omega^*(s)|) \big], \tag{4.3.8}$$

where $\omega^*(x)$ is defined as the reflection of $\omega(x)$ through vertical axis, that is

$$\omega^*(x) = \left(-\sqrt{r_x} \cos\left(\tfrac{\theta_x}{2}\right), \sqrt{r_x} \sin\left(\tfrac{\theta_x}{2}\right) \right),$$

where we refer to Figure 4.1 for a visualisation.

It is easy to see that

$$\hat{G}(x,s) = \hat{G}(s,x), \tag{4.3.9}$$

since

$$|\omega(x) - \omega(s)||\omega(x) - \omega^*(s)| = |\omega(x) - \omega(s)||\omega^*(x) - \omega(s)|,$$

thus $\hat{G}$ also solves (4.3.7). It is worth recalling that the complex square root mapping is also used to construct $\hat{u}$.

Finally, bearing in mind that $\hat{G}(s,s)$ is not well-defined in the pointwise sense, the predictor $\hat{\mathcal{G}} : \Lambda \times \Lambda \to \mathbb{R}$ we prescribe is given by

$$\hat{\mathcal{G}}(m,s) := \begin{cases} \hat{G}(m,s) & \text{if } m \neq s, \\ 0 & \text{if } m = s, \end{cases} \tag{4.3.10}$$

since near the point-source it will always be true that $\mathcal{G}(s,s) \sim \mathcal{O}(1)$.

4.3.1 Proof of Theorem 4.2.2, Part 1: existence of a Green's function

We begin by investigating the predictor $\hat{\mathcal{G}}$ and estimate the decay of its derivatives of relevant order.

Lemma 4.3.2. *For any $x, s \in \mathbb{R}^2 \setminus \Gamma_0$ with $x, s \neq 0$ and $x \neq s$, and $\alpha \in \{1, 2, 3, 4\}$*

$$\begin{aligned} |\nabla_x^\alpha \hat{G}(x,s)| &\lesssim (1 + |\omega_x|^{2\alpha-1}|\omega_{xs}^-|)^{-1} + (1 + |\omega_x|^\alpha |\omega_{xs}^-|^\alpha)^{-1} \\ &=: g_\alpha^{(a)}(x,s) + g_\alpha^{(b)}(x,s) \end{aligned} \tag{4.3.11}$$

and

$$\begin{aligned} |\nabla_x^\alpha \nabla_s \hat{G}(x,s)| &\lesssim (1 + |\omega_x|^{2\alpha-1}|\omega_s||\omega_{xs}^-|^2)^{-1} + (1 + |\omega_x|^\alpha |\omega_s||\omega_{xs}^-|^{\alpha+1})^{-1} \\ &=: h_\alpha^{(a)}(x,s) + h_\alpha^{(b)}(x,s). \end{aligned} \tag{4.3.12}$$

Consequently, if m, $s \in \Lambda$ and $\rho \in \mathcal{R}(m)$ and $\sigma \in \mathcal{R}(s)$, then

$$|D_{1\rho} D_{2\sigma} \hat{\mathcal{G}}(m,s)| \lesssim h_1^{(a)}(m,s).$$

Proof. We first notice that it is sufficient to estimate $L(x,s) := \log(|\omega_{xs}^-|)$, since the part of (4.3.8) that includes $\omega^*(s)$ does not decay any slower. We calculate that

$$\nabla_x L(x,s) = \frac{1}{|\omega_{xs}^-|^2} \nabla\omega(x)\omega_{xs}^- \implies |\nabla_x L(x,s)| \lesssim |\omega_{xs}^-|^{-1}|\nabla\omega(x)| \lesssim |\omega_x|^{-1}|\omega_{xs}^-|^{-1}.$$

Similarly,

$$\nabla_x^2 L(x,s) = \frac{1}{|\omega_{xs}^-|^2}\left(\nabla^2\omega(x)[\omega_{xs}^-] + \nabla\omega(x)\cdot\nabla\omega(x)\right) - \frac{2}{|\omega_{xs}^-|^4}\left(\nabla\omega(x)\omega_{xs}^-\right)^{\otimes 2},$$

which implies that

$$\begin{aligned} |\nabla_x^2 L(x,s)| &\lesssim |\omega_{xs}^-|^{-1}|\nabla^2\omega(x)| + |\omega_{xs}^-|^{-2}|\nabla\omega(x)|^2 \\ &\lesssim |\omega_x|^{-3}|\omega_{xs}^-|^{-1} + |\omega_x|^{-2}|\omega_{xs}^-|^{-2}. \end{aligned}$$

For mixed derivatives we first calculate

$$\begin{aligned} \nabla_s\nabla_x L(x,s) &= \frac{2}{|\omega_{xs}^-|^4}\left(\nabla\omega(x)\omega_{xs}^-\right)\otimes\left(\nabla\omega(s)\omega_{xs}^-\right) - \frac{1}{|\omega_{xs}^-|^2}\nabla\omega(x)\cdot\nabla\omega(s) \\ \implies |\nabla_s\nabla_x L(x,s)| &\lesssim |\omega_{xs}^-|^{-2}|\nabla\omega(x)||\nabla\omega(s)| \lesssim |\omega_x|^{-1}|\omega_s|^{-1}|\omega_{xs}^-|^{-2} \end{aligned}$$

and further realise that

$$\begin{aligned}\nabla_x^2\nabla_s L(x,s) = &\frac{-8}{|\omega_{xs}^-|^6}\left(\nabla\omega(x)\omega_{xs}^-\right)^{\otimes 2}\otimes\left(\nabla\omega(s)\omega_{xs}^-\right)\\ &+\frac{2}{|\omega_{xs}^-|^4}\left(\nabla^2\omega(x)[\omega_{xs}^-]+\nabla\omega(x)\cdot\nabla\omega(x)\right)\otimes\left(\nabla\omega(s)\omega_{xs}^-\right)\\ &+\frac{4}{|\omega_{xs}^-|^4}\left(\nabla\omega(x)\omega_{xs}^-\right)\otimes\left(\nabla\omega(s)\cdot\nabla\omega(x)\right)-\frac{1}{|\omega_{xs}^-|^2}\nabla^2\omega(x)[\nabla\omega(s)],\end{aligned}$$

which leads to

$$|\nabla_x^2\nabla_s L(x,s)| \lesssim |\omega_x|^{-3}|\omega_s|^{-1}|\omega_{xs}^-|^{-2}+|\omega_x|^{-2}|\omega_s|^{-1}|\omega_{xs}^-|^{-3}.$$

Remaining cases can be calculated along similar lines, but for the sake of brevity we choose to omit these tedious calculations. In particular, for $\alpha \geq 3$ there begin to appear extra terms corresponding to intermediate permutations of powers, but these can always be bounded by the two extreme permutations stated.

The facts that $|D_{1\rho}D_{2\sigma}\hat{\mathcal{G}}(m,s)| \lesssim |\nabla_m\nabla_s\hat{\mathcal{G}}(m,s)|$ and $h_1^{(a)} \equiv h_1^{(b)}$ conclude the proof. □

Proposition 4.3.3. *For any $s \in \Lambda$ ($m \in \Lambda$ respectively) the energy difference functional $\hat{\mathcal{E}}_1$ ($\hat{\mathcal{E}}_2$ resp.) in* (4.3.4) *(*(4.3.5) *resp.) is well-defined on $\dot{\mathcal{H}}^1$ and infinitely many times differentiable.*

Proof. Here we will explicitly consider the part of the proof related to $\tilde{\mathcal{E}}_1$, as then the variable symmetry of the predictor, i.e. $\hat{\mathcal{G}}(m,s) = \hat{\mathcal{G}}(s,m)$, implies the other part.

For any $v \in \dot{\mathcal{H}}^1$ we can rewrite the energy difference functional $\tilde{\mathcal{E}}_1$ given by (4.3.4) as

$$\tilde{\mathcal{E}}_1(v) = \tilde{\mathcal{E}}_0(v) + \langle \delta\tilde{\mathcal{E}}_1(0),\, v\rangle,$$

where

$$\begin{aligned}\tilde{\mathcal{E}}_0(v) := \sum_{m\in\Lambda}\Bigg[&\frac{1}{2}|D_1\hat{\mathcal{G}}(m,s)+Dv(m)|^2-\frac{1}{2}|D_1\hat{\mathcal{G}}(m,s)|^2\\ &-D_1\hat{\mathcal{G}}(m,s)\cdot Dv(m)-\delta_{ms}\hat{\mathcal{G}}(m,s)\Bigg]\end{aligned}$$

and

$$\langle \delta\tilde{\mathcal{E}}_1(0),\, v\rangle = \sum_{m\in\Lambda}\Big(D_1\hat{\mathcal{G}}(m,s)\cdot Dv(m)-\delta_{ms}v(m)\Big).$$

Due to the quadratic nature of the energy, $\tilde{\mathcal{E}}_0$ reduces to $\tilde{\mathcal{E}}_0(v) = \frac{1}{2}\|v\|_{\dot{\mathcal{H}}^1}^2 - \hat{\mathcal{G}}(s,s)$

and thus is well-defined on $\dot{\mathcal{H}}^1$.

For the second term, we aim to establish that $\delta\tilde{\mathcal{E}}_1(0)$ is a bounded linear functional on $\dot{\mathcal{H}}^1$ and to achieve that we use the fact that $\hat{G}$ solves the equation given by (4.3.6) by applying the same interpolation construction as in Section 3.5.2. Consequently, we can write

$$\sum_{m\in\Lambda} \delta_{ms} v(m) = v(s) = C_\Lambda \int_{\mathbb{R}^2\setminus\Gamma_0} \nabla\hat{G}(x,s)\cdot\nabla Iv(x)\,dx,$$

and in particular the second equality follows from the weak form of (4.3.6) and the boundary term is not there due to the boundary condition in (4.3.6). Mirroring the argument in Section 3.5.2 we can conclude that

$$\begin{aligned}\langle\delta\tilde{\mathcal{E}}_1(0),\, v\rangle = &\sum_{b(m,\rho)\not\subset\Gamma}\left(D_{1\rho}\hat{\mathcal{G}}(m,s) - \int_{U_{m\rho}} \nabla_\rho\hat{G}(x,s)\,dx\right) D_\rho v(m)\\ &+ \sum_{b(m,\rho)\subset\Gamma}\left(D_{1\rho}\hat{\mathcal{G}}(m,s) - \int_{U_{m\rho}} \nabla_\rho\hat{G}(x,s)\,dx\right.\\ &\qquad\left. - \int_{Q_{m\rho}} \nabla_\rho\hat{G}(x,s)\,dx\right) D_\rho v(m)\\ &+ \sum_{b(m,\rho)\subset Q_0} f(m,s) D_\rho v(m),\end{aligned}$$

where this time $|f(m,s)| \lesssim |\omega_s|^{-1}$, as

$$\int_{B_1(0)\setminus\Gamma_0} |\nabla\hat{G}(x,s)|dx \lesssim |\omega_s|^{-1}\int_0^1 |x|^{-1/2}dx \lesssim |\omega_s|^{-1}.$$

Once again employing a Taylor expansion followed by a standard quadrature result (as discussed in Section 3.5.2) results in

$$b(m,\rho)\not\subset\Gamma \implies \left|D_{1\rho}\hat{\mathcal{G}}(m,s) - \int_{U_{m\rho}} \nabla_\rho\hat{G}(x,s)\,dx\right| \lesssim |\nabla_x^3\hat{G}(x,s)|$$

and

$$b(m,\rho)\subset\Gamma\setminus Q_0 \implies \left|D_{1\rho}\hat{\mathcal{G}}(m,s) - \int_{U_{m\rho}} \nabla_\rho\hat{G}(x,s)\,dx\right| \lesssim |\nabla_x^2\hat{G}(x,s)|.$$

Finally, since Lemma 4.3.2 implies that for both $j = 2,3$ and $x_0 \approx 0$ we have $|\nabla_x^j\hat{G}(x_0,s)| \sim |\omega_s|^{-1}$, we can incorporate any bond $b(m,\rho)\subset Q_0$ into the general

conclusion that

$$|\langle \delta\tilde{\mathcal{E}}_1(0),\, v\rangle| \lesssim \sum_{i=1}^{4} I_i(v),$$

with

$$I_1(v) := \sum_{b(m,\rho)\not\subset\Gamma} g_3^{(a)}(m)|D_\rho v(m)|, \quad I_2(v) := \sum_{b(m,\rho)\not\subset\Gamma} g_3^{(b)}(m)|D_\rho v(m)| \tag{4.3.13}$$

and

$$I_3(v) := \sum_{b(m,\rho)\subset\Gamma} g_2^{(a)}(m)|D_\rho v(m)|, \quad I_4(v) := \sum_{b(m,\rho)\subset\Gamma} g_2^{(b)}(m)|D_\rho v(m)|, \tag{4.3.14}$$

where $g_\alpha^{(a)}$ and $g_\alpha^{(b)}$ were defined in (4.3.11).

Since $|\omega_m| = |m|^{1/2}$, we have $|g_3^{(a)}|, |g_3^{(b)}| \lesssim |m|^{-3/2}$, which is enough to conclude that $I_1(\cdot)$ and $I_2(\cdot)$ are bounded on $\dot{\mathcal{H}}^1$.

Similarly, $|g_2^{(a)}|, |g_2^{(b)}| \lesssim |m|^{-1}$ and thus $I_3(\cdot)$ and $I_4(\cdot)$ are bounded on $\dot{\mathcal{H}}^1$, since their domain of summation is one–dimensional. Hence we can conclude that for any $v \in \dot{\mathcal{H}}^1$,

$$\langle \delta\tilde{\mathcal{E}}_1(0),\, v\rangle \lesssim \|Dv\|_{\ell^2}.$$

To conclude $\tilde{\mathcal{E}}_1$ is C^∞ we first note that $\frac{1}{2}|D\mathcal{F}(m)|^2 = \sum_{\rho\in\mathcal{R}(m)} \tilde{\phi}(D_\rho\mathcal{F}(m))$, where $\tilde{\phi}(r) := \frac{1}{2}r^2$ is a quadratic pair-potential, with $\tilde{\phi}^{(j)} \equiv 0$ for $j \geq 3$, thus, similarly as in the corresponding part of the proof of Theorem 3.2.1, the argument of [68] applies. Likewise, the first variation of the Kronecker delta term can be explicitly calculated and all subsequent ones vanish, thus giving the result. □

Lemma 4.3.4. *For any $s \in \Lambda$, the minimisation problem* (4.3.3) *for $i = 1$ has a unique solution $\tilde{\mathcal{G}}_1(\cdot, s) \in \dot{\mathcal{H}}^1$. Similarly, for any $m \in \Lambda$, the minimisation problem* (4.3.3) *for $i = 2$ has a unique solution $\tilde{\mathcal{G}}_2(m, \cdot) \in \dot{\mathcal{H}}^1$.*

Proof. The existence $\tilde{\mathcal{G}}_1(\cdot, s)$ and $\tilde{\mathcal{G}}_2(m, \cdot)$ is guaranteed by the quadratic nature of the energy $\tilde{\mathcal{E}}_i$, which implies that the problem of finding its critical point is linear, thus allowing us to invoke the standard Lax-Milgram lemma. The minimisers satisfy

$$\langle \delta\tilde{\mathcal{E}}_1(\tilde{\mathcal{G}}_1),\, v\rangle = 0 \quad \text{and} \quad \langle \delta\tilde{\mathcal{E}}_2(\tilde{\mathcal{G}}_2),\, v\rangle = 0 \quad \forall v \in \dot{\mathcal{H}}^1, \tag{4.3.15}$$

where

$$\langle \delta\tilde{\mathcal{E}}_1(\tilde{\mathcal{G}}_1),\, v\rangle = \sum_{m\in\Lambda} (D_1\hat{\mathcal{G}}(m, s) + D_1\tilde{\mathcal{G}}_1(m, s)) \cdot Dv(m) \, - \delta_{ms} v(m),$$

$$\langle \delta\tilde{\mathcal{E}}_2(\tilde{\mathcal{G}}_2),\, v\rangle = \sum_{s\in\Lambda}(D_2\hat{\mathcal{G}}(m,s) + D_2\tilde{\mathcal{G}}_2(m,s))\cdot Dv(s) \; - \delta_{sm}v(s).$$

□

It can be readily checked that in fact $\tilde{\mathcal{G}}_2(m,s) = \tilde{\mathcal{G}}_1(s,m)$, in particular since the restriction in the definition of $\dot{\mathcal{H}}^1$ is satisfied, that is for $m \in \Lambda$ we indeed have $\tilde{\mathcal{G}}_2(m,\hat{x}) = \tilde{\mathcal{G}}_1(\hat{x},m) = 0$, with $\hat{x}$ defined in (4.3.2).

To conclude the result one thus requires to establish that in fact $\tilde{\mathcal{G}}_1 \equiv \tilde{\mathcal{G}}_2$, or in other words that $\tilde{\mathcal{G}}_1(m,s) = \tilde{\mathcal{G}}_1(s,m)$. The reason why two minimisation problems were introduced in (4.3.3), however, is that this cannot be guaranteed without making a suitable adjustment that correctly takes into account the definition of $\dot{\mathcal{H}}^1$. The following weaker preliminary result is first obtained. For notational convenience in what follows we set $\tilde{\mathcal{G}} \equiv \tilde{\mathcal{G}}_1$.

Lemma 4.3.5. *For any $l, s \in \Lambda$ and $\lambda \in \mathcal{R}(l)$, $\tau \in \mathcal{R}(s)$, the unique solution $\tilde{\mathcal{G}}$ from Lemma 4.3.4 satisfies*

$$D_{1\lambda}D_{2\tau}\tilde{\mathcal{G}}(l,s) = D_{2\lambda}D_{1\tau}\tilde{\mathcal{G}}(s,l).$$

Proof. The first equation in (4.3.15) implies that, for any $v \in \dot{\mathcal{H}}^1$ and any $l \in \Lambda$,

$$v(l) = \sum_{m\in\Lambda} D_1(\hat{\mathcal{G}} + \bar{\mathcal{G}})(m,l)\cdot Dv(m). \tag{4.3.16}$$

Since for any $\lambda \in \mathcal{R}(l)$ we have $l + \lambda \in \Lambda$, we also have

$$v(l+\lambda) = \sum_{m\in\Lambda} D_1(\hat{\mathcal{G}} + \bar{\mathcal{G}})(m,l+\lambda)\cdot Dv(m). \tag{4.3.17}$$

Subtracting (4.3.16) from (4.3.17) and letting $v = D_{2\tau}\bar{G}(\cdot,s)$, we obtain

$$D_{1\lambda}D_{2\tau}\tilde{\mathcal{G}}(l,s) = \sum_{m\in\Lambda} D_1D_{2\lambda}(\hat{\mathcal{G}} + \tilde{\mathcal{G}})(m,l)\cdot D_1D_{2\tau}\tilde{\mathcal{G}}(m,s)$$

and since Lemma 4.3.2 ensures that $\left(D_{2\lambda}\hat{\mathcal{G}}(\cdot,l) - D_{2\lambda}\hat{\mathcal{G}}(\hat{x},l)\right) \in \dot{\mathcal{H}}^1$, we can split this infinite sum and write

$$D_{1\lambda}D_{2\tau}\tilde{\mathcal{G}}(l,s) = A + B,$$

where

$$A := \sum_{m\in\Lambda} D_1D_{2\tau}\tilde{\mathcal{G}}(m,s)\cdot D_1D_{2\lambda}\tilde{\mathcal{G}}(m,l)$$

and

$$B := \sum_{m \in \Lambda} D_1 D_{2\tau} \tilde{\mathcal{G}}(m, s) \cdot D_1 D_{2\lambda} \hat{\mathcal{G}}(m, l).$$

Since $\delta\tilde{\mathcal{E}}_1$ is linear, one starts by observing that the first equation of (4.3.15) implies, for all $v \in \dot{\mathcal{H}}^1$,

$$0 = \langle \delta\tilde{\mathcal{E}}_1(\tilde{\mathcal{G}}(\cdot, s+\tau)),\, v\rangle - \langle \delta\tilde{\mathcal{E}}_1(\tilde{\mathcal{G}}(\cdot, s)),\, v\rangle = \langle \delta\tilde{\mathcal{E}}_1(D_{2\tau}\tilde{\mathcal{G}}(\cdot, s)),\, v\rangle. \tag{4.3.18}$$

Treating $\left(D_{2\lambda}\hat{\mathcal{G}}(\cdot, l) - D_{2\lambda}\hat{\mathcal{G}}(\hat{x}, l)\right) \in \dot{\mathcal{H}}^1$ as a test function in (4.3.18), we subtract this expression from B to conclude that

$$B = \sum_{m \in \Lambda} -D_1 D_{2\tau} \hat{\mathcal{G}}(m, s) \cdot D_1 D_{2\lambda} \hat{\mathcal{G}}(m, l) + D_{1\tau} D_{2\lambda} \hat{\mathcal{G}}(s, l).$$

The same analysis can be employed to further conclude that

$$D_{2\lambda} D_{1\tau} \tilde{\mathcal{G}}(s, l) = A + C,$$

where A is defined above and

$$\begin{aligned} C :&= \sum_{m \in \Lambda} D_1 D_{2\lambda} \tilde{\mathcal{G}}(m, l) \cdot D_1 D_{2\tau} \hat{\mathcal{G}}(m, s) \\ &= \sum_{m \in \Lambda} -D_1 D_{2\lambda} \hat{\mathcal{G}}(m, l) \cdot D_1 D_{2\tau} \hat{\mathcal{G}}(m, s) + D_{1\lambda} D_{2\tau} \hat{\mathcal{G}}(l, s), \end{aligned}$$

where the final passage follows from applying the first equality in (4.3.15).

Finally, noting that the variable symmetry of $\hat{\mathcal{G}}$ stated in (4.3.9) implies that

$$D_{1\tau} D_{2\lambda} \hat{\mathcal{G}}(s, l) = D_{1\lambda} D_{2\tau} \hat{\mathcal{G}}(l, s),$$

we can conclude that $B \equiv C$, thus establishing the result. □

We are now in a position to prove the main result of this section.

Proof of Theorem 4.2.2, Part 1: existence of a Green's function. Starting with the equality established in Lemma 4.3.5, we can apply the indefinite sum operator (discrete anologue of indefinite integration, cf. [52]) in the second variable to conclude that

$$D_{1\lambda} \tilde{\mathcal{G}}(m, s) = D_{2\lambda} \tilde{\mathcal{G}}(s, m) + f_\lambda(m),$$

for some lattice function $f_\lambda : \Lambda \to \mathbb{R}$. Similarly, applying indefinite sum operator in

the first variable implies that

$$\tilde{\mathcal{G}}(m,s) = \tilde{\mathcal{G}}(s,m) + F(m) + K_1(s), \tag{4.3.19}$$

where $D_\lambda F(m) = f_\lambda(m)$ and K_1 a is a lattice function to be determined and originating from indefinite summation. We can repeat the procedure in the reverse order to obtain

$$D_{2\tau}\tilde{\mathcal{G}}(m,s) = D_{1\tau}\tilde{\mathcal{G}}(s,m) + k_\tau(s).$$

Taking $\tau = \lambda$ and exchanging m and s we obtain that for any lattice direction λ we have $k_\lambda(m) = -f_\lambda(m)$. Indefinitely summing one more time results in

$$\tilde{\mathcal{G}}(m,s) = \tilde{\mathcal{G}}(s,m) - F(s) + K_2(m). \tag{4.3.20}$$

Comparing (4.3.19) and (4.3.20) we conclude that $K_1(s) = -F(s)$ and $K_2(m) = F(m)$ and thus

$$\tilde{\mathcal{G}}(m,s) = \tilde{\mathcal{G}}(s,m) + F(m) - F(s), \tag{4.3.21}$$

for some F that arises from the restriction in the definition of the energy space $\dot{\mathcal{H}}^1$. By adding and subtracting the same constant we can in fact also write that

$$\tilde{\mathcal{G}}(m,s) + F_2(s) = \tilde{\mathcal{G}}(s,m) + F_2(m),$$

where $F_2(m) := F(m) - F(\hat{x})$, which conveniently implies that $F_2(\hat{x}) = 0$. We now let $m = \hat{x}$ and realise that

$$F_2(s) = \tilde{\mathcal{G}}(s,\hat{x}).$$

Thus the actual relation is given by

$$\tilde{\mathcal{G}}(m,s) + \tilde{\mathcal{G}}(s,\hat{x}) = \tilde{\mathcal{G}}(s,m) + \tilde{\mathcal{G}}(m,\hat{x}) \tag{4.3.22}$$

and we can conclude the proof by stating that the atomistic correction $\bar{\mathcal{G}}$ we sought is given by $\bar{\mathcal{G}}(m,s) := \tilde{\mathcal{G}}(m,s) + \tilde{\mathcal{G}}(s,\hat{x})$, as it clearly satisfies both equations in (4.3.15) and in addition, due to (4.3.22), $\bar{\mathcal{G}}(m,s) = \bar{\mathcal{G}}(s,m)$. □

4.4 Proof of Theorem 4.2.2, Part 2: Green's function decay estimate

4.4.1 Preliminaries

The decay of $|D_1 D_2 \hat{G}|$ is explicitly calculated in Lemma 4.3.2, thus we turn our attention to the decay of the corrector $\bar{\mathcal{G}}$. The general approach we employ is to get insight in the decay behaviour of $\bar{\mathcal{G}}$ in different regions on Λ. For a fixed $s \in \Lambda$ with $|s|$ large enough, we carve the lattice into three regions:

$$\Omega_1(s) := B_{|s|/2}(0) \cap \Lambda, \quad \mathcal{A}(s) := \left(B_{3|s|/2}(0) \setminus B_{|s|/2}(0)\right) \cap \Lambda,$$
$$\Omega_2(s) := \left(\mathbb{R}^2 \setminus B_{3|s|/2}(0)\right) \cap \Lambda.$$

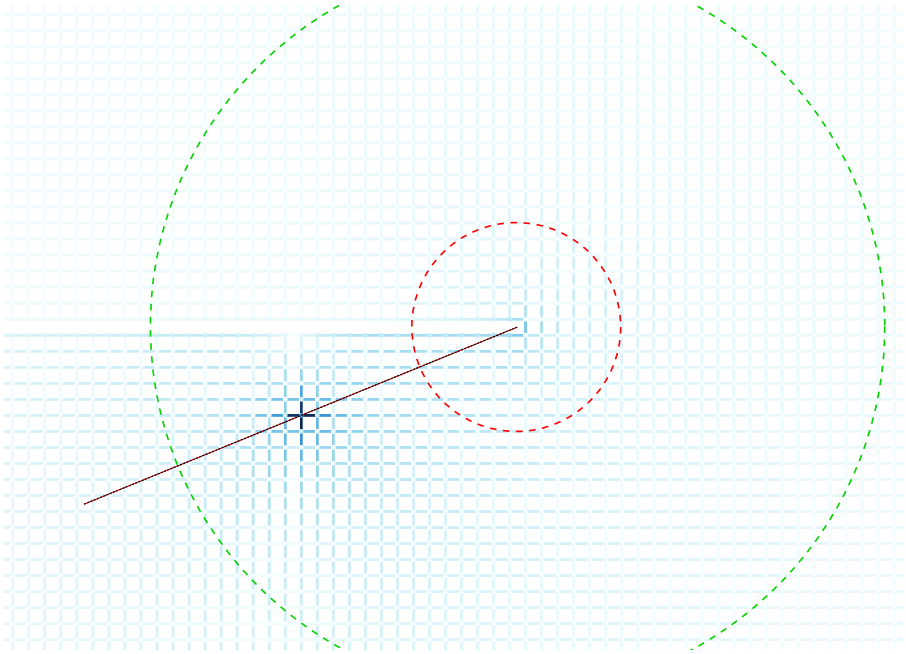

Figure 4.2: The lattice with point-source s depicted in dark blue and $\Omega_1(s)$ being the inner ball with red boundary, $\Omega_2(s)$ the outer region with green boundary and $\mathcal{A}(s)$ the annulus in-between.

In the following we will extensively use the fact that locally the defective lattice does not differ from a homogeneous lattice and thus the result from the spatially homogeneous setup apply, as long as we introduce suitable cut-offs. The general idea behind the cut-off function $\eta : \mathbb{R}^2 \to \mathbb{R}$ to be used throughout is as follows. We define it as $\eta(x) := \hat{\eta}(|x - \hat{y}|/R)$, where $\hat{\eta} : \mathbb{R} \to \mathbb{R}$ is such that $\hat{\eta}(x) = 1$

for $x \in [0, c_1]$, $\eta(x) = 0$ for $x > c_2$, and smooth and decreasing inbetween. As a result $D\eta$ will only be non-zero on an annulus that scales like R. It is also clear, by Taylor expansion, that $|D^j \eta(x)| \lesssim R^{-j}$. The radius R, the lattice point $\hat{y}$, and constants $c_1 < c_2$ will be chosen as needed.

Finally, we also recall the existence and the decay of the homogeneous lattice Green's function $\mathcal{G}^{\text{hom}}$ corresponding to the homogenous hessian operator $\tilde{H}$:

$$\tilde{H}u(m) := \text{Div}\, \tilde{D}u(m), \tag{4.4.1}$$

where we recall the definition of discrete divergence in (4.1.1) and also from (2.1.3) that $\tilde{D}u(m) = (D_\rho u(m))_{\rho \in \mathcal{R}}$, i.e. we always use full stencils. It is proven in [34] in a much more general setup that there exists $\mathcal{G}^{\text{hom}} : \Lambda \to \mathbb{R}$ such that

$$\tilde{H}\mathcal{G}^{\text{hom}}(m - l) = \delta_{ml} \quad \forall m, l \in \Lambda,$$

where δ denotes the Kronecker delta, and

$$|D^j \mathcal{G}^{\text{hom}}(m - l)| \lesssim (1 + |m - l|^j)^{-1}. \tag{4.4.2}$$

With these tools in hand we can gain preliminary insight into the decay behaviour of $\bar{\mathcal{G}}$, however the appearance of the cut-off function restricts us to a suboptimal result.

We proceed in a number of steps, listed in separate section for clarity.

4.4.2 Decay of the first derivative of $\bar{\mathcal{G}}$ away from the origin

Lemma 4.4.1. *If $l \in \Lambda \setminus \Omega_1(s)$ and $\tau \in \mathcal{R}(l)$, then*

$$|D_{1\tau}\bar{\mathcal{G}}(l, s)| \lesssim (1 + |\omega_l||\omega_{ls}^-|)^{-1}.$$

Proof. Due to the spatial restriction on l, we can always choose $\hat{y} = l$,

$$R = |\omega_l||\omega_{ls}^-|$$

with c_1 and c_2 such that the support of the cut-off function η does not reach the origin, e.g. $c_1 = \frac{1}{12}$, $c_2 = \frac{1}{6}$. This is true because $|\omega_l| = |l|^{1/2}$ and trivially $|\omega_{ls}^-| \leq |\omega_l| + |\omega_s| \leq (1 + \sqrt{2})|\omega_l|$.

We distinguish two cases and deal with them separately. The distinction is motivated by the fact that the first case concerns the region away from the crack and translates almost verbatim to vectorial models on an arbitrary Bravais lattice with a finite-range interatomic potential. On the other hand, in Case 2 we handle

the near-crack region with an argument that heavily exploits the setting of a scalar anti-plane model posed on a square lattice under a nearest-neighbour pair-potential.

Case 1: $\operatorname{supp}\eta \cap \Gamma = \emptyset$ **(bulk).**
With the support of the cut-off function not crossing the crack surface, we can directly write

$$\begin{aligned} D_{1\tau}\bar{\mathcal{G}}(l,s) &= D_{1\tau}[\bar{\mathcal{G}}(l,s)\eta(l)] \\ &= \sum_{m\in\Lambda} \tilde{H} D_\tau \mathcal{G}^{\hom}(m-l)]\bar{\mathcal{G}}(m,s)\eta(m) \\ &= \sum_{m\in\Lambda}\sum_{\rho\in\mathcal{R}} D_\rho D_\tau \mathcal{G}^{\hom}(m-l) D_{1\rho}[\bar{\mathcal{G}}(m,s)\eta(m)], \end{aligned} \tag{4.4.3}$$

where the first equality is due to the fact that near l the cut-off is just 1, the second follows from the definition of the homogeneous lattice Green's function and the fact that with the cut-off in place we effectively sum over a finite region, where there is no disparity between H and $\tilde{H}$. The last equality is just summation by parts.

In order to use the fact that $\bar{\mathcal{G}}$ satisfies equation given in (4.3.15), we need to push the cut-off onto the other term by exploiting the discrete product rule satisfied by any $f, g : \Lambda \to \mathbb{R}$ and given by

$$D_\rho[fg](m) = f(m+\rho)D_\rho g(m) + f(m)D_\rho g(m) \tag{4.4.4a}$$
$$= g(m+\rho)D_\rho f(m) + g(m)D_\rho f(m) \tag{4.4.4b}$$
$$= A_\rho f(m) D_\rho g(m) + D_\rho f(m) A_\rho g(m), \tag{4.4.4c}$$

where $A_\rho f(m) := \frac{1}{2}\left(f(m+\rho) + f(m)\right)$ is the average operator.

This leads to

$$D_{1\tau}\bar{\mathcal{G}}(l,s) = S_1 + S_2,$$

where the first term is in the form allowing us to exploit the equation, namely

$$S_1 = \sum_{m\in\Lambda}\sum_{\rho\in\mathcal{R}} D_\rho[D_\tau \mathcal{G}^{\hom}(m-l)\eta(m)] D_{1\rho}\bar{\mathcal{G}}(m,s)$$

and the second term makes sure that the right-hand side is consistent with (4.4.3),

that is

$$S_2 = \sum_{m\in\Lambda}\sum_{\rho\in\mathcal{R}} D_\rho\eta(m)\Big[A_\rho D_\tau \mathcal{G}^{\mathrm{hom}}(m-l)D_{1\rho}\bar{\mathcal{G}}(m,s) + D_\rho D_\tau \mathcal{G}^{\mathrm{hom}}(m-l)A_{1\rho}\bar{\mathcal{G}}(m,s)\Big].$$

Here $A_{1\rho}f(m,s) := \frac{1}{2}\left(f(m+\rho,s)+f(m,s)\right)$.

We deal with both terms separately. For S_1 we realise that

$$v(m) := D_\tau \mathcal{G}^{\mathrm{hom}}(m-l)\eta(m) \tag{4.4.5}$$

is in fact compactly-supported, so is an admissible test function in the energy space $\dot{\mathcal{H}}^1$. In particular, it satisfies $|D_\rho v(m)| \lesssim |m-l|^{-2} = |\omega_{ml}^-|^{-2}|\omega_{ml}^+|^{-2}$, a relation established in (4.3.1), and for $m \in B_{c_2R}(l)$, which is equal to $\operatorname{supp}\eta$, we trivially have that $|\omega_{ml}^+| \geq |\omega_m|$, from which it further follows that

$$|\omega_{ml}^-| = \frac{|m-l|}{\omega_{ml}^+} \leq \frac{|m-l|}{|\omega_m|},$$

where the first equality is due to (4.3.1). We can further establish that $m \in B_{c_2R}(l)$ implies $|m-l| \leq c_2R \leq \frac{1+\sqrt{2}}{6}|l|$ and $|l|\left(1-\frac{1+\sqrt{2}}{6}\right) \leq |m|$, which after elementary rearranging implies that $|\omega_{ml}^+| \geq |\omega_m| \geq |\omega_{ml}^-|$, which ultimately leads to

$$|m-l|^{-2} \lesssim |\omega_{ml}^-|^{-2}|\omega_m|^{-2} \lesssim |\omega_{ml}^-|^{-4}. \tag{4.4.6}$$

Exploiting the fact that $\bar{\mathcal{G}}$ satisfies (4.3.15) we conclude that

$$|S_1| = \left|-\langle \delta\tilde{E}_1(0),\, v\rangle\right| \lesssim \sum_{i=1}^{4} I_i(v),$$

where $I_1,\dots,I_4$ are defined in (4.3.13) and (4.3.14).

We look at each term separately and begin by noting that

$$I_1(v) \lesssim \sum_{m\in B_{c_2R}(l)} (1+|\omega_m|^5|\omega_{ms}^-|)^{-1}(1+|\omega_{ml}^-|^2|\omega_m|^2)^{-1} =: \sum_{m\in B_{c_2R}(l)} f_1(m)$$

and observe that away from the potential sharp spikes at $m=l$ and $m=s$ we can

bound this series by the corresponding integral, that is we can say

$$I_1(v) \lesssim f_1(l) + f_1(s)\mathbb{1}_{B_{c_2R}(l)}(s) + \int_{D_R(l)} f_1(x)dx,$$

where $D_R(l) := B_{c_2R}(l)\setminus(B_1(l)\cup B_1(s))$. The indicator function $\mathbb{1}$ covers cases when $s \notin B_{c_2R}(l)$. Clearly

$$f_1(l) = (1+|\omega_l|^5|\omega_{ls}^-|)^{-1},$$

whereas $f_1(s)\mathbb{1}_{B_{c_2R}(l)}(s) \neq 0$ only if $s \in B_{c_2R}(l)$, but then $|s| \sim |l|$, which implies

$$f_1(s)\mathbb{1}_{B_{c_2R}(l)}(s) \lesssim (1+|\omega_l|^2|\omega_{ls}^-|^2)^{-1}. \tag{4.4.7}$$

For the integral term we introduce a change of variables $\xi = \omega_m$, and set $\gamma := \omega_s$, $\zeta := \omega_l$, leading to $dm = |\xi|^2 d\xi$. As a result we have

$$\begin{aligned}\int_{D_R(l)} f_1(x)dx &\leq \int_{\omega(D_R(l))} \frac{|\xi|^2}{(1+|\xi|^5|\xi-\gamma|)(1+|\xi-\zeta|^4)}d\xi \\ &=: \int_{\omega(D_R(l))} \tilde{f}_1(\xi)d\xi,\end{aligned}$$

where the first inequality follows from (4.4.6).

Carving the region of integration into

$$\Omega_\gamma := B_{\frac{|\gamma-\zeta|}{2}}(\gamma) \cap \omega(D_R(l)), \tag{4.4.8a}$$

$$\Omega_\zeta := B_{\frac{|\gamma-\zeta|}{2}}(\zeta) \cap \omega(D_R(l)), \tag{4.4.8b}$$

$$\Omega' := \omega(D_R(l)) \setminus (\Omega_\gamma \cup \Omega_\zeta) \tag{4.4.8c}$$

and noting that depending on where l and s are, some of them could be empty, we can estimate the integral as follows.

First we notice the following spatial relations

$$\xi \in \omega(D_R(l)) \implies |\xi| \sim |\zeta|, \tag{4.4.9a}$$

$$\xi \in \Omega_\gamma \implies |\xi-\zeta| \gtrsim |\zeta-\gamma|, \tag{4.4.9b}$$

$$\xi \in \Omega_\zeta \implies |\xi-\gamma| \gtrsim |\zeta-\gamma|. \tag{4.4.9c}$$

Thus

$$\begin{aligned}\int_{\Omega_\gamma} \tilde{f}_1 d\xi &\lesssim \frac{|\zeta|^2}{1+|\zeta-\gamma|^4} \int_{\Omega_\gamma} \frac{1}{1+|\zeta|^5|\xi-\gamma|} d\xi \\ &\lesssim \frac{|\zeta|^2}{1+|\zeta-\gamma|^4} \int_{\frac{1}{|\gamma|}}^{\frac{|\zeta-\gamma|}{2}} \frac{r}{1+|\zeta|^5 r} dr \\ &\lesssim (1+|\zeta|^3|\zeta-\gamma|^3)^{-1},\end{aligned}$$

where the lower limit of integration in the third integral follows from the fact that we exclude a unit ball around $|s|$ in the original domain. The same reasoning was used to estimate (3.5.18).

Likewise,

$$\int_{\Omega_\zeta} \tilde{f}_1 d\xi \lesssim \frac{|\zeta|^2}{1+|\zeta|^5|\zeta-\gamma|} \int_{\Omega_\zeta} \frac{1}{1+|\zeta-\gamma|^4} d\xi \lesssim (1+|\zeta|^3|\zeta-\gamma|)^{-1} \tag{4.4.10}$$

and

$$\int_{\Omega'} \tilde{f}_1 d\xi \lesssim \frac{1}{(1+|\zeta|^5|\zeta-\gamma|)(1+|\zeta-\gamma|^4)} \int_{\Omega'} |\xi|^2 d\xi \lesssim (1+|\zeta|^3|\zeta-\gamma|^3)^{-1},$$

where the final passage relies on the fact that we can map back to $B_{c_2R}(l)$ and have a volume term that scales like $R^2 = |\zeta|^2|\zeta-\gamma|^2$.

For $I_2(v)$ (recalling its definition from (4.3.13)), similarly,

$$I_2(v) \lesssim \sum_{m \in B_{c_2R}(l)} (1+|\omega_m|^3|\omega_{ms}^-|)^{-3}(1+|\omega_{ml}^-|^2|\omega_m|^2)^{-1} =: \sum_{m \in B_{c_2R}(l)} f_2(m)$$

and hence

$$I_2(v) \lesssim f_2(l) + f_2(s)\mathbb{1}_{B_{c_2R}(l)}(s) + \int_{D_R(l)} f_2(x)dx.$$

We observe that, due to the same reasoning as in (4.4.7), we have

$$f_2(l) = (1+|\omega_l|^3|\omega_{ls}^-|^3)^{-1} \quad \text{and} \quad f_2(s)\mathbb{1}_{B_{c_2R}(l)}(s) \lesssim (1+|\omega_l|^2|\omega_{ls}^-|^2)^{-1}. \tag{4.4.11}$$

Furthermore,

$$\begin{aligned}\int_{D_R(l)} f_2(x)dx &= \int_{\omega(D_R(l))} \frac{|\xi|^2}{(1+|\xi|^3|\xi-\gamma|^3)(1+|\xi|^2|\xi-\zeta|^2)} d\xi \\ &=: \int_{D_R(l))} \tilde{f}_2(\xi) d\xi,\end{aligned}$$

with estimates, again arising from the spatial relations established in (4.4.9),

$$\begin{aligned}\int_{\Omega_\gamma} \tilde{f}_2 d\xi &\lesssim \frac{|\zeta|^2}{1+|\zeta|^2|\zeta-\gamma|^2} \int_{\Omega_\gamma} \frac{1}{1+|\zeta|^3|\xi-\gamma|^3} d\xi \\ &\lesssim \frac{|\zeta|^2}{1+|\zeta|^2|\zeta-\gamma|^2} \int_{\frac{1}{|\gamma|}}^{\frac{|\zeta-\gamma|}{2}} \frac{r}{1+|\zeta|^3 r^3} dr \\ &\lesssim (1+|\zeta|^2|\zeta-\gamma|^2)^{-1}, \end{aligned} \tag{4.4.12}$$

$$\begin{aligned}\int_{\Omega_\zeta} \tilde{f}_2 d\xi &\lesssim \frac{|\zeta|^2}{1+|\zeta|^3|\zeta-\gamma|^3} \int_{\Omega_\zeta} \frac{1}{1+|\zeta|^2|\xi-\zeta|^2} d\xi \\ &\lesssim (1+|\zeta|^3|\zeta-\gamma|^3)^{-1} \log|\zeta-\gamma| \end{aligned}$$

and

$$\begin{aligned}\int_{\Omega'} \tilde{f}_2 d\xi &\lesssim \frac{1}{(1+|\zeta|^3|\zeta-\gamma|^3)(1+|\zeta|^2|\zeta-\gamma|^2)} \int_{\Omega'} |\xi|^2 d\xi \\ &\lesssim (1+|\zeta|^3|\zeta-\gamma|^3)^{-1}, \end{aligned}$$

Finally, since for now we assume that $\operatorname{supp}\eta \cap \Gamma = \emptyset$, we trivially have that $I_3(v) = I_4(v) = 0$. It can be thus concluded that $S_1 \lesssim (1+|\zeta|^2|\zeta-\gamma|)^{-1} = (1+|\omega_l|^2|\omega_{ls}^-|)^{-1}$, with the exponents taken from combining (4.4.10), (4.4.11) and (4.4.12).

For S_2 we realise that $D_\rho\eta(m)$ is only non-zero for $m \in \mathcal{A}_R := B_{c_2R}(l) \setminus B_{c_1R}(l)$, which corresponds to a volume term that scales like $R^2 = |\omega_l|^2|\omega_{ls}^-|^2$. It also in particular implies that $|m-l|$ and $|\omega_l||\omega_{ls}^-|$ are comparable. We can thus use Cauchy-Schwarz inequality and the decay of each term to conclude that

$$\begin{aligned}|S_2| &\lesssim \left(|\omega_l|^{(-4+2)}|\omega_{ls}^-|^{(-4+2)}\right)^{1/2} \|D\bar{\mathcal{G}}(\cdot,s)\|_{\ell^2} \\ &\quad + \left(|\omega_l|^{(-6+2)}|\omega_{ls}^-|^{(-6+2)}\right)^{1/2} \|A\bar{\mathcal{G}}(\cdot,s)\|_{\ell^2(\mathcal{A}_R)} \\ &\lesssim (1+|\omega_l||\omega_{ls}^-|)^{-1}, \end{aligned}$$

where the last inequality is due to $\|A\bar{\mathcal{G}}(\cdot,s)\|_{\ell^2(\mathcal{A}_R)} \lesssim R\|D\bar{\mathcal{G}}(\cdot,s)\|_{\ell^2}$, a result that immediately follows from [33, Lemma 7.1].

Case 2: $\operatorname{supp}\eta \cap \Gamma \neq \emptyset$ **(near crack surface).**

To cover this more problematic case we resort to a technical trick at present only

seems to be applicable to a square lattice with NN interactions. We begin by constructing a discrete equivalent of a Riemann surface corresponding to the complex square root map,

$$\mathcal{M} := \mathbb{Z}^2 \times \{-1, 1\}, \tag{4.4.13}$$

that is, we look at two copies of the square lattice and so $k \in \mathcal{M}$ is such that $k = (k_l, k_b)$, where k_l corresponds to a lattice site and k_b determines whether we are on the positive branch or the negative branch (as with the complex square root mapping).

For $\boldsymbol{u} : \mathcal{M} \to \mathbb{R}$ and a lattice direction $\rho \in \mathcal{R}$, we also define the notion of a finite difference $\mathcal{D}_\rho$ and of a swapping finite difference $\mathcal{D}^s_\rho$ as

$$\begin{aligned} \mathcal{D}_\rho \boldsymbol{u}(k) &:= \boldsymbol{u}(k_l + \rho, k_b) - \boldsymbol{u}(k_l, k_b) \\ \mathcal{D}^s_\rho \boldsymbol{u}(k) &:= \boldsymbol{u}(k_l + \rho, -k_b) - \boldsymbol{u}(k_l, k_b). \end{aligned}$$

Since $k_b \in \{-1, 1\}$, we note that in the latter case we simply jump from one branch to another. The corresponding manifold discrete gradient operator as $\mathcal{D}\boldsymbol{u}(k) \in \mathbb{R}^{\mathcal{R}}$ can then be defined as

$$\big(\mathcal{D}\boldsymbol{u}(k)\big)_\rho = \begin{cases} \mathcal{D}_\rho \boldsymbol{u}(k) & \text{if } \rho \in \mathcal{R}(k_l), \\ \mathcal{D}^s_\rho \boldsymbol{u}(k) & \text{if } \rho \notin \mathcal{R}(k_l). \end{cases} \tag{4.4.14}$$

Comparing this with the definition of the discrete gradient in (2.1.3), we observe that the they only differ at lattice points on $\Gamma_+ \cup \Gamma_-$. This underlines the reasoning behind the construction - we take two copies of the lattice and glue them together at the 'cut' created by the crack, thus ensuring that in fact we always work with full stencils. Consequently, we can again locally use the homogeneous lattice Green's function $\mathcal{G}^{\text{hom}}$, as long as we avoid the origin of $\mathcal{M}$.

We further define the manifold equivalent of $\dot{\mathcal{H}}^1$ defined in (2.2.1) as

$$\dot{\mathcal{H}}^1_{\mathcal{M}} := \left\{ \boldsymbol{u} : \mathcal{M} \to \mathbb{R} \mid \mathcal{D}\boldsymbol{u} \in \ell^2 \text{ and } \boldsymbol{u}(\hat{x}, \pm 1) = 0 \right\}. \tag{4.4.15}$$

Likewise, we can extend the notion of the predictor $\hat{\mathcal{G}}$ defined in (4.3.10) to the manifold setup by defining $\hat{\mathcal{G}}_{\mathcal{M}} : \mathcal{M} \times \mathbb{Z}^2 \to \mathbb{R}$ as

$$\hat{\mathcal{G}}_{\mathcal{M}}(k, s) := \begin{cases} \hat{\mathcal{G}}(k_l, s) & \text{if } k_b = 1, \\ \hat{\mathcal{G}}((k_{l_1}, -k_{l_2}), s) & \text{if } k_b = -1, \end{cases}$$

that is, for the negative branch, we reflect the original predictor across x-axis. Note

that the manifold finite difference operators are always applied with respect to the first variable.

Finally, we can also consider a manifold equivalent of the energy-difference $\tilde{\mathcal{E}}_1$ defined in (4.3.4), which we define as

$$\tilde{\mathcal{E}}_{\mathcal{M}}(\mathcal{G}_{\mathcal{M}}) = \sum_{k\in\mathcal{M}} \Bigg[\frac{1}{2}\Big(\sum_{\rho\in\mathcal{R}} (\mathcal{D}\hat{\mathcal{G}}_{\mathcal{M}}(k,s))_\rho + (\mathcal{D}\mathcal{G}_{\mathcal{M}}(k,s))_\rho)^2 - (\mathcal{D}\hat{\mathcal{G}}_{\mathcal{M}}(k,s))_\rho^2 \Big) \\ - (\delta(k,(s,1)) + \delta(k,((s_1,-s_2),-1))) \left(\hat{\mathcal{G}}_{\mathcal{M}}(k,s) + \mathcal{G}_{\mathcal{M}}(k,s)\right) \Bigg]. \tag{4.4.16}$$

It follows immediately from Proposition 4.3.3 that $\tilde{\mathcal{E}}_{\mathcal{M}}$ is well-defined over $\dot{\mathcal{H}}^1_{\mathcal{M}}$ and smooth. Thus we can again look at the problem of finding a stationary point $\bar{\mathcal{G}}_{\mathcal{M}}$ which satisfies

$$\langle \delta\tilde{\mathcal{E}}_{\mathcal{M}}(\bar{\mathcal{G}}_{\mathcal{M}}),\, \boldsymbol{u}\rangle = 0 \quad \forall \boldsymbol{u} \in \dot{\mathcal{H}}^1_{\mathcal{M}}, \tag{4.4.17}$$

where

$$\langle \delta\tilde{\mathcal{E}}_{\mathcal{M}}(\bar{\mathcal{G}}_{\mathcal{M}}),\, \boldsymbol{u}\rangle = \sum_{k\in\mathcal{M}} \Bigg[\sum_{\rho\in\mathcal{R}} \left(\mathcal{D}_\rho\hat{\mathcal{G}}_{\mathcal{M}}(k,s) + \mathcal{D}_\rho\bar{\mathcal{G}}_{\mathcal{M}}(k,s)\right) \mathcal{D}_\rho\boldsymbol{u}(m) \\ - (\delta(k,(s,1)) + \delta(k,((s_1,-s_2),-1)))\, \boldsymbol{u}(k) \Bigg].$$

Crucially, the way we define $\hat{\mathcal{G}}_{\mathcal{M}}$ implies that the contribution from the new bonds across Γ is null, as e.g. for $l \in \Gamma_-$ we have $l+e_2 = (l_1,-l_2)$, hence $\mathcal{D}^s_{e_2}\hat{\mathcal{G}}_{\mathcal{M}}((l,1),s) = 0$. This in turn tells us the solution to (4.4.17) is given by

$$\bar{\mathcal{G}}_{\mathcal{M}}(k,s) := \begin{cases} \bar{\mathcal{G}}(k_l,s) & \text{if } k_b = 1, \\ \bar{\mathcal{G}}((k_{l_1},-k_{l_2}),s) & \text{if } k_b = -1. \end{cases}$$

Thus to obtain the decay estimate for $|D_{1\tau}\bar{\mathcal{G}}(l,s)|$, we proceed as follows. Without loss of generality we can assume that $l_2 < 0$ and accordingly define a reflected version of $\mathcal{G} = \hat{\mathcal{G}} + \bar{\mathcal{G}}$ as $\mathcal{G}_{\text{ref}} : \Lambda \to \mathbb{R}$ with $\mathcal{G}_{\text{ref}} = \hat{\mathcal{G}}_{\text{ref}} + \bar{\mathcal{G}}_{\text{ref}}$, where

$$\hat{\mathcal{G}}_{\text{ref}}(m,s) := \begin{cases} \hat{\mathcal{G}}(m,s) & \text{if } m_2 < 0, \\ \hat{\mathcal{G}}((m_1,-m_2),s) & \text{if } m_2 > 0 \end{cases}$$

and

$$\bar{\mathcal{G}}_{\mathrm{ref}}(m,s) := \begin{cases} \bar{\mathcal{G}}(m,s) & \text{if } m_2 < 0, \\ \bar{\mathcal{G}}((m_1,-m_2),s) & \text{if } m_2 > 0. \end{cases}$$

Hence, by construction we have $D_{1\tau}\bar{G}(l,s) = D_{1\tau}\bar{G}_{\mathrm{ref}}(l,s)$ and we can write

$$\begin{aligned} D_{1\tau}\bar{\mathcal{G}}(l,s) &= D_{1\tau}[\bar{\mathcal{G}}_{\mathrm{ref}}(l,s)\eta(l)] = \sum_{m\in\Lambda} \tilde{H} D_\tau \mathcal{G}^{\mathrm{hom}}(m-l)\bar{\mathcal{G}}_{\mathrm{ref}}(m,s)\eta(m) \\ &= \sum_{m\in\Lambda}\sum_{\rho\in\mathcal{R}} D_\rho D_\tau \mathcal{G}^{\mathrm{hom}}(m-l) D_{1\rho}[\bar{\mathcal{G}}_{\mathrm{ref}}(m,s)\eta(m)] \\ &= S_1 + S_2, \end{aligned}$$

with

$$S_1 = \sum_{m\in\Lambda}\sum_{\rho\in\mathcal{R}} D_\rho[D_\tau \mathcal{G}^{\mathrm{hom}}(m-l)\eta(m)] D_{1\rho}\bar{\mathcal{G}}_{\mathrm{ref}}(m,s),$$

and

$$S_2 = \sum_{m\in\Lambda}\sum_{\rho\in\mathcal{R}} D_\rho\eta(m)\Big[A_\rho D_\tau \mathcal{G}^{\mathrm{hom}}(m-l) D_{1\rho}\bar{\mathcal{G}}_{\mathrm{ref}}(m,s) + D_\rho D_\tau \mathcal{G}^{\mathrm{hom}}(m-l) A_{1\rho}\bar{\mathcal{G}}_{\mathrm{ref}}(m,s)\Big].$$

Noting that the nullity of bonds across the x-axis of $\bar{\mathcal{G}}_{\mathrm{ref}}$ due to reflection ensures that $\|D_1\bar{\mathcal{G}}_{\mathrm{ref}}(\cdot,s)\|_{\ell^2} < \infty$, the argument for S_2 is unaffected, thus we can immediately conclude that $S_2 \lesssim (1+|\omega_l||\omega_{ls}^-|)^{-1}$. For S_1 we recall the definition of v in (4.4.5) and define its manifold equivalent $v_{\mathcal{M}} : \mathcal{M} \to \mathbb{R}$ by

$$v_{\mathcal{M}}(k) := \begin{cases} v(k_l) & \text{if } (k_{l_2} < 0 \ \wedge k_b = 1) \vee (k_{l_2} > 0 \wedge k_b = -1), \\ 0 & \text{otherwise.} \end{cases}$$

As a result we have

$$S_1 = \sum_{k\in\mathcal{M}} \mathcal{D}\bar{\mathcal{G}}_{\mathcal{M}}(k,s)\cdot\mathcal{D}v_{\mathcal{M}}(k)$$

and thus we can exploit (4.4.17) to conclude that

$$S_1 = \sum_{k\in\mathcal{M}} -\mathcal{D}\hat{\mathcal{G}}_{\mathcal{M}}(k,s)\cdot\mathcal{D}v_{\mathcal{M}}(k) + v_{\mathcal{M}}((s,1)) + v_{\mathcal{M}}((s,-1)).$$

We can now introduce

$$\hat{\mathcal{G}}_+(m,s) := \begin{cases} \hat{\mathcal{G}}_{\mathcal{M}}((m,1),s) & \text{if } m_2 < 0, \\ 0 & \text{if } m_2 > 0, \end{cases}$$

$$\hat{\mathcal{G}}_-(m,s) := \begin{cases} \hat{\mathcal{G}}_{\mathcal{M}}((m,-1),s) & \text{if } m_2 > 0, \\ 0 & \text{if } m_2 < 0, \end{cases}$$

$$v_+(m) := \begin{cases} v(m) & \text{if } m_2 < 0, \\ 0 & \text{if } m_2 > 0, \end{cases} \quad v_-(m) := \begin{cases} v(m) & \text{if } m_2 > 0, \\ 0 & \text{if } m_2 < 0. \end{cases} \tag{4.4.18}$$

and are able to conclude that in fact

$$\begin{aligned} S_1 &= \left(\sum_{m \in \Lambda} -D_1 \hat{\mathcal{G}}_+(m,s) \cdot Dv_+(m) + v_+(s) \right) \\ &\quad + \left(\sum_{m \in \Lambda} -D_1 \hat{\mathcal{G}}_-(m,s) \cdot Dv_-(m) + v_-((s_1,-s_2)) \right) \\ &=: S_+ + S_-, \end{aligned}$$

i.e., we look at the positive and negative branch separately. We further note that due to reflection we always have

$$|D_1 \hat{\mathcal{G}}_-(m,s) \cdot Dv_-(m)| \leq |D_1 \hat{\mathcal{G}}_+((m_1,-m_2),s) \cdot Dv_+((m_1,-m_2))|,$$

and consequently any estimate that applies to $|S_+|$ equally applies to $|S_-|$. Furthermore, $|S_+|$ can be estimated as in Case 1, except now $I_3(v_+), I_4(v_+) \neq 0$, but we can estimate them as follows.

With $\Gamma_l := B_{c_2 R}(l) \cap \Gamma$, we first note that

$$I_3(v_+) \lesssim \sum_{m \in \Gamma_l} (1 + |\omega_m|^3 |\omega_{ms}^-|)^{-1} (1 + |\omega_{ml}^-|^2 |\omega_{ml}^+|^2)^{-1} =: \sum_{m \in \Gamma_l} f_3(m)$$

and again argue that

$$I_3(v_+) \lesssim f_3(l) \mathbb{1}_{\Gamma_l}(l) + f_3(s) \mathbb{1}_{\Gamma_l}(s) + \int_{\tilde{\Gamma}_l} f_3(x) dx,$$

where $\tilde{\Gamma}_l := \Gamma_l \setminus (B_1(l) \cup B_1(s))$. The indicator function $\mathbb{1}$ is there to cover cases

when $l, s \notin \Gamma_l$. It is clear that

$$f_3(l) = (1 + |\omega_l|^3 |\omega_{ls}^-|)^{-1} \quad \text{and} \quad f_3(s)\mathbb{1}_{\Gamma_l}(s) \lesssim (1 + |\omega_l|^2 |\omega_{ls}^-|^2)^{-1},$$

where in particular for the second inequality we argue as in (4.4.7).

For the integral term we again introduce a change of variables $\xi = \omega_m$ and due to $\omega(\Gamma_l)$ being a one-dimensional line, we can conclude that $dm \lesssim |\xi| d\xi$. As a result, we have

$$\begin{aligned}\int_{\tilde{\Gamma}_l} f_3(x)dx &= \int_{\omega(\tilde{\Gamma}_l)} \frac{|\xi|}{(1 + |\xi|^3|\xi - \gamma|)(1 + |\xi - \zeta|^2||\xi + \zeta|^2)} d\xi \\ &=: \int_{\omega(\tilde{\Gamma}_l)} \tilde{f}_3(\xi) d\xi.\end{aligned}$$

Mimicking the approach for $I_1(v)$ and $I_2(v)$, we carve the region of integration into

$$\Gamma_\gamma := B_{\frac{|\gamma-\zeta|}{2}}(\gamma) \cap \omega(\tilde{\Gamma}_l), \tag{4.4.19a}$$

$$\Gamma_\zeta := B_{\frac{|\gamma-\zeta|}{2}}(\zeta) \cap \omega(\tilde{\Gamma}_l), \tag{4.4.19b}$$

$$\Gamma_l' := \omega(\tilde{\Gamma}_l) \setminus (\Gamma_\gamma \cup \Gamma_\zeta) \tag{4.4.19c}$$

and observe that the spatial relations in (4.4.9) remain valid. Hence,

$$\begin{aligned}\int_{\Gamma_\gamma} \tilde{f}_3 d\xi &\lesssim \frac{|\zeta|}{1 + |\zeta|^2|\zeta - \gamma|^2} \int_{\Gamma_\gamma} \frac{1}{1 + |\zeta|^3|\xi - \gamma|} d\xi \\ &\lesssim (1 + |\zeta|^4|\zeta - \gamma|^2)^{-1}(\log|\zeta| + \log|\zeta - \gamma|),\end{aligned}$$

$$\int_{\Gamma_\zeta} \tilde{f}_3 d\xi \lesssim \frac{|\zeta|}{1 + |\zeta|^3|\zeta - \gamma|} \int_{\Gamma_\zeta} \frac{1}{1 + |\zeta|^2|\xi - \zeta|^2} d\xi \lesssim (1 + |\zeta|^4|\zeta - \gamma|)^{-1}$$

and

$$\int_{\Gamma_l'} \tilde{f}_3 d\xi \lesssim \frac{1}{(1 + |\zeta|^2|\zeta - \gamma|^2)(1 + |\zeta|^3|\zeta - \gamma|)} \int_{\Gamma_\gamma} |\xi| d\xi \lesssim (1 + |\zeta|^4|\zeta - \gamma|^2)^{-1},$$

thus allowing us to conclude that

$$I_3(v_+) \lesssim (1 + |\zeta|^2|\zeta - \gamma|)^{-1} = (1 + |\omega_l|^2|\omega_{ls}^-|)^{-1}.$$

The exact same argument can also be employed to establish that

$$I_4(v_+) \lesssim (1 + |\zeta|^2|\zeta - \gamma|)^{-1} = (1 + |\omega_l|^2|\omega_{ls}^-|)^{-1},$$

which implies $|S_1| \lesssim (1 + |\omega_l|^2|\omega_{ls}^-|)^{-1}$. This concludes the proof. □

4.4.3 Decay of the mixed second derivative of $\bar{\mathcal{G}}$ in an annulus

Lemma 4.4.1 sets the scene for the rest of the proof. In particular we exploit it to establish the first result for the mixed derivative of $\bar{\mathcal{G}}$.

Lemma 4.4.2. *If $l \in \mathcal{A}(s)$, $\tau \in \mathcal{R}(l)$, and $\lambda \in \mathcal{R}(s)$, then*

$$|D_{1\tau}D_{2\lambda}\bar{\mathcal{G}}(l,s)| \lesssim (1 + |\omega_l||\omega_s||\omega_{ls}^-|^2)^{-1}.$$

Proof. Using the same cut-off function η as in Lemma 4.4.1, we again distinguish two cases.

Case 1: $\operatorname{supp}\eta \cap \Gamma = \emptyset$**.**
We write

$$D_{1\tau}D_{2\lambda}\bar{\mathcal{G}}(l,s) = S_1 + S_2,$$

where this time

$$S_1 = \sum_{m\in\Lambda}\sum_{\rho\in\mathcal{R}} D_\rho[D_\tau\mathcal{G}^{\hom}(m-l)\eta(m)]D_{1\rho}D_{2\lambda}\bar{\mathcal{G}}(m,s)$$

and

$$S_2 = \sum_{m\in\Lambda}\sum_{\rho\in\mathcal{R}} D_\rho\eta(m)\Big[A_\rho D_\tau\mathcal{G}^{\hom}(m-l)D_{1\rho}D_{2\lambda}\bar{\mathcal{G}}(m,s) + D_\rho D_\tau\mathcal{G}^{\hom}(m-l)A_{1,\rho}D_{2\lambda}\bar{\mathcal{G}}(m,s)\Big].$$

The S_1 part can be treated similarly to before, with the key difference being that we have an extra s-derivative on terms corresponding to the predictor. We thus let $v(m) := D_\tau\mathcal{G}^{\hom}(m-l)\eta(m)$ and estimate

$$|S_1| \lesssim \sum_{i=1}^{4} J_i(v),$$

where (J_i) are defined as similarly (I_i) in (4.3.13)-(4.3.14), but with an additional derivative with respect to s, namely

$$J_1(v) = \sum_{b(m,\rho)\not\subset\Gamma} h_3^{(a)}(m)|D_\rho v(m)|, \quad J_2(v) = \sum_{b(m,\rho)\not\subset\Gamma} h_3^{(b)}(m)|D_\rho v(m)| \tag{4.4.20}$$

and

$$J_3(v) = \sum_{b(m,\rho)\subset\Gamma} h_2^{(a)}(m)|D_\rho v(m)|, \quad J_4(v) = \sum_{b(m,\rho)\subset\Gamma} h_2^{(b)}(m)|D_\rho v(m)|, \tag{4.4.21}$$

with $h_\alpha^{(a)}$ and $h_\alpha^{(b)}$ defined in (4.3.12).

Throughout we apply the same procedure as in the proof of Lemma 4.4.1, thus we omit some repetitions. We begin by recalling the decay estimate of the homogeneous Green's function $\mathcal{G}^{\text{hom}}$ given in (4.4.2) and the subsequent discussion following the definition in (4.4.5), which together imply that

$$J_1(v) \lesssim \sum_{m\in B_{c_2R}(l)} (1+|\omega_m|^5|\omega_s||\omega_{ms}^-|^2)^{-1}(1+|\omega_{ml}^-|^2|\omega_m|^2)^{-1} =: \sum_{m\in B_{c_2R}(l)} g_1(m)$$

which then leads to

$$J_1(v) \lesssim g_1(l) + g_1(s)\mathbb{1}_{B_{c_2R}(l)}(s) + \int_{D_R(l)} g_1(x)dx.$$

It is further true that

$$g_1(l) = (1+|\omega_l|^5|\omega_s||\omega_{ls}^-|^2)^{-1} \quad \text{and} \quad g_1(s)\mathbb{1}_{B_{c_2R}(l)}(s) \lesssim (1+|\omega_l||\omega_s||\omega_{ls}^-|^2)^{-1}.$$

We then consider

$$\int_{D_R(l)} g_1(x)dx = \int_{\omega(D_R(l))} \frac{|\xi|^2}{(1+|\xi|^5|\gamma||\xi-\gamma|^2)(1+|\xi-\zeta|^4)}d\xi =: \int_{\omega(D_R(l))} \tilde{g}_1(\xi)d\xi$$

and recall the regions of integration from (4.4.8). Following the same logic as in the

proof of Lemma 4.4.1, we can thus conclude that

$$\begin{aligned}\int_{\Omega_\gamma} \tilde{g}_1 d\xi &\lesssim \frac{|\zeta|^2}{1+|\zeta-\gamma|^4}\int_{\Omega_\gamma}\frac{1}{1+|\zeta|^5|\gamma||\xi-\gamma|^2}d\xi \\ &\lesssim \frac{|\zeta|^2}{1+|\zeta-\gamma|^4}\int_{\frac{1}{|\gamma|}}^{\frac{|\zeta-\gamma|}{2}}\frac{r}{1+|\zeta|^5|\gamma|r^2}dr \\ &\lesssim (1+|\zeta|^3|\gamma||\zeta-\gamma|^4)^{-1}\log|\zeta-\gamma|,\end{aligned}$$

$$\int_{\Omega_\zeta}\tilde{g}_1 d\xi \lesssim \frac{|\zeta|^2}{1+|\zeta|^5|\gamma||\zeta-\gamma|^2}\int_{\Omega_\zeta}\frac{1}{1+|\zeta-\gamma|^4}d\xi \lesssim (1+|\zeta|^3|\gamma||\zeta-\gamma|^2)^{-1}$$

and

$$\int_{\Omega'}\hat{g}_1 d\xi \lesssim \frac{1}{(1+|\zeta|^5|\gamma||\zeta-\gamma|^2)(1+|\zeta-\gamma|^4)}\int_{\Omega'}|\xi|^2 d\xi \lesssim (1+|\zeta|^3|\gamma||\zeta-\gamma|^4)^{-1}.$$

For $J_2(v)$, similarly,

$$J_2(v) \lesssim \sum_{m\in B_{c_2R}(l)}(1+|\omega_m|^3|\omega_s||\omega_{ms}^-|^4)^{-1}(1+|\omega_{ml}^-|^2|\omega_m|^2)^{-1} =: \sum_{m\in B_{c_2R}(l)} g_2(m)$$

and thus

$$J_2(v) \lesssim g_2(l) + g_2(s)\mathbb{1}_{B_{c_2R}(l)}(s) + \int_{D_R(l)} g_2(x)dx.$$

We further note that

$$g_2(l) = (1+|\omega_l|^3|\omega_s||\omega_{ls}^-|^4)^{-1} \quad \text{and} \quad g_2(s)\mathbb{1}_{B_{c_2R}(l)}(s) \lesssim (1+|\omega_l||\omega_s||\omega_{ls}^-|^2)^{-1}$$

and

$$\begin{aligned}\int_{D_R(l)} g_2(x)dx, &= \int_{\omega(D_R(l))}\frac{|\xi|^2}{(1+|\xi|^3|\gamma||\xi-\gamma|^4)(1+|\xi|^2|\xi-\zeta|^2)}d\xi \\ &=: \int_{D_R(l))}\tilde{g}_2(\xi)d\xi,\end{aligned}$$

with estimates

$$\begin{aligned}\int_{\Omega_\gamma}\tilde{g}_2 d\xi &\lesssim \frac{|\zeta|^2}{1+|\zeta|^2|\zeta-\gamma|^2}\int_{\Omega_\gamma}\frac{1}{1+|\zeta|^3|\gamma||\xi-\gamma|^4}d\xi \\ &\lesssim \frac{|\zeta|^2}{1+|\zeta|^2|\zeta-\gamma|^2}\int_{\frac{1}{|\gamma|}}^{\frac{|\zeta-\gamma|}{2}}\frac{r}{1+|\zeta|^3|\gamma|r^4}dr \lesssim (1+|\zeta|^3|\gamma||\zeta-\gamma|^2)^{-1},\end{aligned}$$

$$\int_{\Omega_\zeta} \tilde{g}_2 d\xi \lesssim \frac{|\zeta|^2}{1+|\zeta|^3|\gamma||\zeta-\gamma|^4} \int_{\Omega_\zeta} \frac{1}{1+|\zeta|^2|\xi-\zeta|^2} d\xi \lesssim (1+|\zeta|^3|\gamma||\zeta-\gamma|^4)^{-1} \log|\xi-\gamma|$$

and

$$\int_{\Omega'} \tilde{g}_2 d\xi \lesssim \frac{1}{(1+|\zeta|^3|\gamma||\zeta-\gamma|^4)(1+|\zeta|^2|\zeta-\gamma|^2)} \int_{\Omega'} |\xi|^2 d\xi \lesssim (1+|\zeta|^3|\gamma||\zeta-\gamma|^4)^{-1}.$$

This establishes that

$$|S_1| \lesssim (1+|\zeta||\gamma||\zeta-\gamma|^2)^{-1} = (1+|\omega_l||\omega_s||\omega_{ls}^-|^2)^{-1}.$$

For S_2, we note that due to variable symmetry we have $D_{2\lambda}\bar{\mathcal{G}}(m,s) = D_{1\lambda}\bar{\mathcal{G}}(s,m)$ and since $l \in \mathcal{A}$, then $m \in B_{c_2R}(l)$ is such that

$$\begin{aligned} |m| \leq |l| + c_2R \leq |l|(1+c_2(1+\sqrt{2})) \leq \frac{3}{2}(1+c_2(1+\sqrt{2}))|s| \\ \implies |s| \geq \frac{2}{3(1+c_2(1+\sqrt{2}))}|m|. \end{aligned}$$

As a result, with $c_2 = \frac{1}{6}$ we have that $s \in \Lambda \setminus \Omega_1(m)$ and the result of Lemma 4.4.1 applies, thus $D_{2\lambda}\bar{\mathcal{G}}(m,s) \lesssim |\omega_s|^{-1}|\omega_{ms}|^{-1}$. We can exploit this fact by summing the first term by parts and hence consider

$$\begin{aligned} S_2 = S_{2a} + S_{2b} := &\sum_{m\in\Lambda} -\operatorname{Div}\Big(D\eta(m) \odot AD_\tau \mathcal{G}^{\hom}(m-l)\Big) D_{2\lambda}\bar{\mathcal{G}}(m,s) \\ &+ \sum_{m\in\Lambda}\sum_{\rho\in\mathcal{R}} D_\rho\eta(m) D_\rho D_\tau \mathcal{G}^{\hom}(m-l) A_{1\rho} D_{2\lambda}\bar{\mathcal{G}}(m,s), \end{aligned}$$

where $D\eta(m) \odot AD_\tau\mathcal{G}^{\hom}(m-l) = \big(D_\rho\eta(m)A_{1\rho}D_\tau\mathcal{G}^{\hom}(m-l)\big)_{\rho\in\mathcal{R}}$.

For S_{2b} we note that since $|D\eta(m)| \lesssim R^{-1} = |\omega_l|^{-1}|\omega_{ls}^-|^{-1}$, we can estimate

$$|S_{2b}| \lesssim (1+|\omega_l||\omega_{ls}^-|)^{-1} \sum_{m\in\mathcal{A}_l} (1+|m-l|^2)^{-1}(1+|\omega_s||\omega_{ms}^-|)^{-1},$$

where again $\mathcal{A}_l = B_{c_2R}(l) \setminus B_{c_1R}(l)$. With the substitution $\xi = \omega_m$ and the identity in (4.3.1), we thus obtain

$$\begin{aligned} |S_{2b}| &\lesssim (1+|\zeta||\zeta-\gamma|)^{-1} \int_{\omega(\mathcal{A}_l)} \frac{|\xi|^2}{(1+|\gamma||\xi-\gamma|)(1+|\xi-\zeta|^2|\xi+\zeta|^2)} d\xi \\ &=: \int_{\omega(\mathcal{A}_l)} \hat{f}_1(\xi) d\xi \end{aligned}$$

We carve $\omega(\mathcal{A}_l)$ into $U_\gamma := B_{|\zeta-\gamma|/2}(\gamma) \cap \omega(\mathcal{A}_l)$ and $\omega(\mathcal{A}_l) \setminus U_\gamma$, noting that in some

cases U_γ can be empty, but it does not affect the argument.

We first note that

$$\int_{U_\gamma} \hat{f}_1 d\xi \lesssim \frac{|\zeta|^2}{(1+|\zeta|^3|\zeta-\gamma|^3)} \int_{U_\gamma} \frac{1}{1+|\gamma||\xi-\gamma|} d\xi \lesssim (1+|\zeta||\gamma||\zeta-\gamma|^2)^{-1}.$$

On the other hand, if $\xi \in \mathcal{A}_l \setminus U_\gamma$, then $|\xi-\gamma| \gtrsim |\zeta-\gamma|$. Furthermore, (4.3.1) together with how $\mathcal{A}_l$ is defined implies that

$$|\xi-\zeta||\xi+\zeta| \sim R = |\omega_l|\omega_{ls}^-| = |\zeta||\zeta-\gamma|. \tag{4.4.22}$$

Hence

$$\int_{\omega(\mathcal{A}_l)\setminus U_\gamma} \hat{f}_1 d\xi \lesssim \frac{1}{(1+|\zeta|^3|\gamma||\zeta-\gamma|^4)} \int_{\omega(\mathcal{A}_l)\setminus U_\gamma} |\xi|^2 \lesssim (1+|\zeta||\gamma||\zeta-\gamma|^2)^{-1}.$$

As a result

$$|S_{2b}| \lesssim (1+|\zeta||\gamma||\zeta-\gamma|^2)^{-1}.$$

For S_{2a}, when we apply the discrete divergence operator, we use the product rule discussed in (4.4.4) to obtain two sub-terms

$$S_{2a}^{(i)} := \sum_{m\in\Lambda} \sum_{\rho\in\mathcal{R}} D_\rho\eta(m) \left(A_\rho D_\tau \mathcal{G}^{\hom}(m-\rho-l) - A_\rho D_\tau \mathcal{G}^{\hom}(m-l) \right) D_{2\lambda}\bar{\mathcal{G}}(m,s)$$

and

$$S_{2a}^{(ii)} := \sum_{m\in\Lambda} \sum_{\rho\in\mathcal{R}} \left(D_\rho\eta(m-\rho) - D_\rho\eta(m) \right) A_\rho D_\tau \mathcal{G}^{\hom}(m-\rho-l) D_{2\lambda}\bar{\mathcal{G}}(m,s).$$

In the first one the additional derivative goes onto $D_\tau \mathcal{G}^{\hom}(m-l)$ and thus this can be estimated in the same way as S_{2b}.

For the other sub-term we have the additional derivative on the cut-off function, which leads us to exploit $|D^2\eta(m)| \lesssim R^{-2} \lesssim (1+|\omega_l|^2|\omega_{ls}^-|^2)^{-1}$. Hence

$$|S_{2a}^{(ii)}| \lesssim (1+|\omega_l|^2|\omega_{ls}^-|^2)^{-1} \sum_{m\in\mathcal{A}_l} (1+|m-l|)^{-1}(1+|\omega_s||\omega_{ms}|)^{-1}.$$

Similarly to how we argued for S_{2b}, we write

$$|S_{2a}^{(ii)}| \lesssim (1+|\zeta|^2|\zeta-\gamma|^2)^{-1}\int_{\omega(\mathcal{A}_l)} \frac{|\xi|^2}{(1+|\gamma||\xi-\gamma|)(1+|\xi-\zeta||\xi+\zeta|)}d\xi$$
$$=: \int_{\omega(\mathcal{A}_l)} \hat{f}_2(\xi,\zeta,\gamma)d\xi$$

Looking at sets U_γ and $\omega(\mathcal{A}_l)\setminus U_\gamma$ separately again, we get that

$$\int_{U_\gamma} \hat{f}_2 d\xi \lesssim \frac{|\zeta|^2}{(1+|\zeta|^3|\zeta-\gamma|^3)}\int_{U_\gamma}\frac{1}{1+|\gamma||\xi-\gamma|}d\xi \lesssim (1+|\zeta||\gamma||\zeta-\gamma|^2)^{-1},$$

whereas, again exploiting (4.4.22), we have

$$\int_{\omega(\mathcal{A}_l)\setminus U_\gamma} \hat{f}_2 d\xi \lesssim \frac{1}{(1+|\zeta|^3|\gamma||\zeta-\gamma|^4)}\int_{\omega(\mathcal{A}_l)\setminus U_\gamma}|\xi|^2 \lesssim (1+|\zeta||\gamma||\zeta-\gamma|^2)^{-1}.$$

Hence

$$|S_{2a}^{(ii)}| \lesssim (1+|\zeta||\gamma||\zeta-\gamma|^2)^{-1},$$

which concludes the result.

Case 2: $\operatorname{supp}\eta \cap \Gamma \neq \emptyset$**.**

Looking at the corresponding proof in Lemma 4.4.1, we notice that the result will follow from the same manifold $\mathcal{M}$ construction introduced in (4.4.13), as long as we correctly estimate $J_3(v_+)$ and $J_4(v_+)$, defined in (4.4.21), with a formula for v_+ given in (4.4.18). We proceed as follows.

We first note that

$$J_3(v_+) \lesssim \sum_{m\in\Gamma_l}(1+|\omega_m|^3|\omega_s||\omega_{ms}^-|^2)^{-1}(1+|\omega_{ml}^-|^2|\omega_{ml}^+|^2)^{-1} =: \sum_{m\in\Gamma_l} g_3(m)$$

and thus

$$J_3(v_+) \lesssim g_3(l)\mathbb{1}_{\Gamma_l}(l) + g_3(s)\mathbb{1}_{\Gamma_l}(s) + \int_{\tilde{\Gamma}_l} g_3(x)dx,$$

where

$$g_3(l) = (1+|\omega_l|^3|\omega_s|\omega_{ls}^-|^2)^{-1}$$

and

$$g_3(s)\mathbb{1}_{\Gamma_l}(s) = (1+|\omega_s|^2|\omega_{ls}^-|^2)^{-1} \lesssim (1+|\omega_l||\omega_s||\omega_{ls}^-|^2)^{-1}.$$

For the integral term we argue that

$$\int_{\tilde{\Gamma}_l} g_3(x)dx = \int_{\omega(\tilde{\Gamma}_l)} \frac{|\xi|}{(1+|\xi|^3|\gamma||\xi-\gamma|^2)(1+|\xi-\zeta|^2||\xi+\zeta|^2)}d\xi =: \int_{\omega(\tilde{\Gamma}_l)} \tilde{g}_3(\xi)d\xi.$$

As before we now look at regions defined in (4.4.19) and observe that

$$\int_{\Gamma_\gamma} \tilde{g}_3 d\xi \lesssim \frac{|\zeta|}{1+|\zeta|^2|\zeta-\gamma|^2} \int_{\Gamma_\gamma} \frac{1}{1+|\zeta|^3|\gamma||\xi-\gamma|^2} d\xi \lesssim (1+|\zeta|^4|\gamma||\zeta-\gamma|^2)^{-1},$$

$$\int_{\Gamma_\zeta} \tilde{g}_3 d\xi \lesssim \frac{|\zeta|}{1+|\zeta|^3|\gamma||\zeta-\gamma|^2} \int_{\Gamma_\zeta} \frac{1}{1+|\zeta|^2|\xi-\zeta|^2} d\xi \lesssim (1+|\zeta|^4|\gamma||\zeta-\gamma|^2)^{-1}$$

$$\int_{\Gamma_l'} \tilde{g}_3 d\xi \lesssim \frac{1}{(1+|\zeta|^2|\zeta-\gamma|^2)(1+|\zeta|^3|\gamma||\zeta-\gamma|^2)} \int_{\Gamma_\gamma} |\xi| d\xi \lesssim (1+|\zeta|^4|\gamma||\zeta-\gamma|^3)^{-1},$$

thus allowing us to conclude that

$$J_3(v_+) \lesssim (1+|\zeta||\omega|\zeta-\gamma|^2)^{-1} = (1+|\omega_l||\omega_s||\omega_{ls}^-|^2)^{-1}.$$

Finally, a corresponding argument can be employed to establish that

$$J_4(v_+) \lesssim (1+|\zeta||\gamma||\zeta-\gamma|^2)^{-1} = (1+|\omega_l||\omega_s||\omega_{ls}^-|^2)^{-1},$$

which implies $|S_1| \lesssim (1+|\omega_l||\omega_s||\omega_{ls}^-|^2)^{-1}$ and concludes the proof. □

4.4.4 Preliminary norm estimates for the mixed second derivative of $\bar{\mathcal{G}}$

The procedure described in Lemma 4.4.2 cannot be employed if we are too close or too far away from the origin relative to s. It turns out, however, that for $l \in \Omega_1(s) \cup \Omega_2(s)$ one can obtain a preliminary result in the form of norm estimates.

Lemma 4.4.3. *For any s with $|s|$ large enough and $\tau \in \mathcal{R}(s)$, the function $\bar{g}(m,s) := D_{2\tau}\bar{\mathcal{G}}(m,s)$ satisfies*

$$\|D_1\bar{g}(\cdot,s)\|_{\ell^2(\Omega_1(s))} \lesssim |\omega_s|^{-2} \quad \textit{and} \quad \|D_1\bar{g}(\cdot,s)\|_{\ell^2(\Omega_2(s))} \lesssim |\omega_s|^{-2}.$$

Proof. We begin by noting that the equation that $\bar{g}$ satisfies is

$$H\bar{g}(m,s) = -H\hat{g}(m,s) \quad \text{for } m \in \Omega_1(s) \cup \Omega_2(s)$$

where $\hat{g}(m,s) := D_{2\tau}\hat{\mathcal{G}}(m,s)$. This point-wise equation is obtained from (4.3.15)

after testing with $v(l) = \delta_{lm}$ (the Kronecker delta) and noting that inside $\Omega_i(s)$ we are away from s.

We multiply both sides by $\bar{g}(\cdot, s)\eta_1^2$ or $\bar{g}(\cdot, s)\eta_2^2$ and sum over m. The cut-off function η_i is defined to be identically 1 inside $\Omega_i(s)$ and to go smoothly and monotonically to zero over an annulus of radius $c_3|s|$ where the choice of c_3 ensures that $\operatorname{dist}(\operatorname{supp}\eta_i, s) \sim |s|$. A particular choice of η_1 and η_2 that works is as follows: $\eta_1(m) = 1$ for $m \in B_{5|s|/8}(0)$ and $\eta_1(m) = 0$ for $m \in \Lambda \setminus B_{6|s|/8}(0)$. Similarly, $\eta_2(m) = 1$ for $m \in \Lambda \setminus B_{11|s|/8}(0)$ and $\eta_2(m) = 0$ for $m \in B_{10|s|/8}(0)$. Thus $c_3 = \frac{1}{8}$ and the aforementioned annuli are still at least $\frac{|s|}{4}$ away from s.

Note that as a result we have $|D^j\eta_i| \lesssim |s|^{-j} = |\omega_s|^{-2j}$ and also that it is non-zero only in the region where the result from Lemma 4.4.2 can be applied. It can be essentially thought of as imposing a boundary condition on a discrete variant of the Poisson equation on $\Omega_i(s)$. Following summation by parts on the left-hand side we get

$$\sum_{m\in\Lambda} D_1\bar{g}(m,s)\cdot D_1[\bar{g}(m,s)\eta_i^2(m)] = -\sum_{m\in\Lambda}\left(H\hat{g}(m,s)\right)\bar{g}(m,s)\eta_i^2(m). \tag{4.4.23}$$

Furthermore, we can rewrite the left-hand side of (4.4.23) due to the discrete product rule identities discussed in (4.4.4) which establish that any two $f, g : \Lambda \to \mathbb{R}$ satisfy

$$\begin{aligned} D_\rho[fg](m) &= f(m+\rho)D_\rho g(m) + f(m)D_\rho g(m) \\ &= g(m+\rho)D_\rho f(m) + g(m)D_\rho f(m), \end{aligned}$$

which implies that (suppressing the s-dependence of $\bar{g}$ and i-dependence of η in notation for brevity)

$$\begin{aligned} D_\rho\bar{g}(m)\cdot D_\rho[(\bar{g}\eta)\eta](m) =& D_\rho\bar{g}(m)\cdot[\bar{g}(m+\rho)\eta(m+\rho)D_\rho\eta(m) + \eta(m)D_\rho[\bar{g}\eta](m)] \\ =& D_\rho\bar{g}(m)D_\rho\eta(m)\bar{g}(m+\rho)\eta(m+\rho) \\ &+ D_\rho\bar{g}(m)^2\eta(m)\eta(m+\rho) + D_\rho\bar{g}(m)\eta(m)\bar{g}(m)D_\rho\eta(m). \end{aligned}$$

A similar calculation reveals that

$$D[\bar{g}\eta](m)\cdot D[\bar{g}\eta](m) = D_\rho\bar{g}(m)\cdot D_\rho[(\bar{g}\eta)\eta](m) + D_\rho\eta(m)^2\bar{g}(m+\rho)\bar{g}(m),$$

which allows us to rewrite (4.4.23) as

$$\|D_1[\bar{g}(\cdot,s)\eta_i]\|_{\ell^2}^2 = -\sum_{m\in\Lambda}\left(H\hat{g}(m,s)\right)\bar{g}(m,s)\eta_i^2(m) + \sum_{m\in\Lambda}\sum_{\rho\in\mathcal{R}}\left(D_\rho\eta_i(m)\right)^2\bar{g}(m,s)\bar{g}(m+\rho,s) \tag{4.4.24}$$

and subsequently we hope to estimate the right-hand side, in particular noting that $|\bar{g}(m+\rho,s)| \sim |\bar{g}(m,s)|$ inside $\operatorname{supp}\eta_1 \cup \operatorname{supp}\eta_2$.

We first deal with terms that are not on the crack surface. For $m \notin \Gamma$ we know that H coincides with the homogeneous Hessian operator $\tilde{H}$ defined in (4.4.1), thus a Taylor expansion of

$$H\hat{g}(m,s) = \sum_{\rho\in\mathcal{R}} D_{1\rho}\hat{g}(m-\rho,s) - D_{1\rho}\hat{g}(m,s)$$

up to fourth order, as calculated explicitly in the proof of [19, Theorem 5.6], together with the fact that $\hat{\mathcal{G}}(,\cdot,s)$ solves the Laplace equation away from s we can conclude that

$$|H\hat{g}(m,s)| \lesssim \|\nabla_m^4\nabla_s\hat{G}(\cdot,s)\|_{L^\infty(B_{1/2}(m))}.$$

Hence, bearing in mind (4.3.12),

$$|H\hat{g}(m,s)| \lesssim h_4^{(a)}(m,s) + h_4^{(b)}(m,s).$$

If, on the other hand, $m \in \Gamma$, then a careful examination of terms in $H\hat{g}(m)$ reveals that

$$H\hat{g}(m,s) = 2\sum_{\rho\in\mathcal{R}(m)} D_{1\rho}\hat{g}(m,s).$$

Applying a Taylor expansion, this implies

$$\begin{aligned}|H\hat{g}(m,s)| &\lesssim \left|\sum_{\rho\in\mathcal{R}(m)}\left(2\nabla_m\bar{g}(m,s)\cdot\rho + \nabla_m^2\hat{g}(m,s)[\rho,\rho] + \frac{1}{3}\nabla_m^3\bar{g}(m,s)[\rho,\rho,\rho]\right)\right| \\ &\quad + \|\nabla_m^4\nabla_s\hat{G}(\cdot,s)\|_{L^\infty(B_{1/2}(m))} \\ &\lesssim \|\nabla_m\bar{g}(m,s)\cdot e_2\|_{L^\infty(B_{1/2}(m))} + \|\nabla_m^4\nabla_s\hat{G}(\cdot,s)\|_{L^\infty(B_{1/2}(m))},\end{aligned} \tag{4.4.25}$$

where the final line follows from the fact that

$$m \in \Gamma_\pm \implies \sum_{\rho\in\mathcal{R}(m)} 2\nabla_m\bar{g}(m,s)\cdot\rho = \pm 2\nabla_m\bar{g}(m,s)\cdot e_2,$$

$$m \in \Gamma_\pm \implies \sum_{\rho \in \mathcal{R}(m)} \nabla_m^2 \bar{g}(m,s)[\rho,\rho] = 2\Delta_m \bar{g}(m,s) - \nabla_m^2 \bar{g}(m,s)[\pm e_2, \pm e_2]$$
$$= -\nabla_m^2 \bar{g}(m,s)[\pm e_2, \pm e_2],$$

since $\bar{g}(m,s)$ solve the Laplace equation away from s. Finally,

$$m \in \Gamma_\pm \implies \sum_{\rho \in \mathcal{R}(m)} \nabla_m^3 \bar{g}(m,s)[\rho,\rho,\rho] = \pm\frac{1}{3}\nabla_m^3 \bar{g}(m,s)[\pm e_2, \pm e_2, \pm e_2].$$

The second term in 4.4.25 can be estimated as in (4.3.12). For the first term, using the boundary condition in (4.3.6), we can Taylor-expand this around $m_0 \in \Gamma$ vertically aligned with m, allowing us to gain one extra derivative. As a result

$$\|\nabla_m \bar{g}(m,s) \cdot e_2\|_{L^\infty(B_{1/2}(m))} \lesssim h_2^{(a)}(m) + h_2^{(b)}(m).$$

For $i = 1$ we note that in the first term on the right-hand side of (4.4.24) we only sum over $m \in B_{\frac{3|s|}{4}}(0)$, thus Lemma 4.4.1 ensures that $\bar{g}(m,s) \lesssim |\omega_s|^{-1}|\omega_{ms}^-|^{-1}$. Furthermore, recalling (4.3.1), we can rewrite $|\omega_{ms}^-| = |m-s||\omega_{ms}^+|^{-1}$ and exploit the fact in the region of interest $|m-s| \gtrsim |s| = |\omega_s|^2$ and $|\omega_{ms}^+| \leq |\omega_m| + |\omega_s| \lesssim |\omega_s|$. Finally, we note that due to placing the defect core at the origin, we always have $m \in \Lambda \implies |m| > 1/\sqrt{2}$. Thus we can estimate

$$\sum_{m \in B_{\frac{3|s|}{4}}(0)} h_4^{(a)}(m,s)|\bar{g}(m,s)| \lesssim \sum_{m \in B_{\frac{3|s|}{4}}(0)} (1 + |\omega_m|^7 |\omega_s||\omega_{ms}^-|^2)^{-1}(1 + |\omega_{ms}^-|\omega_s|)^{-1}$$
$$\lesssim |\omega_s|^{-5} \sum_{m \in \Lambda} |\omega_m|^{-7} \lesssim |\omega_s|^{-5}, \tag{4.4.26}$$

$$\sum_{m \in B_{\frac{3|s|}{4}}(0)} h_4^{(b)}(m,s)|\bar{g}(m,s)| \lesssim \sum_{m \in B_{\frac{3|s|}{4}}(0)} (1 + |\omega_m|^4 |\omega_s||\omega_{ms}^-|^5)^{-1}(1 + |\omega_{ms}^-||\omega_s|)^{-1}$$
$$\lesssim |\omega_s|^{-8} \sum_{m \in B_{\frac{3|s|}{4}}(0)} |\omega_m|^{-4} \lesssim |\omega_s|^{-8} \log|\omega_s|, \tag{4.4.27}$$

$$\sum_{m\in B_{\frac{3|s|}{4}}(0)\cap\Gamma} h_2^{(a)}(m,s)|\bar{g}(m,s)| \tag{4.4.28}$$
$$\lesssim \sum_{m\in B_{\frac{3|s|}{4}}(0)\cap\Gamma} (1+|\omega_m|^3|\omega_s||\omega_{ms}^-|^2)^{-1}(1+|\omega_{ms}^-||\omega_s|)^{-1}$$
$$\lesssim |\omega_s|^{-5}\sum_{m\in B_{\frac{3|s|}{4}}(0)\cap\Gamma} |\omega_m|^{-3} \lesssim |\omega_s|^{-5},$$

$$\sum_{m\in B_{\frac{3|s|}{4}}(0)\cap\Gamma} h_2^{(b)}(m,s)|\bar{g}(m,s)| \tag{4.4.29}$$
$$\lesssim \sum_{m\in B_{\frac{3|s|}{4}}(0)\cap\Gamma} (1+|\omega_m|^2|\omega_s||\omega_{ms}^-|^3)^{-1}(1+|\omega_{ms}^-||\omega_s|)^{-1}$$
$$\lesssim |\omega_s|^{-6}\sum_{m\in B_{\frac{3|s|}{4}}(0)\cap\Gamma} |\omega_m|^{-2} \lesssim |\omega_s|^{-6}\log|\omega_s|.$$

Similarly, for the boundary term we note that if $i=1$ then we only sum over $m\in B_{\frac{3|s|}{4}}(0)\setminus B_{\frac{5|s|}{8}}(0)$ and we can estimate

$$\sum_{m\in\Lambda}\sum_{\rho\in\mathcal{R}(m)} (D_\rho\eta_i(m)\bar{g}(m,s))^2 \lesssim |\omega_s|^{-8}\sum_{m\in B_{\frac{3|s|}{4}}(0)\setminus B_{\frac{5|s|}{8}}(0)} 1 \lesssim |\omega_s|^{-4}. \tag{4.4.30}$$

For $i=2$ the estimate of boundary term in (4.4.30) still holds with the only difference being that we now sum over $m\in B_{\frac{11|s|}{8}}(0)\setminus B_{\frac{5|s|}{4}}(0)$. On the other hand, as now we sum over $m\in\Lambda\setminus B_{\frac{5|s|}{4}}(0)$, the result of Lemma 4.4.1 does not apply to $\bar{g}(m,s)$. However, we can reproduce the proof of Lemma 4.4.1 using a cut-off function η, as introduced at the beginning of Section 4.4, with $R=|s|$ and $c_1=\frac{1}{2}$ and $c_2=\frac{3}{4}$. One can readily check that the argument for S_1 remains unaffected, whereas the for S_2 a general result for this type of argument is that $|S_2|\lesssim R^{-1}$ and in this case $R^{-1}=|s|^{-1}=|\omega_s|^{-2}$. Thus we obtain

$$|\bar{g}(m,s)| = |D_{1\tau}\bar{\mathcal{G}}(s,m)| \lesssim (1+|\omega_s||\omega_{ms}^-|+|\omega_s|^2)^{-1} \lesssim (1+|\omega_s|^2)^{-1},$$

since $|\omega_{ms}^-| = |m-s||\omega_{ms}^+| \gtrsim |m||(|\omega_m|+|\omega_s|)^{-1} \gtrsim |\omega_m| \gtrsim |\omega_s|$, as in the region of interest $|m|$ $(=|\omega_m|^2)$ and $|m-s|$ are comparable and $|m-s|\gtrsim|s|$.

Thus we can estimate

$$\sum_{m\in\Lambda\setminus B_{\frac{5|s|}{4}}(0)} \left(h_4^{(a)}(m,s)\right)|\bar{g}(m,s)| \tag{4.4.31}$$

$$\lesssim \sum_{m\in\Lambda\setminus B_{\frac{5|s|}{4}}(0)} (1+|\omega_m|^7|\omega_s|^1|\omega_{ms}^-|^2)^{-1}(1+|\omega_s|^2)^{-1}$$

$$\lesssim |\omega_s|^{-5}\sum_{m\in\Lambda\setminus B_{\frac{5|s|}{4}}(0)} |\omega_m|^{-7} \lesssim |\omega_s|^{-5}\int_{\frac{5|s|}{4}}^{\infty} r^{-7/2}rdr \lesssim |\omega_s|^{-8}.$$

Analogous calculations result in

$$\sum_{m\in\Lambda\setminus B_{\frac{5|s|}{4}}(0)} \left(h_4^{(b)}(m,s)\right)|\bar{g}(m,s)| \lesssim |\omega_s|^{-8}, \tag{4.4.32}$$

$$\sum_{m\in\Lambda\setminus B_{\frac{5|s|}{4}}(0)\cap\Gamma} \left(h_2^{(a)}(m,s)\right)|\bar{g}(m,s)| \lesssim |\omega_s|^{-6}, \tag{4.4.33}$$

$$\sum_{m\in\Lambda\setminus B_{\frac{5|s|}{4}}(0)\cap\Gamma} \left(h_2^{(b)}(m,s)\right)|\bar{g}(m,s)| \lesssim |\omega_s|^{-6}. \tag{4.4.34}$$

Since the particular choice of the cut-off functions specified at the start of the proof implies that

$$\Omega_i(s) \subset \{m\in\Lambda :\ \eta_i(m)=1\},$$

we have thus established that

$$\|D\bar{g}(\cdot,s)\|_{\ell^2(\Omega_i(s))} \leq \|D[\bar{g}(\cdot,s)\eta_i]\|_{\ell^2} \lesssim |\omega_s|^{-2}.$$

□

4.4.5 Improving norm estimates for mixed second derivative of $\bar{\mathcal{G}}$ through bootstrapping

Arguments in Sections 4.4.2-4.4.4 together provide the preliminary suboptimal estimates of $\bar{\mathcal{G}}$ over the whole space. Together with Lemma 4.3.2, they make $\mathcal{G}=\hat{\mathcal{G}}+\bar{\mathcal{G}}$ a partially-functioning technical tool for estimating the decay of discrete functions defined on $\dot{\mathcal{H}}^1$ in a crack geometry. In particular, we can use it to improve the decay estimates of $\bar{\mathcal{G}}$ to get better norm estimates over Ω_i.

By looking at the estimates (4.4.26)-(4.4.34), it is evident that we can improve these sub-optimal norm estimates as long as we are able to get a better rate in

(4.4.30), with the summation over an annulus near the boundary of $\Omega_1(s)$, namely for $m \in B_{\frac{3|s|}{4}}(0) \setminus B_{\frac{5|s|}{8}}(0)$ and likewise over an annulus near the boundary of $\Omega_2(s)$, namely for $m \in B_{\frac{11|s|}{8}}(0) \setminus B_{\frac{5|s|}{4}}(0)$. This is possible if, instead of using a cut-off function and the homogeneous lattice Green's function $\mathcal{G}^{\text{hom}}$, we employ $\mathcal{G}$.

Lemma 4.4.4. *Let $\tilde{s} \in \Lambda$ be such that $|\tilde{s}|$ is large enough. If $m \in \Lambda$ is such that $m \in B_{\frac{3|\tilde{s}|}{4}}(0) \setminus B_{\frac{5|\tilde{s}|}{8}}(0)$ or $m \in B_{\frac{11|\tilde{s}|}{8}}(0) \setminus B_{\frac{5|\tilde{s}|}{4}}(0)$, then*

$$|\bar{g}(m, \tilde{s})| \lesssim |\omega(\tilde{s})|^{-3},$$

where $\bar{g}(m, \tilde{s}) = D_{2\tau}\bar{\mathcal{G}}(m, \tilde{s})$.

Proof. Since $\bar{g}(m, \tilde{s}) = D_{1\tau}\bar{\mathcal{G}}(\tilde{s}, m)$, we change the notation to keep it in line with previous proofs by letting $l = \tilde{s}$ and $m = s$. Consequently we will in fact estimate $D_{1\tau}\bar{\mathcal{G}}(l, s)$ for $l \in B_{\frac{8|s|}{5}}(0) \setminus B_{\frac{4|s|}{3}}(0)$ and $l \in B_{\frac{4|s|}{5}}(0) \setminus B_{\frac{8|s|}{11}}(0)$ with the hope that we can conclude that $D_{1\tau}\bar{\mathcal{G}}(l, s) \lesssim |\omega_l|^{-3}$. With $\mathcal{G}$ and its suboptimal decay established, we can write

$$D_{1\tau}\bar{\mathcal{G}}(l, s) = \sum_{m \in \Lambda} \left(H D_{2\tau}\mathcal{G}(m, l)\right) \bar{\mathcal{G}}(m, s) = \sum_{m \in \Lambda} D_1\bar{\mathcal{G}}(m, s) \cdot D_1 g(m, l),$$

where $g = \hat{g} + \bar{g}$ defined in the proof of Lemma 4.4.3. Noting that both $\hat{g}, \bar{g} \in \dot{\mathcal{H}}^1$, we exploit the fact that $\bar{\mathcal{G}}$ satisfies (4.3.15) and, similarly to the strategy employed in the proof of Lemma 4.4.1, we conclude that

$$|D_{1\tau}\bar{\mathcal{G}}(l, s)| \lesssim \sum_{i=1}^{4} I_i(\hat{g}) + I_i(\bar{g}), \tag{4.4.35}$$

where the terms are as in (4.3.13)-(4.3.14). Recalling that Lemma 4.3.2 establishes that $|D_{1\rho}\hat{g}(m, l)| = |D_{1\rho}D_{2\tau}\hat{\mathcal{G}}(m, l)| \lesssim (1 + |\omega_m||\omega_l||\omega^-_{ml}|^2)^{-1}$ and noting the fact that in the region of interest $|l - s|$, $|l|$, and $|s|$ are all comparable, we can directly estimate four summands corresponding to this term arguing as in the proof of Lemma 4.4.1.

We begin by writing

$$I_1(\hat{g}) \lesssim \sum_{m \in \Lambda} (1 + |\omega_m|^5 |\omega^-_{ms}|)^{-1} (1 + |\omega_m||\omega_l||\omega^-_{ml}|^2)^{-1} =: \sum_{m \in \Lambda} h_1(m).$$

We first observe that

$$\sum_{m \in \Lambda} h_1(m) \lesssim h_1(l) + h_1(s) + \int_D \tilde{h}_1(\xi) d\xi,$$

where

$$\tilde{h}_1(\xi) := \frac{|\xi|^2}{(1+|\xi|^5|\xi-\gamma|)(1+|\xi||\zeta||\xi-\zeta|^2)}$$

and

$$D := \mathbb{R}^2_+ \setminus (B_{\epsilon_*}(0) \cup B_{\frac{1}{|\zeta|}}(\zeta) \cup B_{\frac{1}{\gamma}}(\gamma)),$$

with $\epsilon_* = \sqrt{1/\sqrt{2}}$. The fact that we exclude balls of radii $\frac{1}{|\zeta|}$ and $\frac{1}{|\gamma|}$ is as in (4.4.8). It is clear to see that

$$\begin{aligned} h_1(l) &= (1+|\omega_l|^5|\omega_{ls}^-|)^{-1} \lesssim |\omega_l|^{-6}, \\ h_1(s) &= (1+|\omega_s||\omega_l||\omega_{ls}^-|^2)^{-1} \lesssim |\omega_l|^{-4} \end{aligned}$$

and away from the spikes we would like to estimate the integral term separately for regions close to the origin, γ and ζ separately.

To this end, we define radii

$$R_0 := \min\{|\gamma|, |\zeta|\}, \tag{4.4.36a}$$

$$R_\gamma := \min\{|\gamma|, |\gamma-\zeta|\}, \tag{4.4.36b}$$

$$R_\zeta := \min\{|\zeta|, |\zeta-\gamma|\}, \tag{4.4.36c}$$

$$R_1 := \max\{|\zeta|, |\gamma|\} + \frac{\max\{R_\zeta, R_\gamma\}}{2} \tag{4.4.36d}$$

and look at

$$\Omega_0 := (D \cap B_{\frac{R_0}{2}}(0)), \tag{4.4.37a}$$

$$\Omega_\gamma := (D \cap B_{\frac{R_\gamma}{2}}(\gamma)), \tag{4.4.37b}$$

$$\Omega_\zeta := (D \cap B_{\frac{R_\zeta}{2}}(\zeta)), \tag{4.4.37c}$$

$$\Omega_1 := (D \cap B_{R_1}(0)) \setminus (\Omega_0 \cup \Omega_\gamma \cup \Omega_\zeta), \tag{4.4.37d}$$

$$\Omega' := (D \setminus B_{R_1}(0)). \tag{4.4.37e}$$

Exploiting the spatial properties of each of these sets and that $|\gamma|, |\zeta|$ and $|\gamma-\zeta|$ are

all comparable, we can conclude that

$$\int_{\Omega_0} \tilde{h}_1 d\xi \lesssim \int_{\Omega_0} \frac{|\xi|^2}{1+|\xi|^6|\gamma|^4} d\xi \lesssim |\gamma|^{-4} \int_{\epsilon_*}^{\frac{R_0}{2}} \frac{1}{r^3} dr \lesssim |\zeta|^{-4},$$

$$\int_{\Omega_\gamma} \tilde{h}_1 d\xi \lesssim |\gamma|^{-2} \int_{\Omega_\gamma} \frac{1}{1+|\gamma|^5|\xi-\gamma|} d\xi \lesssim |\gamma|^{-2} \int_{\frac{1}{|\gamma|}}^{\frac{R_\gamma}{2}} \frac{r}{1+|\gamma|^5 r} dr \lesssim |\gamma|^{-7} R_\gamma \lesssim |\zeta|^{-6},$$

$$\begin{aligned}\int_{\Omega_\zeta} \tilde{h}_1 d\xi &\lesssim |\gamma|^{-4} \int_{\Omega_\zeta} \frac{1}{1+|\gamma|^2|\xi-\zeta|^2} d\xi \lesssim |\gamma|^{-4} \int_{\frac{1}{|\zeta|}}^{\frac{R_\zeta}{2}} \frac{r}{1+|\gamma|^2 r^2} dr \\ &\lesssim |\gamma|^{-6} \log(R_\zeta) \lesssim |\zeta|^{-6} \log|\zeta|,\end{aligned}$$

$$\int_{\Omega_1} \tilde{h}_1 d\xi \lesssim |\gamma|^{-4} \int_{\Omega_1} |\xi|^{-4} d\xi \lesssim |\gamma|^{-4} \int_{\frac{R_0}{2}}^{R_1} \frac{1}{r^3} dr \lesssim |\zeta|^{-6},$$

$$\int_{\Omega'} \tilde{h}_1 d\xi \lesssim |\gamma|^{-4} \int_{\Omega'} |\xi|^{-4} d\xi \lesssim |\gamma|^{-4} \int_{R_1}^{\infty} \frac{1}{r^3} dr \lesssim |\zeta|^{-6}.$$

Likewise for the second term we begin by saying

$$I_2(\hat{g}) \lesssim \sum_{m\in\Lambda} (1+|\omega_m|^3|\omega_{ms}^-|^3)^{-1}(1+|\omega_m||\omega_l||\omega_{ml}^-|^2)^{-1} =: \sum_{m\in\Lambda} h_2(m)$$

and

$$\sum_{m\in\Lambda} h_2(m) \lesssim h_2(l) + h_2(s) + \int_D \tilde{h}_2 d\xi,$$

where

$$\tilde{h}_2(\xi) := \frac{|\xi|^2}{(1+|\xi|^3|\xi-\gamma|^3)(1+|\xi||\zeta||\xi-\zeta|^2)}.$$

It is clear that

$$\begin{aligned} h_2(l) &= (1+|\omega_l|^3|\omega_{ls}^-|^3)^{-1} \lesssim |\omega_l|^{-6}, \\ h_2(s) &= (1+|\omega_s||\omega_l||\omega_{ls}^-|^2)^{-1} \lesssim |\omega_l|^{-4} \end{aligned}$$

and for the integral term we look at regions defined in (4.4.37) again to obtain

$$\begin{aligned}
&\int_{\Omega_0} \tilde{h}_2 d\xi \lesssim \int_{\Omega_0} \frac{|\xi|^2}{1+|\xi|^4|\gamma|^6} d\xi \lesssim |\gamma|^{-6} \int_{\epsilon_*}^{\frac{R_0}{2}} \frac{1}{r} dr \lesssim |\zeta|^{-6} \log|\zeta|,\\
&\int_{\Omega_\gamma} \tilde{h}_2 d\xi \lesssim |\gamma|^{-2} \int_{\Omega_\gamma} \frac{1}{1+|\gamma|^3|\xi-\gamma|^3} d\xi \lesssim |\gamma|^{-2} \int_{\frac{1}{|\gamma|}}^{\frac{R_\gamma}{2}} \frac{r}{1+|\gamma|^3 r^3} dr \lesssim |\zeta|^{-4}\\
&\int_{\Omega_\zeta} \tilde{h}_2 d\xi \lesssim |\gamma|^{-4} \int_{\Omega_\gamma} \frac{1}{1+|\gamma|^2|\xi-\zeta|^2} d\xi \lesssim |\gamma|^{-4} \int_{\frac{1}{|\zeta|}}^{\frac{R_\zeta}{2}} \frac{r}{1+|\gamma|^2 r^2} dr\\
&\qquad\qquad \lesssim |\gamma|^{-6} \log(R_\zeta) \lesssim |\zeta|^{-6} \log|\zeta|,\\
&\int_{\Omega_1} \tilde{h}_2 d\xi \lesssim |\gamma|^{-6} \int_{\Omega_1} |\xi|^{-2} d\xi \lesssim |\gamma|^{-6} \int_{\frac{R_0}{2}}^{R_1} \frac{1}{r} dr \lesssim |\zeta|^{-6} \log|\zeta|,\\
&\int_{\Omega'} \tilde{h}_2 d\xi \lesssim |\gamma|^{-1} \int_{\Omega'} |\xi|^{-7} d\xi \lesssim |\gamma|^{-1} \int_{R_1}^{\infty} \frac{1}{r^6} dr \lesssim |\zeta|^{-6}.
\end{aligned}$$

The same strategy applies to the boundary terms, as we can write

$$I_3(\hat{g}) \lesssim \sum_{m\in\Gamma} (1+|\omega_m|^3|\omega_{ms}^-|^1)^{-1}(1+|\omega_m||\omega_l||\omega_{ml}^-|^2)^{-1} =: \sum_{m\in\Gamma} h_3(m),$$

and

$$\sum_{m\in\Lambda} h_3(m) \lesssim h_3(l)\mathbb{1}_\Gamma(l) + h_3(s)\mathbb{1}_\Gamma(s) + \int_D \tilde{h}_3 d\xi,$$

where

$$\tilde{h}_3(\xi) := \frac{|\xi|}{(1+|\xi|^3|\xi-\gamma|)(1+|\xi||\zeta||\xi-\zeta|^2)}.$$

It is clear that

$$\begin{aligned}
h_3(l) &= (1+|\omega_l|^3|\omega_{ls}^-|)^{-1} \lesssim |\omega_l|^{-4},\\
h_3(s) &= (1+|\omega_s||\omega_l||\omega_{ls}^-|^2)^{-1} \lesssim |\omega_l|^{-4}
\end{aligned}$$

and also

$$\int_{\Omega_0\cap\omega(\Gamma)}\tilde{h}_3d\xi\lesssim\int_{\Omega_0\cap\omega(\Gamma)}\frac{|\xi|}{1+|\xi|^4|\gamma|^4}d\xi\lesssim|\gamma|^{-4}\int_{\epsilon_*}^{\frac{R_0}{2}}\frac{1}{r^3}dr\lesssim|\zeta|^{-4},$$

$$\begin{aligned}\int_{\Omega_\gamma\cap\omega(\Gamma)}\tilde{h}_3d\xi&\lesssim|\gamma|^{-3}\int_{\Omega_\gamma\cap\omega(\Gamma)}\frac{1}{1+|\gamma|^3|\xi-\gamma|}d\xi\lesssim|\gamma|^{-3}\int_{\frac{1}{|\gamma|}}^{\frac{R_\gamma}{2}}\frac{1}{|\gamma|^3r}dr\\&\lesssim|\zeta|^{-6}\log R_\gamma\lesssim|\zeta|^{-6}\log|\zeta|,\end{aligned}$$

$$\int_{\Omega_\zeta\cap\omega(\Gamma)}\tilde{h}_3d\xi\lesssim|\gamma|^{-3}\int_{\Omega_\zeta\cap\omega(\Gamma)}\frac{1}{1+|\gamma|^2|\xi-\zeta|^2}d\xi\lesssim|\gamma|^{-3}\int_{\frac{1}{|\zeta|}}^{\frac{R_\zeta}{2}}\frac{1}{|\gamma|^2r^2}dr\lesssim|\zeta|^{-4},$$

$$\int_{\Omega_1\cap\omega(\Gamma)}\tilde{h}_3d\xi\lesssim|\gamma|^{-4}\int_{\Omega_1\cap\omega(\Gamma)}|\xi|^{-3}d\xi\lesssim|\gamma|^{-4}\int_{\frac{R_0}{2}}^{R_1}\frac{1}{r^3}dr\lesssim|\zeta|^{-6},$$

$$\int_{\Omega'\cap\omega(\Gamma)}\tilde{h}_3d\xi\lesssim|\gamma|^{-4}\int_{\Omega'\cap\omega(\Gamma)}|\xi|^{-3}d\xi\lesssim|\gamma|^{-4}\int_{R_1}^{\infty}\frac{1}{r^3}dr\lesssim|\zeta|^{-6}.$$

Finally,

$$I_4(\hat{g})\lesssim\sum_{m\in\Gamma}(1+|\omega_m|^2|\omega_{ms}^-|^2)^{-2}(1+|\omega_m||\omega_l||\omega_{ml}^-|^2)^{-1}=:\sum_{m\in\Gamma}h_4(m),$$

and

$$\sum_{m\in\Lambda}h_4(m)\lesssim h_4(l)\mathbb{1}_\Gamma(l)+h_4(s)\mathbb{1}_\Gamma(s)+\int_D\tilde{h}_4d\xi,$$

where

$$\tilde{h}_4(\xi):=\frac{|\xi|}{(1+|\xi|^2|\xi-\gamma|^2)(1+|\xi||\zeta||\xi-\zeta|^2)}.$$

It is clear that

$$\begin{aligned}h_4(l)&=(1+|\omega_l|^2|\omega_{ls}^-|^2)^{-1}\lesssim|\omega_l|^{-4},\\h_4(s)&=(1+|\omega_s||\omega_l||\omega_{ls}^-|^2)^{-1}\lesssim|\omega_l|^{-4}\end{aligned}$$

and also

$$\int_{\Omega_0\cap\omega(\Gamma)}\tilde{h}_4 d\xi \lesssim \int_{\Omega_0\cap\omega(\Gamma)}\frac{|\xi|}{1+|\xi|^3|\gamma|^5}d\xi \lesssim |\gamma|^{-5}\int_{\epsilon_*}^{\frac{R_0}{2}}\frac{1}{r^2}dr \lesssim |\zeta|^{-5},$$
$$\int_{\Omega_\gamma\cap\omega(\Gamma)}\tilde{h}_4 d\xi \lesssim |\gamma|^{-3}\int_{\Omega_\gamma\cap\omega(\Gamma)}\frac{1}{1+|\gamma|^2|\xi-\gamma|^2}d\xi \lesssim |\gamma|^{-3}\int_{\frac{1}{|\gamma|}}^{\frac{R_\gamma}{2}}\frac{1}{|\gamma|^2r^2}dr \lesssim |\zeta|^{-4},$$
$$\int_{\Omega_\zeta\cap\omega(\Gamma)}\tilde{h}_4 d\xi \lesssim |\gamma|^{-3}\int_{\Omega_\zeta\cap\omega(\Gamma)}\frac{1}{1+|\gamma|^2|\xi-\zeta|^2}d\xi \lesssim |\gamma|^{-3}\int_{\frac{1}{|\zeta|}}^{\frac{R_\zeta}{2}}\frac{1}{|\gamma|^2r^2}dr \lesssim |\zeta|^{-4},$$
$$\int_{\Omega_1\cap\omega(\Gamma)}\tilde{h}_4 d\xi \lesssim |\gamma|^{-5}\int_{\Omega_1\cap\omega(\Gamma)}|\xi|^{-2}d\xi \lesssim |\gamma|^{-5}\int_{\frac{R_0}{2}}^{R_1}\frac{1}{r^2}dr \lesssim |\zeta|^{-6},$$
$$\int_{\Omega'\cap\omega(\Gamma)}\tilde{h}_4 d\xi \lesssim |\gamma|^{-5}\int_{\Omega'\cap\omega(\Gamma)}|\xi|^{-2}d\xi \lesssim |\gamma|^{-5}\int_{R_1}^{\infty}\frac{1}{r^2}dr \lesssim |\zeta|^{-6}.$$

Since in each estimate we get at least $|\zeta|^{-4} = |\omega_l|^{-4}$, we can conclude that

$$\sum_{i=1}^{4} I_i(\hat{g}) \lesssim |\omega_l|^{-4}.$$

For the other four terms on the right-hand side of (4.4.35), in light of Lemma 4.4.3, we look separately at the summation over $\Omega_1(l)$, $\Omega_2(l)$ and $\mathcal{A}(l)$. The first two we investigate in detail, but for the sum over $\mathcal{A}(l)$, we simply note that in there we have a point-wise estimate $D_{1\rho}\bar{g}(m,l) \lesssim (1+|\omega_m||\omega_l||\omega_{ml}^-|^2)^{-1}$, as established in Lemma 4.4.2, so the above estimates translate verbatim and we get

$$\sum_{i=1}^{4} I_i(\bar{g}, \mathcal{A}(l)) \lesssim |\omega_l|^{-4},$$

where

$$I_1(v,\mathcal{A}(l)) := \sum_{\substack{b(m,\rho)\not\subset\Gamma \\ m\in\mathcal{A}(l)}} g_3^{(a)}(m)|D_\rho v(m)|, \quad I_2(v,\mathcal{A}(l)) := \sum_{\substack{b(m,\rho)\not\subset\Gamma \\ m\in\mathcal{A}(l)}} g_3^{(b)}(m)|D_\rho v(m)| \tag{4.4.38}$$

and

$$I_3(v,\mathcal{A}(l)) := \sum_{\substack{b(m,\rho)\subset\Gamma \\ m\in\mathcal{A}(l)}} g_2^{(a)}(m)|D_\rho v(m)|, \quad I_4(v,\mathcal{A}(l)) := \sum_{\substack{b(m,\rho)\subset\Gamma \\ m\in\mathcal{A}(l)}} g_2^{(b)}(m)|D_\rho v(m)|, \tag{4.4.39}$$

Due to the spatial restriction on l relative to s, we have that $m \in \Omega_i(l) \implies |m-s| \gtrsim |s|$, which also implies that $|\omega_{ms}^-| = |m-s||\omega_{ms}^+| \gtrsim |\omega_s|^2(|\omega_m|+|\omega_s|)^{-1}$. As a result we can conclude that

$$I_1(\bar{g}) \lesssim \sum_{i=1}^{2} \left(\sum_{m \in \Omega_i(l)} |\omega_m|^{-10} |\omega_{ms}^-|^{-2} \right)^{1/2} \|D\bar{g}\|_{\ell^2(\Omega_i(l))} + |\omega_l|^{-4} \lesssim |\omega_l|^{-3}.$$

An analogous argument for the remaining terms reveals that

$$I_2(\bar{g}) \lesssim \sum_{i=1}^{2} \left(\sum_{m \in \Omega_i(l)} |\omega_m|^{-6} |\omega_{ms}^-|^{-6} \right)^{1/2} \|D\bar{g}\|_{\ell^2(\Omega_i(l))} + |\omega_l|^{-4} \lesssim |\omega_l|^{-4},$$

$$I_3(\bar{g}) \lesssim \sum_{i=1}^{2} \left(\sum_{m \in \Omega_i(l)} |\omega_m|^{-6} |\omega_{ms}^-|^{-2} \right)^{1/2} \|D\bar{g}\|_{\ell^2(\Omega_i(l))} + |\omega_l|^{-4} \lesssim |\omega_l|^{-3},$$

$$I_4(\bar{g}) \lesssim \sum_{i=1}^{2} \left(\sum_{m \in \Omega_i(l)} |\omega_m|^{-4} |\omega_{ms}^-|^{-4} \right)^{1/2} \|D\bar{g}\|_{\ell^2(\Omega_i(l))} + |\omega_l|^{-4} \lesssim |\omega_l|^{-4}.$$

We have thus estimated each summand in (4.4.35) and this concludes the proof. □

As a result, we can improve the norm estimates in Lemma 4.4.3 slightly.

Lemma 4.4.5. *For any s with $|s|$ large enough and $\tau \in \mathcal{R}(s)$, the function $\bar{g}(m,s) := D_{2\tau}\bar{\mathcal{G}}(m,s)$ satisfies*

$$\|D\bar{g}(\cdot,s)\|_{\ell^2(\Omega_1)} \lesssim |\omega_s|^{-5/2} \quad \textit{and} \quad \|D\bar{g}(\cdot,s)\|_{\ell^2(\Omega_2)} \lesssim |\omega_s|^{-3}.$$

Proof. With Lemma 4.4.4 in hand, the estimate (4.4.30) now becomes

$$\sum_{m \in \Lambda} \sum_{\rho \in \mathcal{R}(m)} \left(D_\rho \eta_i(m) \bar{g}(m,s) \right)^2 \lesssim |\omega_s|^{-6}, \tag{4.4.40}$$

which is enough to conclude the result, as now the terms with the lowest rate of decay are given by (4.4.26) and (4.4.28), but these only apply to $\Omega_1(s)$. □

To proceed further we improve upon the estimates in (4.4.26) and (4.4.28).

Lemma 4.4.6. *Let $s \in \Lambda$ be such that $|s|$ is large enough. If $m \in \Lambda$ is such that $m \in B_{\frac{3|s|}{4}}(0)$ then*

$$|\bar{g}(m,s)| \lesssim |\omega_s|^{-5/2}.$$

Proof. Proceeding as in Lemma 4.4.4, we will estimate $D_{1\tau}\bar{\mathcal{G}}(l,s)$ for $l \in \Lambda \setminus B_{\frac{4|s|}{3}}(0)$, which can be achieved by arguing that

$$|D_{1\tau}\bar{\mathcal{G}}(l,s)| \lesssim \sum_{i=1}^{4} I_i(\hat{g}) + I_i(\bar{g}), \tag{4.4.41}$$

where the terms are as in (4.3.13)-(4.3.14). The terms corresponding to $\hat{g}$ can be estimated as in Lemma 4.4.4, with the only difference being that we longer have $|\zeta| \sim |\gamma|$, but now $|\zeta| \gtrsim |\gamma|$. We still have that $|\zeta| \sim |\zeta - \gamma|$. It can be thus verified by redoing the estimates from Lemma 4.4.4 that in fact

$$\sum_{i=1}^{4} I_i(\hat{g}) \lesssim |\zeta|^{-3} = |\omega_l|^{-3}.$$

For the other four terms we can still write, e.g.

$$I_1(\bar{g}) \lesssim \sum_{i=1}^{2} \left(\sum_{m \in \Omega_i(l)} (1 + |\omega_m|^{-5} |\omega_{ms}^{-}|^{-1})^{-2} \right)^{1/2} \|D\bar{g}\|_{\ell^2(\Omega_i(l))} + |\omega_l|^{-4},$$

but since as $|l|$ grows larger, we eventually have $s \in \Omega_1(l)$, it implies that the summation over $\Omega_1(l)$ is $\mathcal{O}(1)$, thus we can only rely on the result of Lemma 4.4.5, which tells us that $\|D\bar{g}\|_{\ell^2(\Omega_1(l))} \lesssim |\omega_l|^{-5/2}$ and so it easy to see that we can only conclude that

$$\sum_{i=1}^{4} I_i(\bar{g}) \lesssim |\omega_l|^{-5/2},$$

thus giving us the result of the lemma. □

Lemma 4.4.7. *For any s with $|s|$ large enough and $\tau \in \mathcal{R}(s)$, and any $\delta > 0$, the function $\bar{g}(m,s) := D_{2\tau}\bar{\mathcal{G}}(m,s)$ satisfies*

$$\|D\bar{g}(\cdot,s)\|_{\ell^2(\Omega_1)} \lesssim |\omega_s|^{-3+\delta}.$$

Proof. The result of Lemma 4.4.6 in particular implies that the terms (4.4.26) and

(4.4.28) can now be estimated, respectively, by

$$\begin{aligned}\sum_{m\in B_{\frac{3|s|}{4}}(0)} h_4^{(a)}(m,s)|\bar{g}(m,s)| &\lesssim \sum_{m\in B_{\frac{3|s|}{4}}(0)} (1+|\omega_m|^7|\omega_s||\omega_{ms}^-|^2)^{-1}(1+|\omega_s|^{5/2})^{-1} \\ &\lesssim |\omega_s|^{-11/2}\sum_m |\omega_m|^{-7} \lesssim |\omega_s|^{-11/2},\end{aligned} \tag{4.4.42}$$

$$\begin{aligned}\sum_{m\in B_{\frac{3|s|}{4}}(0)\cap\Gamma} h_2^{(a)}(m,s)|\bar{g}(m,s)| &\lesssim \sum_{m\in B_{\frac{3|s|}{4}}(0)\cap\Gamma} (1+|\omega_m|^3|\omega_s||\omega_{ms}^-|^2)^{-1}(1+|\omega_s|)^{-5/2} \\ &\lesssim |\omega_s|^{-11/2}\sum_{m\in B_{\frac{3|s|}{4}}(0)\cap\Gamma} |\omega_m|^{-3} \lesssim |\omega_s|^{-11/2},\end{aligned} \tag{4.4.43}$$

which in particular, repeating the argument in Lemma 4.4.5, implies that

$$\|D\bar{g}(\cdot,s)\|_{\ell^2(\Omega_1)} \lesssim |\omega_s|^{-11/4}.$$

We can thus redo the argument in Lemma 4.4.6 to conclude that for $|m| \leq \frac{3|s|}{4}$ we have $|\bar{g}(m,s)| \lesssim |\omega_s|^{-11/4}$, which in turn implies that

$$\|D\bar{g}(\cdot,s)\|_{\ell^2(\Omega_1)} \lesssim |\omega_s|^{-23/4}.$$

It is hence apparent that we can repeat this process ad infinitum with the result after k iterations given by

$$\|D\bar{g}(\cdot,s)\|_{\ell^2(\Omega_1)} \lesssim |\omega_s|^{-d(k)},$$

where

$$d(k) = 3\left(\sum_{i=1}^{k}\frac{1}{2^i} + \frac{b}{2^k}\right),$$

where $b = \frac{2}{3} < 1$, which ensures that $d(k) < 3\ \forall k \in \mathbb{N}$, but with $\lim_{k\to\infty} d(k) = 3$, thus establishing the premise of the lemma. □

4.4.6 The concluding pointwise estimate for the mixed second derivative of $\mathcal{G}$

The bootstrapping argument of Section 4.4.5 ensures we can obtain a global pointwise decay estimate for $|D_1 D_2 \bar{\mathcal{G}}|$ and hence for $|D_1 D_2 \mathcal{G}|$ as well.

Lemma 4.4.8. *If $l \in \Omega_1(s) \cup \Omega_2(s)$, $\tau \in \mathcal{R}(l)$, and $\lambda \in \mathcal{R}(s)$, then for any $\delta > 0$*

$$|D_{1\tau} D_{2\lambda} \bar{\mathcal{G}}(l,s)| \lesssim (1 + |\omega_l||\omega_s||\omega_{ls}^-|^{2-\delta})^{-1}.$$

Proof. Consider $s, l \in \Lambda$ such that $|s|$ is large enough and $|l| \leq \frac{|s|}{3}$ and $|l| \geq 4$. We create a cut-off function η that scales with $|l|$, namely we say $\eta \equiv 1$ in $B_{\frac{|l|}{4}}(l)$ and $\eta \equiv 0$ outside $B_{\frac{|l|}{2}}(l)$ and smooth and decreasing in-between. Mimicking the approach in Lemma 4.4.2, we conclude that

$$D_{1\tau} D_{2\lambda} \bar{\mathcal{G}}(l,s) = S_1 + S_2$$

where

$$|S_1| \lesssim \sum_{i=1}^{4} J_i(v) \lesssim (1 + |\omega_l||\omega_s||\omega_{ls}^-|^2)^{-1},$$

due to a verbatim repetition of the argument in Lemma 4.4.2. Likewise, we can immediately conclude that

$$|S_2| \lesssim |\omega_l|^{-2} \|D_1 \bar{g}(\cdot, s)\|_{\ell^2(\mathcal{A}_l)},$$

where $\bar{g}(m,s) := D_{2\tau} \bar{\mathcal{G}}(m,s)$ and $\mathcal{A}_l := B_{\frac{|l|}{2}}(l) \setminus B_{\frac{|l|}{4}}(l)$. Crucially, we observe that in the region under consideration we have $B_{\frac{|l|}{2}}(l) \subset \Omega_1(s)$, thus allowing us to employ Lemma 4.4.7 to conclude that

$$|S_2| \lesssim (1 + |\omega_l|^2 |\omega_s|^{3-\delta})^{-1} \lesssim (1 + |\omega_l|^2 |\omega_s||\omega_{ls}^-|^{2-\delta})^{-1},$$

where the final passage follows from the fact that we have $|\omega_s| \gtrsim |\omega_{ls}^-|$ in the region of interest.

We further note that this partial result together with the norm estimate over $\Omega_1(s)$ in Lemma 4.4.7 implies that if $|l| \leq 4$, then

$$|D_{1\tau} D_{2\lambda} \bar{\mathcal{G}}(l,s)| \lesssim |\omega_s|^{-3+\delta} \lesssim |\omega_s|^{-1} |\omega_{ls}^-|^{-2+\delta},$$

which is precisely the result we want for $l \approx 0$. Finally, for l such that $\frac{|s|}{3} \leq |l| \leq \frac{|s|}{2}$, we simply note that the choice of regions $\Omega_1(s), \mathcal{A}(s)$, and $\Omega_2(s)$ at the start of

Section 4.4 was arbitrary in the sense that we can always choose different constants with the $|s|$ scaling and none of the arguments are affected except for having to readjust the constants for $|s|$ scaling of the cut-off functions used throughout. Thus we have shown that if $l \in \Omega_1(s)$ then

$$|D_{1\tau}D_{2\lambda}\bar{\mathcal{G}}(l,s)| \lesssim (1+|\omega_l||\omega_s||\omega_{ls}^-|^{2-\delta})^{-1},$$

which thanks to variable symmetry of $\bar{\mathcal{G}}$ established in the proof of Theorem 4.2.2 implies the same for $l \in \Omega_2(s)$. □

We are at last ready to prove the main result of this section.

Proof Theorem 4.2.2, Part 2: decay estimate for the mixed derivative of $\mathcal{G}$.
Lemma 4.4.2 and Lemma 4.4.8 together establish that for all $l, s \in \Lambda$ and $\tau \in \mathcal{R}(l)$, $\lambda \in \mathcal{R}(s)$, we have for any $\delta > 0$

$$|D_{1\tau}D_{2\lambda}\bar{\mathcal{G}}(l,s)| \lesssim |\omega_l|^{-1}|\omega_s|^{-1}|\omega_{ls}^-|^{-2+\delta}.$$

Lemma 4.3.2 provides the same result for $\hat{\mathcal{G}}$ (including the case $\delta = 0$) and since $\mathcal{G} = \hat{\mathcal{G}} + \bar{\mathcal{G}}$, then in fact

$$|D_{1\tau}D_{2\lambda}\mathcal{G}(l,s)| \lesssim |\omega_l|^{-1}|\omega_s|^{-1}|\omega_{ls}^-|^{-2+\delta},$$

which is what we set out to prove. □

4.5 Discussion

In the concluding section of this chapter, we discuss to what extent the key ingredients of the proofs presented in Sections 4.3 and 4.4 rely on the present setup of a two-dimensional square lattice under nearest-neighbour interactions and anti-plane displacements and whether we can adapt the proof to work in a greater generality.

We begin by noting that the construction of the Green's function described in Section 4.3 based upon coupling the discrete problem with its continuum counterpart translates verbatim to certain more involved settings, for instance, in the anti-plane setup, to any Bravais lattice under finite-range pair-potential, subject to prescribing the correct constant C_Λ in (4.3.6). In a general case of a vectorial model with under finite-range interatomic potential, however, surface effects play a vital role, potentially rendering the continuum approximation invalid near the crack surface.

This has been discussed already in Chapter 3 in Section 3.6 and requires further thought.

Similarly, most of the decay estimate proof detailed in Section 4.4 can be easily extended to the general case, in particular the pointwise estimates in Sections 4.4.2-4.4.3 applied to the bulk (Case 1 in the proofs of Lemma 4.4.1 and Lemma 4.4.2). This is because these arguments apply to the region where any surface effects are negligible, as we effectively exclude a fixed crack-encompassing infinite cone centered at origin.

However, in order to obtain norm estimates in Sections 4.4.4-4.4.5, which translate verbatim to more complicated setups, one first needs to obtain pointwise estimates of Sections 4.4.2-4.4.3 near the crack surface (Case 2 in the proofs of Lemma 4.4.1 and Lemma 4.4.2). In this crucial step we rely on a construction of a locally isomorphic mapping from the defective lattice to a homogeneous lattice, which preserves the fact that $\bar{\mathcal{G}}$ is a critical point of the associated energy-difference functional.

A similar construction based on a different reflection can also be carried out for the triangular lattice under NN interactions, but this approach is ill-suited to arbitrary finite-range interactions. This is because as we enlarge the radius of interaction, we increase the number of constraints required for the extended version of $\bar{\mathcal{G}}$ to remain a critical point of the corresponding extended functional, whereas any argument based on reflection (possibly coupled with translation and scaling) has a fixed number of degrees of freedom associated with it. For the same reason the current framework only permits many-body terms in the interatomic potential that do not contribute to the Hessian, which is why we restrict ourselves to pair-potentials in the first place.

Chapter 5

Cell size effects in atomistic crack propagation

5.1 Introduction and notation

In this chapter we introduce a framework in which atomistic crack *propagation* can be analysed. In particular, we move away from the small-loading regime of Chapter 3 and introduce the stress intensity factor k discussed in Section 2.4 as a variable in the energy which was introduced in Section 2.5. Furthermore, in order to work with a physically-realistic periodic bifurcation diagram, the interactions across the crack are now included, as discussed in Section 2.1 (recall the notational conventions introduced therein). This setup requires us to assume the premise of Theorem 2 (adjusted to the new setup), but, with a suitable adjustment in the assumption on the interatomic potential V, as discussed in Section 2.3, the equivalents of Theorems 1 and 3 will be proven.

We are again interested in investigating cell size effects in the finite-domain approximation under structural assumptions on the bifurcation diagram. In particular, Theorem 6 will be proven, as well as the superconvergence estimate (1.2.6).

The be precise, we consider the energy difference functional $\mathcal{E} : \dot{\mathcal{H}}^1 \times \mathbb{R} \to \mathbb{R}$ given by

$$\mathcal{E}(u,k) = \sum_{m\in\Lambda} V(\tilde{D}\hat{u}_k(m) + \tilde{D}u(m)) - V(\tilde{D}\hat{u}_k(m)), \tag{5.1.1}$$

where $\hat{u}_k$ was defined in (2.4.3). We recall from (2.1.3) that $\tilde{D}$ is the homogeneous discrete gradient operator, thus interactions across the crack are now included. The interatomic potential V was introduced in (2.3.1), and crucially, following the discussion in Section 2.3 and given that $\tilde{D}$ is employed, we note that (2.3.2) is assumed

throughout this chapter, namely

$$\text{there exists } R_\phi > 0 \text{ such that } \phi'(r) = 0 \quad \forall r \text{ with } |r| \geq R_\phi. \tag{5.1.2}$$

Outline of the chapter: In Section 5.2 we introduce the bifurcation theory machinery, discuss the structural assumptions and state the main results. In Section 5.3 we consider the finite-domain approximation and provide rigorous statements of results about the rate of convergence of the approximate bifurcation diagrams, as introduced in (1.2.4)-(1.2.6). The numerical tests are presented in Section 5.4. The discussion about the model is in Section 5.6. We conclude by gathering proofs in Section 5.5.

5.2 Results about the model

We begin by stating the following result, which will be proven in Section 5.5.2.

Theorem 5.2.1. *Let I be an open bounded interval in $\mathbb{R}_+$ that excludes the origin. The energy difference functional $\mathcal{E}$ expressed in* (5.1.1) *is well-defined on $\dot{\mathcal{H}}^1 \times I$ and is α-times continuously differentiable.*

The inclusion of the stress intensity factor $k \in I$ as a variable in the definition of $\mathcal{E}$ allows us to employ bifurcation analysis to describe the propagation of the crack as a series of bifurcations, which we view as corresponding to bond-breaking events.

The primary task of our analysis is to characterise the set of critical points of the energy, S, defined as

$$S := \big\{(u,k) \in \dot{\mathcal{H}}^1 \times I \,\big|\, \delta_u \mathcal{E}(u,k) = 0 \in (\dot{\mathcal{H}}^1)^*\big\}, \tag{5.2.1}$$

where $\delta_u \mathcal{E} : \dot{\mathcal{H}}^1 \times I \to (\dot{\mathcal{H}}^1)^*$ is the partial Fréchet derivative given by

$$\langle \delta_u \mathcal{E}(u,k),\, v\rangle = \sum_{m \in \Lambda} \nabla V(\tilde{D}\hat{u}_k(m) + \tilde{D}u(m)) \cdot \tilde{D}v(m).$$

For future reference, we summarize our notation for linear and multi-linear forms, in particular defining the meaning of $\langle \delta_u \mathcal{E}(u,k),\, v\rangle$. For any n-linear form L, we write $L[v_1, \dots, v_n]$ to denote its evaluation at $v_1, \dots, v_n$ and if $m < n$, then $L[v_1, \dots, v_m]$ is the $(n-m)$-linear form

$$(w_1, \dots, w_{n-m}) \mapsto L[v_1, \dots, v_m, w_1, \dots, w_{n-m}].$$

For the sake of readability and only when there is no risk of confusion, we often write $\langle L,\, v_1\rangle$ for linear forms and $\langle L_1 v_1,\, v_2\rangle$ as well as $L_1 v_1 = L_1[v_1]$ for bilinear forms.

It is of particular interest to compute continuous paths contained in S, as it allows to characterise the response of the model to variations in SIF. This is often possible if we are able to identify one particular pair, say $(\bar{u}_0, \bar{k}_0) \in S$ and it can be further shown that it is a *regular point*, by which we mean

$$H_0 := \delta^2_{uu}\mathcal{E}(\bar{u}_0, \bar{k}_0) \,:\, \dot{\mathcal{H}}^1 \to (\dot{\mathcal{H}}^1)^* \text{ is an isomorphism.} \tag{5.2.2}$$

In this case, a standard application of the Implicit Function Theorem [57] yields existence of a locally unique path of solutions $(\bar{u}_s, \bar{k}_s)$ in the vicinity of $(\bar{u}_0, \bar{k}_0)$ which we will assume to be parametrised with an index $s \in \mathbb{R}$; exactly this strategy was used in Chapter 3 to show existence of solutions in a static crack problem with crack bonds removed from the definition of $\mathcal{E}$, for k small enough. We will set

$$H_s := \delta^2_{uu}\mathcal{E}(\bar{u}_s, \bar{k}_s) \,:\, \dot{\mathcal{H}}^1 \to (\dot{\mathcal{H}}^1)^*. \tag{5.2.3}$$

As we will see in the numerical examples of Section 5.4, beyond some critical value of k, bifurcations of the following type begin to occur.

Definition 5.2.2. A *(simple quadratic) fold point* occurs at $(\bar{u}_b, \bar{k}_b) \in S$ if there exists $\gamma_b \in \dot{\mathcal{H}}^1$ such that $\mathrm{Ker}(H_b) = \mathrm{span}\{\gamma_b\}$,

$$\delta^2_{uk}\mathcal{E}(\bar{u}_b, \bar{k}_b)[\gamma_b, 1] \neq 0, \tag{5.2.4}$$

$$\delta^3_{uuu}\mathcal{E}(\bar{u}_b, \bar{k}_b)[\gamma_b, \gamma_b, \gamma_b] \neq 0, \tag{5.2.5}$$

with formulae for these variations of energy given in (5.5.12) and (5.5.13), respectively.

A schematic representation of the idea behind Definition 5.2.2 is shown in Figure 5.1a. The fact that the predictor $\hat{u}_k$ introduced in Section 2.4, given by

$$\hat{u}_k(x) = k\sqrt{r_x}\sin\left(\tfrac{\theta_x}{2}\right),$$

is such that $|\nabla^j \hat{u}_k(x)| \lesssim k|x|^{1/2-j}$ implies that $\hat{u}_k \notin \dot{\mathcal{H}}^1$. This is key to (5.2.4) being true, and suggests that a full bifurcation diagram is an infinite non-self-intersecting snaking curve [80], consisting solely of regular and fold points as shown in Figure 5.1b. Our functional setup is well-suited to considering an arbitrary finite segment of it, so we begin with the following set of assumptions.

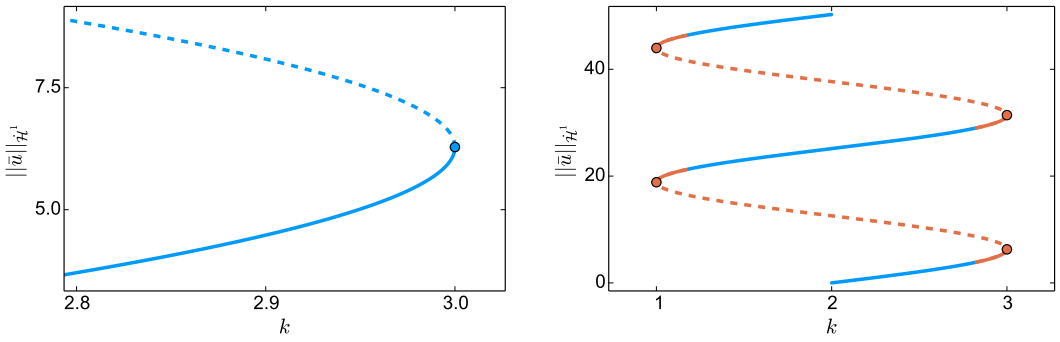

(a) (b)

Figure 5.1: (a) An illustration of typical behaviour near quadratic fold point (depicted as a blue dot). Solid (respectively dashed) lines represent stable (resp. unstable) solutions. A change in stability at such points as shown in Proposition 5.2.4 is guaranteed by (5.2.5), which ensures that the smallest eigenvalue passes through zero with nonzero 'velocity'.
(b): A schematic representation of a snaking curve with dots representing bifurcation points. The sets of solutions $\mathcal{B}_{\text{pos}}$ and $\mathcal{B}_{\text{pt}}$ defined in (5.2.9)-(5.2.10) are represented in blue and red, respectively. Note that $\mathcal{B}_{\text{pt}}$ includes the entirety of the unstable segments, as well as bifurcation points and small parts of the stable segments.

Assumption 1. There exists a bifurcation diagram in the form of an injective continuous path $\mathcal{B} : [0,1] \to \dot{\mathcal{H}}^1 \times I$ given by

$$\mathcal{B}(s) := (\bar{u}_s, \bar{k}_s), \tag{5.2.6}$$

where $\text{Im}(\mathcal{B}) \subset S$ (defined in (5.2.1)) is compact and for each $s \in [0,1]$, $\mathcal{B}(s)$ is either a regular point, as in (5.2.2), or a fold point, as in Definition 5.2.2. We further assume that there are finitely many fold points occuring at $s \in \{b_1, \ldots, b_M\} \subset (0,1)$. In particular, this implies that $\text{Im}(\mathcal{B})$ is a non–self–intersecting curve.

For future reference, if $f : \mathcal{B} \to X$, where X is a Banach space, is differentiable, then we write $f'_s := \frac{d}{ds} f_s$.

Assumption 2. There exists $c > 0$ such that for each $s \in [0,1]$ there exists a subspace U_s of $\dot{\mathcal{H}}^1$ of codimension at most 1 for which it holds that

$$\langle H_s v,\, v \rangle \geq c \, \|v\|^2_{\dot{\mathcal{H}}^1} \tag{5.2.7}$$

for all $v \in U_s$.

Assumption 2 is the natural analogue of the notion of strong stability from Theorem 2, which in Chapter 3 is proven to hold for the locally unique solution in

the small loading regime.

The fact that a succession of fold points occurs is assumed to be an inherent feature of the lattice and the potential in place, much as the existence of a solution to a static dislocation problem is assumed in [34]. Assumption 2 ensures that each $\mathcal{B}(s) = (\bar{u}_s, \bar{k}_s)$ represents either a bifurcation point, a stable solution or an unstable solution which is an index–1 saddle point. This assumption is motivated by the fact that the anti-plane setup and lattice symmetry naturally binds the crack propagation to the x_1-axis, leaving little room for any more involved bifurcating behaviour. Moreover, this is also supported by numerical evidence presented in Section 5.4.

As will be shown in Proposition 5.2.4, requiring that (5.2.5) holds ensures that a change in the stability of the solution occurs at each fold point. This implies that near bifurcation points and on the unstable segments the infimum of the spectrum of H_s is an eigenvalue, which motivates the following decomposition of the parametrisation interval $[0, 1]$: since we look at a finite segment of the full bifurcation diagram, we will assume for notational convenience that it starts on a stable segment and that the number of fold points M lying in $\mathrm{Im}(\mathcal{B})$ is even. We then define sets

$$\mathcal{I}_{\mathrm{pt}} := \bigcup_{k=1}^{M/2} I_k \subset [0,1] \quad \text{and} \quad \mathcal{I}_{\mathrm{pos}} := [0,1] \setminus \mathcal{I}_{\mathrm{pt}}, \tag{5.2.8}$$

where $I_k := (b_{2k-1} - \xi, b_{2k} + \xi)$ with $\xi > 0$ small enough to be specified in in the proof of Proposition 5.2.4. The cases where M is odd or we start on an unstable segment can be handled in an entirely analogous way. We refer to

$$\mathcal{B}_{\mathrm{pt}} := \mathcal{B}(\mathcal{I}_{\mathrm{pt}}) \tag{5.2.9}$$

as the collection of segments of the bifurcation diagram with $\sigma_p(H_s) \neq \emptyset$ (non–empty point spectrum) and to

$$\mathcal{B}_{\mathrm{pos}} := \mathcal{B}(\mathcal{I}_{\mathrm{pos}}) \tag{5.2.10}$$

as the collection of segments with $\sigma(H_s) \subset [c, \infty)$ (positive spectrum, c from Assumption 2).

We note that both the unstable segments and neighbourhoods of the bifurcation points belong to $\mathcal{B}_{\mathrm{pt}}$, thus the constant c in Assumption 2 can be chosen to be small enough so that

$$s \in \mathcal{I}_{\mathrm{pos}} \implies U_s = \dot{\mathcal{H}}^1. \tag{5.2.11}$$

We now establish some initial results about the model. First, a regularity result, to be proven in Section 5.5.2.

Proposition 5.2.3 (Regularity of the diagram)**.** *The set* $\mathrm{Im}(\mathcal{B}) \subset \dot{\mathcal{H}}^1 \times I$ *is a one–dimensional* $C^{\alpha-1}$ *manifold.*

This result entails that without loss of generality, we may make the following assumption concerning the parametrisation $\mathcal{B}$.

Assumption 3. The function $\mathcal{B} : [0,1] \to \dot{\mathcal{H}}^1 \times I$ is a constant speed, $C^{\alpha-1}$ parametrisation of the manifold $\mathrm{Im}(\mathcal{B}) \subset \dot{\mathcal{H}}^1 \times \mathbb{R}$.

Next we state a result concerning the existence of linearly unstable directions and corresponding negative eigenvalues for some sections of the bifurcation diagram. This will be proven in Section 5.5.2.

Proposition 5.2.4 (Existence of an eigen-pair)**.** *Under Assumptions 1, 2 & 3, there exist* $C^{\alpha-2}$ *functions* $\gamma : \mathcal{I}_{\mathrm{pt}} \to \dot{\mathcal{H}}^1$ *and* $\mu : \mathcal{I}_{\mathrm{pt}} \to \mathbb{R}$ *such that*

$$H_s \gamma_s = \mu_s J \gamma_s, \tag{5.2.12}$$

where H_s *was defined in* (5.2.3) *and* J *represents the Riesz mapping [74], i.e. an isometric isomorphism between* $\dot{\mathcal{H}}^1$ *and* $(\dot{\mathcal{H}}^1)^*$*, thus we can equivalently say that*

$$\langle H_s \gamma_s,\, v\rangle = \mu_s (\gamma_s, v)_{\dot{\mathcal{H}}^1} \qquad \text{for all } v \in \dot{\mathcal{H}}^1.$$

Furthermore, for $j = 1, \dots, M$*, we have* $\mu_{b_j} = 0$ *with the corresponding eigenvector* γ_{b_j} *introduced in Definition 5.2.2 and also* $\mu'_{b_j} \neq 0$*, implying that a change of stability occurs at* $s = b_j$*.*

We subsequently establish the following decay and regularity results for the atomistic core corrector, which rely on the precise characterisation of the lattice Green's function for the anti-plane crack geometry developed in Chapter 4. Details are presented in Section 5.5.2.

Theorem 5.2.5 (Decay properties of solutions and eigenvectors)**.** *For any* $s \in [0,1]$ *and* $l \in \Lambda$ *with* $|l|$ *large enough it holds that for any* $\delta > 0$ *the atomistic correction* $\bar{u}_s$ *satisfies*

$$\big|D\bar{u}_s(l)\big| \leq C|l|^{-3/2+\delta}. \tag{5.2.13}$$

If $s \in \mathcal{I}_{\mathrm{unst}}$*, then the eigenvector* $\gamma_s \in \dot{\mathcal{H}}^1$ *from Proposition 5.2.4 satisfies*

$$\big|D\gamma_s(l)\big| \leq C|l|^{-3/2+\delta}. \tag{5.2.14}$$

In both cases C *is a generic constant independent of* s*.*

5.3 Approximation

As numerical simulations are naturally restricted to a computational domain of finite size, we now consider and analyse a finite-dimensional scheme that approximates the solution path $\mathcal{B}$ defined in (5.2.6) and establish rigorous convergence results.

The starting point is a computational domain Ω_R with $B_R \cap \Lambda \subset \Omega_R \subset \Lambda$ (where B_R is a ball of radius R centred at the origin) and the boundary condition prescribed as $\hat{u}$ on $\Lambda \setminus \Omega_R$. The approximation to (5.2.1) can thus be stated as a Galerkin approximation, that is we seek to characterise

$$S_R := \big\{(u^R, k) \in \mathcal{H}_R \times I \,\big|\, \delta_u \mathcal{E}(u^R, k) = 0 \in (\mathcal{H}_R^0)^*\big\}, \tag{5.3.1}$$

where

$$\mathcal{H}_R^0 := \{v : \Lambda \to \mathbb{R} \,|\, v = 0 \text{ in } \Lambda \setminus \Omega_R\}.$$

We can prove the following results, noting that the details of the proofs are presented in Section 5.5.3.

Theorem 5.3.1. *Under Assumptions 1, 2 & 3, there exists $R_0 > 0$, such that for all $R \geq R_0$, there exists a $C^{\alpha-1}$ approximate bifurcation path $\mathcal{B}_R : [0,1] \to \mathcal{H}_R^0 \times I$ given by*

$$\mathcal{B}_R(s) := (\bar{u}_s^R, \bar{k}_s^R),$$

where $\mathrm{Im}(\mathcal{B}_R) \subset S_R$, such that for any $\beta > 0$

$$\|\bar{u}_s^R - \bar{u}_s\|_{\dot{\mathcal{H}}^1} + \big|\bar{k}_s^R - \bar{k}_s\big| \lesssim R^{-1/2+\beta} \tag{5.3.2}$$

and

$$\big|\mathcal{E}(\bar{u}_s^R, \bar{k}_s^R) - \mathcal{E}(\bar{u}_s, \bar{k}_s)\big| \lesssim R^{-1+\beta}, \tag{5.3.3}$$

where $\mathcal{B}(s) = (\bar{u}_s, \bar{k}_s)$ as in (5.2.6).

While the estimate in (5.3.2) appears to be almost sharp (our numerical results in Section 5.4 indicate that this estimate holds with $\beta = 0$, possibly up to log-factors), more can be said about the approximation of the critical values of the stress intensity factor for which fold points occur.

Theorem 5.3.2. *For R suffiently large, the approximate bifurcation path $\mathcal{B}_R$ from Theorem 5.3.1 contains M fold points in the sense of Definition 5.2.2 occuring at $s \in \{b_1^R, \ldots, b_M^R\} \subset (0,1)$, and for each of these we have*

$$\big|\bar{k}_{b_j^R}^R - \bar{k}_{b_j}\big| \lesssim R^{-1+\beta} \quad \text{for any } \beta > 0.$$

This superconvergence result is well-known in bifurcation theory [27], and is observed numerically in our tests in Section 5.4.

5.4 Numerical investigation

In this section we present results of numerical tests that confirm the rate of decay of $|D\bar{u}_s|$ and $|D\gamma_s|$ established in Theorem 5.2.5, as well as the convergence rates from Theorems 5.3.1 and 5.3.2. The computational setup is similar to the one described in [19, Section 3], with Λ and $\mathcal{R}$ as specified in Sections 2.1 and the pair-potential given by

$$\phi(r) = \frac{1}{6}\big(1 - \exp(-3r^2)\big). \tag{5.4.1}$$

We employ a pseudo-arclength numerical continuation scheme to approximate $\mathcal{B}_R$ [7]. To compute equilibria we employ a standard Newton scheme, terminating at an ℓ^∞-residual of 10^{-8}.

Theorems 5.2.5 suggests that $|D\bar{u}_s(l)| \lesssim |l|^{-3/2}$ and $|D\gamma_s(l)| \lesssim |l|^{-3/2}$. This is verified in Figure 5.2. Theorem 5.3.1 suggests that in the supercell approximation of $\mathcal{B}$ in (5.2.6) we expect $\|\bar{u}_s^R - \bar{u}_s\|_{\dot{\mathcal{H}}^1} + |\bar{k}_s^R - \bar{k}_s| \sim \mathcal{O}(R^{-1/2})$, where R is the size of the domain. To verify this numerically, we first compute $\mathcal{B}_R$ for $R = 32, \dots, 256$ via a pseudo–arclength continuation scheme. The results are shown in Figure 5.3, with stable segments plotted as solid lines and unstable segments as dashed lines. To measure the distance between the segments of the bifurcation diagram, we compute the Hausdorff distance [73] with respect to $\|\cdot\|_{\dot{\mathcal{H}}^1}$-norm between the critical points on $\mathcal{B}_R$ (for $R = 32, \dots, 90.51$)and on $\mathcal{B}_{R_*}$, where $R_* = 256$. The result is shown in Figure 5.4a.

Finally, we test the superconvergence result for the bifurcation points from Theorem 5.3.2, which predicts that $|\bar{k}^R_{b_j^R} - \bar{k}_{b_j}| \sim \mathcal{O}(R^{-1})$. To this end we accelerate the convergence of the sequence $\{\bar{k}^R_{b_j^R}\}$ (for $R = 32, \dots, 256$) by employing Richardson extrapolation [72], thus giving us an approximate limit values for $\bar{k}_{b_j}$. The values of the approximate limits, as well as the R^{-1} convergence is exhibited in Figure 5.4b.

Remark 5.4.1. The pair-potential ϕ defined in (5.4.1) does not satisfy the strong assumption of compact support of ϕ' introduced in (5.1.2), but has the slightly weaker property of exponential decay in first derivative. It thus illustrates the point mentioned in Section 2.3 that (5.1.2) is by no means a necessary condition.

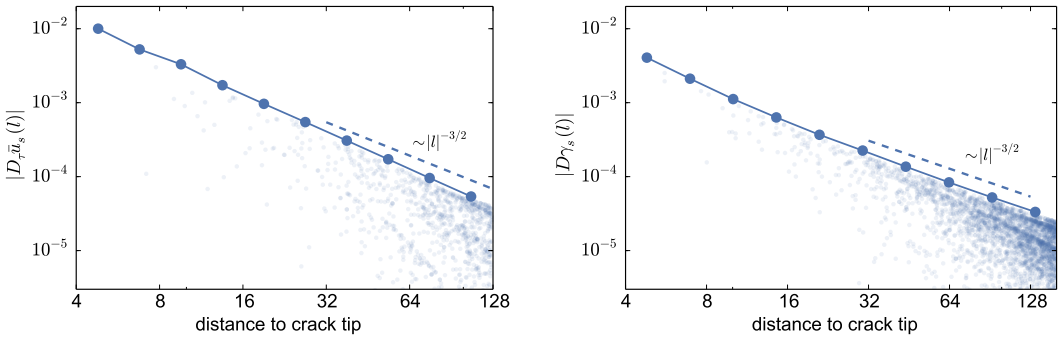

Figure 5.2: The decay of $D\bar{u}_s$ and $D\gamma_s$. Transparent dots denote data points $(|l|, |Du_s(l)|)$, solid curves their envelopes. We observe the expected rate of $|l|^{-3/2}$.

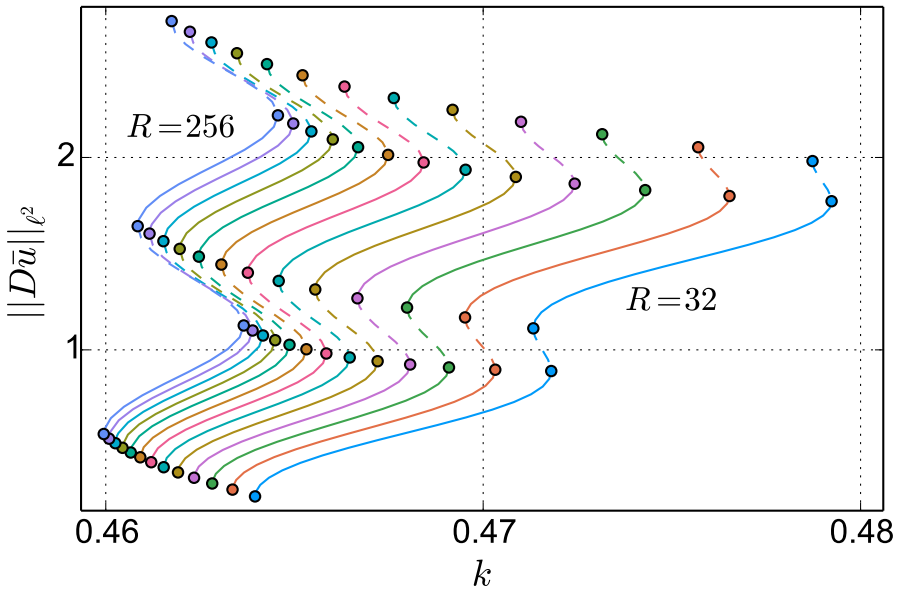

Figure 5.3: The bifurcation paths $\mathcal{B}_R$ for $R = 32, \ldots, 256$, that is for $R = 2^{n/4}$ for $n = 20, \ldots 32$. Solid lines denote stables segments, dashed lines unstable segments and dots the bifurcation points.

5.5 Proofs

5.5.1 Preliminaries

Our approach is based on two classic results from bifurcation analysis on Banach spaces, cf. [27], which we state in this section for convenience. The first result is known as 'ABCD Lemma' and is adapted from [54].

Lemma 5.5.1 (ABCD Lemma)**.** *Let H be a Hilbert space with dual H^* and consider*

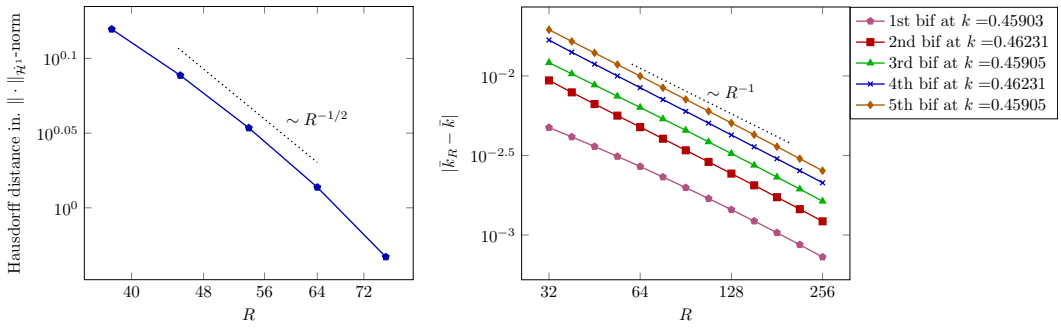

(a) (b)

Figure 5.4: (a) The approximate rate of convergence of the supercell approximation of $\mathcal{B}$, measured by the Hausdorff distance with respect to $\|\cdot\|_{\dot{\mathcal{H}}^1}$-norm, compared against the domain with $R = 256$.
(b) The convergence rate of the values of stress intensity factor at which bifurcations occur. The approximate limit values as predicted by Richardson extrapolation are given in the legend entries. The fact that all unstable-to-stable (and separately stable-to-unstable) fold points occur at the same values indicates that in the limit the bifurcation path is exactly vertical.

the linear operator $M : H \times \mathbb{R} \to H^* \times \mathbb{R}$ *of the form*

$$M := \begin{bmatrix} A & b \\ (c, \cdot)_H & d \end{bmatrix},$$

where $A : H \to H^*$ *is self-adjoint in the sense that* $\langle Av, w\rangle = \langle Aw, v\rangle$ *for all* $v, w \in H$, $b \in H^* \setminus \{0\}$, $c \in H \setminus \{0\}$ *and* $d \in \mathbb{R}$. *Then*

(i) if A *is an isomorphism from* H *to* H^*, *then* M *is an isomorphism between* $H \times \mathbb{R}$ *and* $H^* \times \mathbb{R}$ *if and only if* $d - (c, A^{-1}b)_H \neq 0$; *and*

(ii) if $\dim \mathrm{Ker}(A) = \mathrm{codim}\,\mathrm{Range}(A) = 1$ *with* $\mathrm{Ker}(A) = \mathrm{span}\{\gamma\}$, *then* M *is an isomorphism if and only if* $\langle b, \gamma\rangle \neq 0$ *and* $(c, \gamma)_H \neq 0$.

To state the second result we introduce the following setup: let X, Y and Z be real Banach spaces and $F \in C^k(U \times Y; Z)$ for some $k \geq 1$, where U is a bounded open subset of X. The total derivative of F at $(x, y) \in X \times Y$ is denoted $DF(x, y) \in \mathcal{L}(X \times Y, Z)$, with partial derivatives denoted $D_xF(x, y) \in \mathcal{L}(X, Z)$ and $D_yF(x, y) \in \mathcal{L}(Y, Z)$. We now state a version of [20, Theorem 1] tailored to our setting.

Theorem 5.5.2. *Suppose a function* $y : U \to Y$ *is Lipschitz continuous with Lipschitz constant* c_2, *and there exist constants* c_0 *and* c_1 *and a monotonically increasing function* $L_1 : \mathbb{R} \to \mathbb{R}$ *such that the following hypotheses are satisfied:*

(i) for any $x_0 \in U$, $D_y F\big(x_0, y(x_0)\big)$ is an isomorphism of Y onto Z with

$$\sup_{x_0 \in U} \big\| D_y F\big(x_0, y(x_0)\big)^{-1} \big\| \leq c_0; \tag{5.5.1}$$

(ii) we have the uniform bound

$$\sup_{x_0 \in U} \big\| D_x F\big(x_0, y(x_0)\big) \big\| \leq c_1; \tag{5.5.2}$$

(iii) for any $x_0 \in U$ and all (x, y) satisfying $\|x - x_0\| + \|y - y(x_0)\| \leq \xi$, we have

$$\|DF(x, y) - DF(x_0, y(x_0)\| \leq L_1(\xi)\big(\|x - x_0\| + \|y - y(x_0)\|\big).$$

It then follows that there exist constants $a, d > 0$ depending only on c_0, c_1, c_2 and L_1 so that whenever

$$\sup_{x_0 \in U} \|F(x_0, y(x_0))\| \leq d,$$

then there exists a unique function $g \in C^k(\bigcup_{x_0 \in U} B(x_0, a), Y)$ such that

$$F\big(x, g(x)\big) = 0.$$

Moreover, for all $x_0 \in U$ and all $x \in B(x_0, a)$,

$$\|g(x) - y(x_0)\| \leq K_0\Big(\|x - x_0\| + \big\|F\big(x_0, y(x_0)\big)\big\|\Big), \tag{5.5.3}$$

where $K_0 > 0$ depends only on the constants c_0 and c_1.

For future reference we note that a suitable choice a is given by

$$a = \min\left\{\frac{\hat{a}}{2}, \frac{b}{2c_2}\right\} - \epsilon \tag{5.5.4}$$

where $\hat{a} = \frac{b}{4M}$, b is such that $bL_1(b) \leq \frac{1}{2M}$, $M = \max\{c_0, 1 + c_0 c_1\}$ and $\epsilon > 0$ is sufficiently small to ensure that a is positive. This can be seen by tracing the constants in the proof given in [20].

5.5.2 Proofs about the model

We begin with a technical lemma that is required to prove Theorem 5.2.1.

Lemma 5.5.3. *If $v \in \dot{\mathcal{H}}^1$, then, for any $l \in \Gamma_\pm$,*

$$|v(l)| \lesssim ||v||_{\dot{\mathcal{H}}^1}(1 + \log|l|). \tag{5.5.5}$$

Proof. The argument in [66, Proposition 12(ii)] proves the result for the case without a crack present. In that setting, the proof follows directly from [67, Theorem 2.2]. For a crack geometry, we modify the argument. We distinguish two cases, depending on whether $l \in \Gamma_+$ or $l \in \Gamma_-$. We recall that $\hat{x} = \left(\frac{1}{2}, \frac{1}{2}\right)$ and that by definition $v \in \dot{\mathcal{H}}^1 \implies v(\hat{x}) = 0$.

Case 1: Let $l \in \Gamma_+$, which implies that $(l - \hat{x}) \cdot e_1 = 0$. We consider a sequence of squares $(Q_i)_{i=0}^N \subset \mathbb{R}^2 \setminus (\Omega_\Gamma \cup \Gamma_0)$ (recall the definition of Ω_Γ in (3.5.1)) aligned in the direction e_2 (which is possible due to the assumption on l) and defined as follows. Q_0 and Q_N are unit squares corresponding to sites $\hat{x}$ and l, defined in such a way that $\hat{x}$ (respectively l) is the midpoint of the side of Q_0 (resp. Q_N) which borders Γ_+. The squares $Q_1, \ldots, Q_{N-1}$ are defined to fill the space between $\hat{x}$ and l in such a way that they have disjoint interiors and are such that their side-lengths differ by at most a factor of 2, with one side of the smaller square contained in one side of the larger square. It is easy to see that there is at most

$$N \lesssim (2 + \log|l - \hat{x}|) \lesssim 1 + \log|l|$$

squares in the sequence. See Figure 5.5.

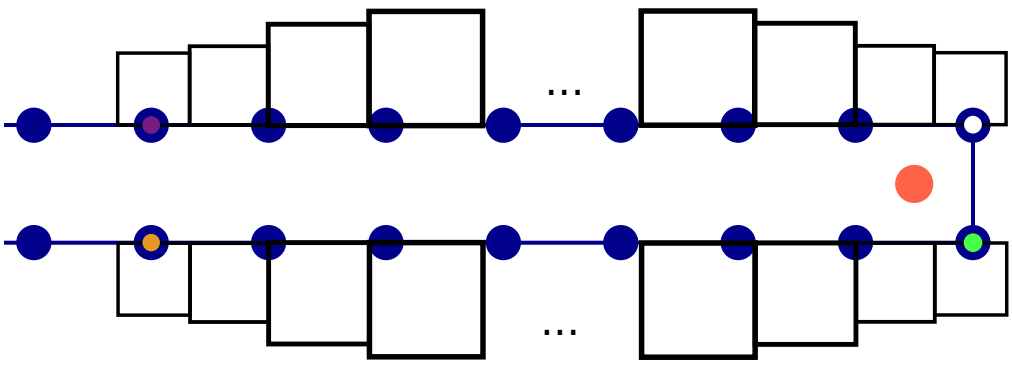

Figure 5.5: An example of construction of squares. The white dot represents $\hat{x}$, the green dot is $\hat{a}$, the purple dot a site in Case 1 and the orange dot is a site in Case 2.

For any two neighbouring squares Q_j, Q_{j+1} it follows from a special case of

[51, Lemma 2] that

$$|(v)_{Q_{j+1}} - (v)_{Q_j}| \lesssim \|\nabla Iv\|_{L^2(\mathbb{R}^2\setminus\Gamma_0)} = \|v\|_{\dot{\mathcal{H}}^1}, \tag{5.5.6}$$

where

$$(v)_{Q_j} := \frac{1}{|Q_j|}\int_{Q_j} Iv(x)\,dx$$

and I denotes the crack domain P1 interpolation operator employed throughout this thesis (in particular first discussed in the proof of Theorem 3.2.1).

As a result

$$\begin{aligned} |(u)_{Q_N} - (u)_{Q_0}| &\leq \sum_{j=1}^{N} |(u)_{Q_j} - (u)_{Q_{j-1}}| \\ &\lesssim \sum_{j=1}^{N} \|\nabla Iv\|_{L^2(\mathbb{R}^2\setminus\Gamma_0)} = N\|v\|_{\dot{\mathcal{H}}^1} \lesssim (2+\log|l|)\|v\|_{\dot{\mathcal{H}}^1}. \end{aligned} \tag{5.5.7}$$

Furthermore, it is naturally true that

$$|(v)_{Q_0} - v(\hat{x})| \leq \|\nabla v\|_{L^\infty(Q_0)} \quad \text{and } |v(l) - (v)_{Q_N}| \leq \|\nabla v\|_{L^\infty(Q_N)} \tag{5.5.8}$$

and since on each Q_i, the piecewise linear interpolant v belongs to a finite-dimensional space, we obtain

$$\|\nabla Iv\|_{L^\infty(Q_i)} \lesssim \|\nabla Iv\|_{L^2(Q_i)} \lesssim \|\nabla v\|_{L^2(\mathbb{R}^2\setminus\Gamma_0)} = \|v\|_{\dot{\mathcal{H}}^1}, \tag{5.5.9}$$

where the first inequality follows from the equivalence of norms for finite-dimensional spaces and the second from extending the domain from Q_i to the whole of $\mathbb{R}^2 \setminus \Gamma_0$.

With (5.5.7) and (5.5.8)-(5.5.9) in hand, we obtain

$$\begin{aligned} |v(l)| = |v(l) - v(\hat{x})| &\leq |v(l) - (v)_{Q_N}| + |(v)_{Q_N} - (v)_{Q_0}| + |(v)_{Q_0} - v(\hat{x})| \\ &\lesssim (1+\log|l|)\|v\|_{\dot{\mathcal{H}}^1}, \end{aligned} \tag{5.5.10}$$

which concludes the proof for $l \in \Gamma_+$.

Case 2: Let $l \in \Gamma_-$. The fact that l is on the other side of the crack relative to $\hat{x}$ deems the previous argument invalid, as we can no longer define the sequence of squares aligned with $\hat{x}$ and l which will be a subset of $\mathbb{R}^2 \setminus (\Omega_\Gamma \cup \Gamma_0)$. Thus we

first 'jump' to the other side. By defining $\hat{a} = \left(\frac{1}{2}, -\frac{1}{2}\right)$ we conclude that

$$\begin{aligned} |v(l) - v(\hat{x})| &\leq |v(l) - v(\hat{a})| + |v(\hat{a}) - v(\hat{x})| \\ &\lesssim \|v\|_{\dot{\mathcal{H}}^1}((1 + \log|l - \hat{a}|)) \\ &\lesssim ||v||_{\dot{\mathcal{H}}^1}(1 + \log|l|), \end{aligned}$$

where the second inequality follows from applying (5.5.10) to a sequence of squares between l and $\hat{a}$ and the fact that a bound on $|v(\hat{a}) - v(\hat{x})|$ can be incorporated into the general form . □

We now show that the model is well-defined, with the particular emphasis on two new elements of the analysis that are distinct from previous arguments of this kind, e.g. [22, 34].

Proof of Theorem 5.2.1. We can decompose the energy into a bulk part and a crack surface part by writing

$$\mathcal{E}(u, k) = \mathcal{E}_{\text{bulk}}(u, k) + \mathcal{E}_{\Gamma}(u, k),$$

where

$$\mathcal{E}_{\text{bulk}}(u, k) := \sum_{m \in \Lambda} \sum_{\rho \in \mathcal{R}(m)} \phi\big(D_\rho \hat{u}_k(m) + D_\rho u(m)\big) - \phi\big(D_\rho \hat{u}_k(m)\big),$$

$$\mathcal{E}_{\Gamma}(u, k) := \sum_{m \in \Gamma_\pm} \sum_{\rho \in \mathcal{R} \setminus \mathcal{R}(m)} \phi\big(D_\rho \hat{u}_k(m) + D_\rho u(m)\big) - \phi\big(D_\rho \hat{u}_k(m)\big).$$

We notice that $\mathcal{E}_{\text{bulk}}$ excludes the bonds across the crack and thus is well-defined on $\dot{\mathcal{H}}^1 \times I$, as shown in the first part of Theorem 3.2.1.

To establish the same for the $\mathcal{E}_\Gamma$, we note that we have the symmetry

$$\hat{u}_{-k}(l) = \hat{u}_k(l_1, -l_2);$$

using this observation, for $m \in \Gamma_\pm$ and $\rho \in \mathcal{R} \setminus \mathcal{R}(m)$ (that is bonds crossing the crack) we have

$$|D_\rho \hat{u}_k(m)| = |-2\hat{u}_k(m)| \sim k|m|^{1/2} \quad \text{as } |m| \to \infty. \tag{5.5.11}$$

We note here that the condition $k \neq 0$ originating from the definition of I is crucial here.

Furthermore, Lemma 5.5.3 establishes that, for any $u \in \dot{\mathcal{H}}^1$ with $m \in \Gamma_\pm$ and $\rho \in \mathcal{R} \setminus \mathcal{R}(m)$, we have $|D_\rho u(m)| \lesssim \log|m|$, which in particular implies that

$$|D_\rho \hat{u}_k(m) + D_\rho u(m)| \geq C_0|m|^{1/2} - C_1 \log|m|,$$

for suitable constants C_0, C_1. Therefore, using assumption (5.1.2), it follows that for any $m \in \Gamma_\pm$ with $|m|$ sufficiently large,

$$\phi\big(D_\rho \hat{u}_k(m) + D_\rho u(m)\big) - \phi\big(D_\rho \hat{u}_k(m)\big) = 0;$$

this entails that for each $u \in \dot{\mathcal{H}}^1$ we effectively only sum over a finite domain, and implies that $\mathcal{E}_\Gamma$ is indeed well-defined over $\dot{\mathcal{H}}^1 \times \mathbb{R}$.

The differentiability properties of the functional follow from a standard argument, see [68]. In particular we note that due to the assumptions on interval I the issues near $k = 0$ do not enter the analysis. Here we simply provide formulae for derivatives of relevance to our subsequent arguments. In particular, we have

$$\begin{aligned}
\langle \delta_k \mathcal{E}(u,k),\, \lambda\rangle &= \sum_{m\in\Lambda} (\nabla V(\tilde{D}\hat{u}_k(m) + \tilde{D}u(m)) - \nabla V(\tilde{D}\hat{u}_k(m)) \cdot (\lambda \tilde{D}\hat{u}_k(m)),\\
\langle \delta_u \mathcal{E}(u,k),\, v\rangle &= \sum_{m\in\Lambda} \nabla V(\tilde{D}\hat{u}_k(m) + \tilde{D}u(m)) \cdot \tilde{D}v(m),\\
\delta^2_{uk}\mathcal{E}(u,k)[v,\lambda] &= \sum_{m\in\Lambda} \nabla^2 V(\tilde{D}\hat{u}_k(m) + \tilde{D}u(m))[\lambda \tilde{D}\hat{u}_k(m)] \cdot \tilde{D}v(m), \qquad (5.5.12)\\
\langle \delta^2_{uu}\mathcal{E}(u,k)v,\, w\rangle &= \sum_{m\in\Lambda} \nabla^2 V(\tilde{D}\hat{u}_k(m) + \tilde{D}u(m))\tilde{D}v(m) \cdot \tilde{D}w(m),\\
\delta^3_{uuu}\mathcal{E}(u,k)[v,w,z] &= \sum_{m\in\Lambda} \nabla^3 V(\tilde{D}\hat{u}_k(m) + \tilde{D}u(m))[\tilde{D}v(m), \tilde{D}w(m), \tilde{D}z(m)]. \qquad (5.5.13)
\end{aligned}$$

□

As stated, the foregoing expressions are valid for $v \in \mathcal{H}^c$. To define them for $v \in \dot{\mathcal{H}}^1$ one requires an extension argument relying on showing that $\delta_u \mathcal{E}(0,k) \in (\dot{\mathcal{H}}^1)^*$, which is proven in Chapter 3 in Theorem 3.2.1, and analogous results for the remaining terms.

We now turn to the analysis of the bifurcation path $\mathcal{B}$.

Proof of Proposition 5.2.3. This is a standard result and follows from Theorem 5.5.2 and the fact that $\mathcal{E}$ is a C^α functional, so we may apply the local uniqueness of the function g whose existence was asserted in Theorem 5.5.2. We therefore only outline

the proof. Define sets corresponding to neighbourhoods of fold points

$$\mathcal{I}_{\mathrm{f}} := \bigcup_{i=1}^{M} (b_i - \xi, b_i + \xi) \quad \text{and} \quad \mathcal{B}_{\mathrm{f}} := \mathcal{B}(\mathcal{I}_{\mathrm{f}}),$$

Since $\mathrm{Im}(\mathcal{B})$ is compact, then so is $\mathrm{Im}(\mathcal{B}) \setminus \mathcal{B}_{\mathrm{f}}$, thus the latter can be covered with a finite collection of neighbourhoods of points $\{(\bar{u}_{s_i}, \bar{k}_{s_i})\}_{i=1,\dots,N}$.

It will be shown in the proof of Theorem 5.3.1 that $H_{s_i} = \delta^2_{uu}\mathcal{E}(\bar{u}_{s_i}, \bar{k}_{s_i})$ at each such point is an isomorphism, thus rendering Theorem 5.5.2 applicable to $\delta_u\mathcal{E}(\bar{u}_{s_i}, \bar{k}_{s_i})$, giving us a locally unique $C^{\alpha-1}$ graph of critical points $k \mapsto u(k)$, which by its uniqueness together with injectivity of $\mathcal{B}$ has to coincide with $(\bar{u}_s, \bar{k}_s)$, thus $\mathrm{Im}(\mathcal{B}) \setminus \mathcal{B}_{\mathrm{f}}$ is a piecewise $C^{\alpha-1}$ manifold.

To establish the same in $\mathcal{B}_{\mathrm{f}}$, for each fold point b_i, one considers an extended system $\tilde{F} : (\dot{\mathcal{H}}^1 \times I) \times \mathbb{R}$ given by $\tilde{F}(u, k, t) = \big(\delta_u\mathcal{E}(u, k), (u - \bar{u}_{b_i}, \gamma_{b_i})_{\dot{\mathcal{H}}^1} - t\big)$, where γ_{b_i} was introduced in Definition 5.2.2. The ABCD Lemma is applicable to this extended system evaluated at $(\bar{u}_{b_i}, \bar{k}_{b_i}, b_i)$, thus ensuring that Theorem 5.5.2 is also applicable, giving us a locally unique $C^{\alpha-1}$ graph $t \mapsto (u(t), k(t))$, where in particular $k(0) = \bar{k}_{b_i}$. Again, due to uniqueness this must coincide with $(\bar{u}_s, \bar{k}_s)$, and hence this finishes the argument. □

Likewise, the existence of an eigen-pair can be established.

Proof of Proposition 5.2.4. In what follows we always consider a system $G : B \times Y \to Z$ where $B \subset [0, 1]$, $Y = \dot{\mathcal{H}}^1 \times \mathbb{R}$ and $Z = (\dot{\mathcal{H}}^1)^* \times \mathbb{R}$, given by

$$G(s, \gamma, \mu) := (H_s\gamma - \mu J\gamma, (c, \gamma)_{\dot{\mathcal{H}}^1} - 1), \tag{5.5.14}$$

where $c \in \dot{\mathcal{H}}^1$ will be chosen appropriately. We consider two subsets of $\mathcal{B}_{pt}$ seperately.

Throughout this proof we endow the product spaces with their canonical norms, for example, $\|(u, k)\|_{\dot{\mathcal{H}}^1 \times \mathbb{R}} = \|u\|_{\dot{\mathcal{H}}^1} + |k|$.

(a) Vicinity of a bifurcation point: We let $c = \gamma_{b_i}$, introduce the notation $y := (\gamma, \mu)$ and observe that

$$D_yG(b_i, \gamma_{b_i}, \mu_{b_i}) = \begin{pmatrix} H_{b_i} - \mu_{b_i}J & -\gamma_{b_i} \\ (c, \cdot)_{\dot{\mathcal{H}}^1} & 0 \end{pmatrix}.$$

Thus, Lemma 5.5.1 and Theorem 5.5.2 together imply that, for $s \in (b_i - \xi, b_i + \xi)$, where $\xi > 0$ is small enough (cf. (5.2.8)), there exists an eigen-pair (μ_s, γ_s). To show

that $\mu_s' := \frac{\mathrm{d}\mu_s}{\mathrm{d}s} \neq 0$ at $s = b_i$, we differentiate both sides of (5.2.12) with respect to s to obtain

$$\delta^3_{uuu}\mathcal{E}(\bar{u}_s, \bar{k}_s)[\bar{u}_s', \gamma_s] + \delta^3_{uuk}\mathcal{E}(\bar{u}_s, \bar{k}_s)[\bar{u}_s, \bar{k}_s'] + H_s[\gamma_s'] = \mu_s' J[\gamma_s] + \mu_s J[\gamma_s']. \quad (5.5.15)$$

By definition, at a fold point we have $\bar{k}_{b_i}' = 0$ and since along the bifurcation path we have $\delta_u\mathcal{E}(\bar{u}_s, \bar{k}_s) = 0$, we can differentiate both sides with respect to s to get $H_s\bar{u}_s' + \bar{k}_s' b_s = 0$, it follows that $\bar{u}_{b_i}' = \alpha\gamma_{b_i}$ for some $\alpha \neq 0$ (constant speed of parametrisation). Testing (5.5.15) at $s = b_i$ with γ_{b_i} and simplifying, we obtain

$$\mu_{b_i}' = \alpha\langle\delta^3_{uuu}\mathcal{E}(\bar{u}_{b_i}, \bar{k}_{b_i})[\gamma_{b_i}, \gamma_{b_i}],\, \gamma_{b_i}\rangle \neq 0, \quad (5.5.16)$$

which is nonzero by Assumption (5.2.5). This completes case (a).

(b) Unstable segment away from bifurcations: We assume without loss of generality that at the bifurcation point b_i we switch from a stable segment to an unstable segment. The result in (a) establishes existence of an eigenvector for $s \in (b_i - \xi, b_i + \xi)$, so we let $t_1 := b_i + \xi - \epsilon$, where $0 < \epsilon < \xi$ and thus are able to set $c = \gamma_{t_1}$ in (5.5.14). A subsequent application of Theorem 5.5.2 to system G with this newly chosen c yields existence of a new interval $(t_1 - \xi_1, t_1 + \xi_1) \subset \mathcal{I}_{\mathrm{pt}}$ for which the premise of the theorem is true. This procedure can be iterated, for example by incrementing $t_2 := t_1 + \xi_1/2$ and repeating the argument. To cover the entire unstable segment in this way we need to bound ξ_j from below, independently of t_j.

Due to (5.5.16) we know that $\mu_t < 0$, which implies that the subspace U_t from Assumption 2 can be characterised as

$$U_t = \{v \in \dot{\mathcal{H}}^1 \,|\, (v, \gamma_t)_{\dot{\mathcal{H}}^1} = 0\}. \quad (5.5.17)$$

With this in hand we consider any $(u, k) \in \dot{\mathcal{H}}^1 \times \mathbb{R}$, decompose u as $u = \alpha\gamma_t + v$, where $\alpha \in \mathbb{R}$ and $v \in U_t$, and aim to uniformly bound

$$\|D_y G(t, \gamma_t, \mu_t)[u, k]\| = \big\|H_t u - \mu_t J u - kJ\gamma_t\big\| + \big|(\gamma_t, u)_{\dot{\mathcal{H}}^1}\big|$$

from below.

To do so, we observe that

$$\langle (H_t - \mu_t J)u - kJ\gamma_t,\, \tfrac{v}{\|v\|_{\dot{\mathcal{H}}^1}}\rangle = \langle (H_t - \mu_t J)v,\, \tfrac{v}{\|v\|_{\dot{\mathcal{H}}^1}}\rangle \geq (c - \mu_t)\|v\|_{\dot{\mathcal{H}}^1}, \quad (5.5.18)$$

$$\langle (H_t - \mu_t J)u - kJ\gamma_t,\, -\gamma_t\rangle = \langle (H_t - \mu_t J)\alpha\gamma_t - kJ\gamma_t,\, -\gamma_t\rangle = k \quad (5.5.19)$$

Together, (5.5.18) and (5.5.19) imply that

$$\begin{aligned}\|H_t u - \mu_t J u - kJ\gamma_t\| &= \sup_{\substack{\tilde{v}\in\dot{\mathcal{H}}^1\\ \|\tilde{v}\|=1}} |\langle H_t u - \mu_t J u - kJ\gamma_t,\, \tilde{v}\rangle| \\ &\geq \max\big(|c-\mu_t|\|v\|_{\dot{\mathcal{H}}^1}, |k|\big) \\ &\geq \tfrac{1}{2}\min\big(|c-\mu_t|, 1\big)\big(\|v\|_{\dot{\mathcal{H}}^1} + |k|\big). \end{aligned} \tag{5.5.20}$$

Moreover, we trivially have

$$|(\gamma_t, u)_{\dot{\mathcal{H}}^1}| = |\alpha| = \|\alpha\gamma_t\|_{\dot{\mathcal{H}}^1}. \tag{5.5.21}$$

Let $\tilde{c}_0(s)^{-1} = \min\{\frac{1}{2}(c-\mu_t), \frac{1}{2}\} > \min\{\frac{1}{2}(c), \frac{1}{2}\} =: c_0^{-1}$, then combining (5.5.20) and (5.5.21) yields

$$\|D_y G(t, \gamma_t, \mu_t)[u,k]\| \geq \tilde{c}_0(t)^{-1}\|(u,k)\|.$$

In a similar vein, we observe that

$$\|D_s G(\gamma_t, \mu_t, t)\| \leq \|\delta^3_{uuu}\mathcal{E}(\bar{u}_t, \bar{k}_t)\| + \|\delta^3_{uuk}\mathcal{E}(\bar{u}_t, \bar{k}_t)\||\bar{k}_t'| =: \tilde{c}_1(t) \leq c_1,$$

where $c_1 := \max_{t\in\mathcal{I}_{pt}} \tilde{c}_1(t)$, which is guaranteed to exist due to $\mathcal{E}$ being a C^α functional and that $\mathcal{B}$ is a $C^{\alpha-1}$ function of s, where $\alpha \geq 5$ by assumption.

It is also evident that Condition (iii) from Theorem 5.5.2 is satisfied with

$$L_1(\xi) := \sup_{(s,y)\in S(\tilde{s},\gamma_{\tilde{s}},\mu_{\tilde{s}},\xi)} \|D^2 G(s,y)\|,$$

where $S(\tilde{s}, \gamma_{\tilde{s}}, \mu_{\tilde{s}}, \xi) = \{(s,\gamma,\mu) \in \mathbb{R}\times\dot{\mathcal{H}}^1\times\mathbb{R} :\ |s-\tilde{s}| + \|\gamma - \gamma_{\tilde{s}}\| + |\mu - \mu_{\tilde{s}}| \leq \xi\}$.

Guided by (5.5.4), we define $M := \max\{c_0, 1 + c_0 c_1\}$, choose b such that $bL_1(b) \geq \frac{1}{2M}$, let $\hat{a} = \frac{b}{4M}$ and recall from (5.5.4) that $\xi = \min\left\{\frac{\hat{a}}{2}, \frac{b}{2c_2}\right\} - \epsilon$ with sufficiently small $\epsilon > 0$ is an admissible choice for ξ which is in particular independent of t.

This completes the proof of part (b).

(c) Regularity: It remains to establish the $C^{\alpha-2}$-regularity of

$$s \mapsto (\mu_s, \gamma_s), s \in \mathcal{I}_{\mathrm{pt}}.$$

To that end, we note that G is a smooth function of γ and μ and $C^{\alpha-2}$ function with respect to s, thus uniqueness and regularity parts of Theorem 5.5.2 immediately

imply that γ and μ are $C^{\alpha-2}(\mathcal{I}_{\text{pt}})$ functions. $\square$

We are now in a position to prove the spatial regularity of $\bar{u}_s$ and γ_s.

Proof of Theorem 5.2.5. We begin by defining $v(m) := D_{2\tau}\mathcal{G}(m,l)$, where $\mathcal{G}$ is the lattice Green's function for the anti-plane crack geometry, as introduced in Theorem 4.2.2 and proven to satisfy decay property

$$|D_1 D_{2\tau}\mathcal{G}(m,l) \lesssim (1+|\omega(m)|\,|\omega(l)|\,|\omega(m)-\omega(l)|^{2-\delta})^{-1},$$

where ω is the complex square root mapping defined in polar coordinates as

$$\omega(l) := r^{1/2}(\cos(\theta/2), \sin(\theta/2))$$

and $\delta > 0$ is arbitrarily small. Here, and throughout this proof, $\lesssim$ should be read as $\leq C_\delta$ where C_δ is a constant that may depend on δ.

Proof of Theorem 5.2.5: estimate (5.2.13)*:* We first prove the decay estimate for $\bar{u}_s$. We can write

$$\begin{aligned} D_\tau \bar{u}_s(l) &= \sum_{m\in\Lambda} D\bar{u}_s(m)\cdot Dv(m) \\ &= \sum_{m\in\Lambda}\sum_{\rho\in\mathcal{R}(m)} (D_\rho \bar{u}_s(m) - \phi'(D_\rho \hat{u}_{\bar{k}_s}(m) + D_\rho \bar{u}_s(m)))D_\rho v(m) \qquad (5.5.22) \\ &\quad + \sum_{m\in\Gamma_\pm}\sum_{\rho\in\mathcal{R}\setminus\mathcal{R}(m)} (-\phi'(D_\rho \hat{u}_{\bar{k}_s}(m) + D_\rho \bar{u}_s(m)))D_\rho v(m), \qquad (5.5.23) \end{aligned}$$

noting that the second equality follows from the fact that $\delta_u\mathcal{E}(\bar{u}_s, \bar{k}_s) = 0$, which implies we effectively subtract zero. The term (5.5.22) can be estimated by $|l|^{-3/2+\delta}$ due to the argument given in Theorem 3.2.2; that is,

$$\left|\sum_{m\in\Lambda}\sum_{\rho\in\mathcal{R}(m)} (D_\rho \bar{u}_s(m) - \phi'(D_\rho \hat{u}_{\bar{k}_s}(m) + D_\rho \bar{u}_s(m)))D_\rho v(m)\right| \lesssim |l|^{-3/2+\delta}.$$

The additional term (5.5.23) appears because we define the energy with the homogeneous discrete gradient operator and can be estimated as follows. Using (5.5.11) we see that we only sum over at most $2R_\phi^3$ lattice sites in (5.5.23) and thus we can decompose $D_\rho v(m)$ into a sum of finite differences along bonds that go around the crack. There will be at most $2R_\phi^3$ many of them and each separately decays like

$|D_{1\rho}D_{2\tau}\mathcal{G}(m,l)| \lesssim |l|^{-3/2+\delta}$, thus ensuring that (5.5.23) can be bounded by

$$\left| \sum_{m\in\Gamma_\pm} \sum_{\rho\in\mathcal{R}\setminus\mathcal{R}(m)} (-\phi'(D_\rho \hat{u}_{\bar{k}_s}(m) + D_\rho \bar{u}_s(m)))D_\rho v(m) \right| \lesssim C|l|^{-3/2+\delta},$$

where $C < 4R_\phi^6$ (though an optimal C might be much smaller). This concludes the proof of (5.2.13).

Proof of Theorem 5.2.5: estimate (5.2.14)*:* To estimate γ_s we employ an analogous argument. We begin by writing

$$\begin{aligned} D_\tau\gamma_s(l) &= \sum_m D\gamma_s(m)\cdot Dv(m) \\ &= \sum_{m\in\Lambda}\sum_{\rho\in\mathcal{R}(m)} (D_\rho\gamma_s(m) - \phi''(D_\rho\hat{u}_{\bar{k}_s}(m) + D_\rho\bar{u}_s(m))D_\rho\gamma_s(m))D_\rho v(m) \qquad (5.5.24) \\ &\quad + \sum_{m\in\Gamma_\pm}\sum_{\rho\in\mathcal{R}\setminus\mathcal{R}(m)} (-\phi''(D_\rho\hat{u}_{\bar{k}_s}(m) + D_\rho\bar{u}_s(m))D_\rho\gamma_s(m))D_\rho v(m). \qquad (5.5.25) \end{aligned}$$

Using precisely the same argument as for (5.5.23) we can bound (5.5.25) by $|l|^{-3/2+\delta}$.

To estimate (5.5.24) we Taylor-expand ϕ'' around 0 and observe that

$$\begin{aligned} &\left| \sum_{m\in\Lambda}\sum_{\rho\in\mathcal{R}(m)} (D_\rho\gamma_s(m) - \phi''(D_\rho\hat{u}_{\bar{k}_s}(m) + D_\rho\bar{u}_s(m))D_\rho\gamma_s(m))D_\rho v(m) \right| \qquad (5.5.26) \\ &\lesssim \|\gamma_s\|_{\dot{\mathcal{H}}^1} \left(\sum_{m\in\Lambda} |R(m)|^2 |Dv(m)|^2 \right)^{1/2}, \end{aligned}$$

where $|R(m)| \lesssim |m|^{-1}$ is the remainder of the expansion. This readily implies that $|D_\tau\gamma_s(l)| \lesssim |l|^{-1}$. Thus looking again at (5.5.26), instead of applying Cauchy-Schwarz inequality, we directly observe that

$$\begin{aligned} &\left| \sum_{m\in\Lambda}\sum_{\rho\in\mathcal{R}(m)} (D_\rho\gamma_s(m) - \phi''(D_\rho\hat{u}_{\bar{k}_s}(m) + D_\rho\bar{u}_s(m))D_\rho\gamma_s(m))D_\rho v(m) \right| \\ &\lesssim \sum_{m\in\Lambda} |R(m)||D\gamma_s(m)||Dv(m)| \lesssim |l|^{-3/2+\delta}, \end{aligned}$$

since $|R(m)||D\gamma_s(m)| \lesssim |m|^{-2}$. As before, $\delta > 0$ is arbitrarily small. This completes the proof of the second bound (5.2.14). □

Remark 5.5.4. It is interesting to note that while the model includes a full interaction between nearest-neighbour atoms, even across the crack, it is nonetheless the lattice Green's function for the fractured domain that is employed to estimate the atomistic solutions. The homogeneous lattice Green's function fails because the finite differences of $\hat{u}_k(m)$ across the crack grow like $\sim |m|^{1/2}$.

5.5.3 Convergence proofs

In tandem with the results from bifurcation theory stated in Section 5.5.1, in order to prove the results from Section 5.3 we rely on the following auxiliary result from [34] that was adapted to domain with cracks in Chapter 3 in Lemma 3.5.6.

Lemma 5.5.5. *There exists a truncation operator $T_R : \dot{\mathcal{H}}^1 \to \mathcal{H}^0_R$ such that $T_R v = 0$ in $\Lambda \setminus B_R$ and which satisfies*

$$\|T_R v - v\|_{\dot{\mathcal{H}}^1} \lesssim \|v\|_{\dot{\mathcal{H}}^1(\Lambda\setminus B_{R/2})} := \left(\sum_{m\in\Lambda\setminus B_{R/2}} |Dv(m)|^2 \right)^{1/2} \qquad \forall v \in \dot{\mathcal{H}}^1. \quad (5.5.27)$$

We can now prove the main result of this section.

Proof of Theorem 5.3.1. We consider an extended system $F : B \times Y \to Z$ where $B = [0,1]$, $Y = \mathcal{H}^0_R \times I$ and $Z = (\mathcal{H}^0_R)^* \times \mathbb{R}$ given by

$$F(s,y) = (\delta_u \mathcal{E}(u_y, k_y), (u_y - \bar{u}_s, \bar{u}'_s)_{\dot{\mathcal{H}}^1}), \quad (5.5.28)$$

where $\bar{u}'_s = \frac{d\bar{u}(s)}{ds}$ and $y = (u_y, k_y)$. We further introduce a mapping $y_R : B \to Y$ given by $y_R(s) = (T_R\bar{u}_s, \bar{k}_s)$. We shall now show that, with the help of ABCD Lemma, F satisfies the conditions of Theorem 5.5.2.

One can easily obtain that

$$D_y F(s, y_R(s)) = \begin{pmatrix} \delta^2_{uu}\mathcal{E}(T_R\bar{u}_s, \bar{k}_s) & \delta^2_{uk}\mathcal{E}(T_R\bar{u}_s, \bar{k}_s) \\ (\bar{u}'_s, \cdot)_{\dot{\mathcal{H}}^1} & 0 \end{pmatrix} =: \begin{pmatrix} A^R_s & b^R_s \\ (\bar{u}'_s, \cdot)_{\dot{\mathcal{H}}^1} & 0 \end{pmatrix}.$$

We further define $A_s := H_s = \delta^2_{uu}\mathcal{E}(\bar{u}_s, \bar{k}_s)$ (renamed to keep intuitive notation) and $b_s := \delta^2_{uk}\mathcal{E}(\bar{u}_s, \bar{k}_s)$ and observe that

$$D_y F(s, y_R(s)) = \begin{pmatrix} A_s & b_s \\ (\bar{u}'_s, \cdot)_{\dot{\mathcal{H}}^1} & 0 \end{pmatrix} + \begin{pmatrix} A^R_s - A_s & b^R_s - b_s \\ 0 & 0 \end{pmatrix} =: M^1_s + M^2_s.$$

Here, we treat A_s as a restriction to $\mathcal{H}^R_0$ and b_s as an element of $(\mathcal{H}^R_0)^*$. Since

$T_R\bar{u}_s \to \bar{u}_s$ as $R \to \infty$ strongly in $\dot{\mathcal{H}}^1$ (a consequence of (5.5.27), the decay estimate from Theorem 5.2.5 and $\mathcal{E} \in C^\alpha$),

$$\|A_s^R - A_s\|_{\mathcal{L}(\dot{\mathcal{H}}^1,(\dot{\mathcal{H}}^1)^*)} + \|b_s^R - b_s\|_{(\dot{\mathcal{H}}^1)^*} \to 0 \tag{5.5.29}$$

as $R \to \infty$. Our strategy will therefore be to apply the ABCD Lemma to M_s^1, interpreted as an operator from $\dot{\mathcal{H}}^1 \times I$ to $(\dot{\mathcal{H}}^1)^* \times \mathbb{R}$, and show that M_s^2 is a small perturbation.

To carry out this strategy we begin by differentiating $\delta_u\mathcal{E}(\bar{u}_s, \bar{k}_s) = 0$ with respect to s to obtain

$$A_s\bar{u}_s' + \bar{k}_s'b_s = 0 \tag{5.5.30}$$

along the bifurcation path $\mathcal{B}$. At a fold point, when $s = b_i$, due to (5.2.4), we have $\bar{k}_s' = 0$, thus revealing that $\bar{u}_{b_i}' = \alpha\gamma_{b_i}$ for some non-zero $\alpha \in \mathbb{R}$. For $s \neq b_i$, the operator A_s is invertible and thus

$$\bar{u}_s' = -\bar{k}_s'(A_s)^{-1}b_s. \tag{5.5.31}$$

We can now show that M_s^1 satisfies the conditions of ABCD Lemma.

Case 1, $s \in \mathcal{I}_{\text{pos}}$: Suppose that $s \in \mathcal{I}_{\text{pos}}$ from (5.2.8). In this case A_s is an isomorphism due to (5.2.7) and (5.2.11). Thus, to apply ABCD Lemma to M_s^1, we have to check that $(\bar{u}_s', (A_s)^{-1}b_s)_{\dot{\mathcal{H}}^1} \neq 0$, which is true since

$$(\bar{u}_s', (A_s)^{-1}b_s)_{\dot{\mathcal{H}}^1} = -\bar{k}_s'(\bar{u}_s', \bar{u}_s')_{\dot{\mathcal{H}}^1} \neq 0,$$

since by definition at a regular point we have $\bar{k}_s' \neq 0$ and $\bar{u}_s' \neq 0$.

Case 2, $s \in \mathcal{I}_{\text{pt}}$: Now suppose $s \in \mathcal{I}_{\text{pt}}$ but $s \neq b_i\ \forall i \in \{1, \dots, M\}$. It can be shown that A_s remains an isomorphism as follows. Proposition 5.2.4 tells us that we have an eigen-pair (μ_s, γ_s) satisfying (5.2.12). Any $v \in \dot{\mathcal{H}}^1$ can be decomposed into $v = \alpha\gamma_s + w$, where $w \in U_s$ with U_s given by (5.5.17) and $\alpha \in \mathbb{R}$. Thus,

$$\|A_sv\| = \sup_{\substack{\tilde{v}\in\dot{\mathcal{H}}^1 \\ \|\tilde{v}\|=1}} |\langle A_sv,\, \tilde{v}\rangle| \geq \frac{1}{2}\left(|\langle A_sv,\, \gamma_s\rangle| + \left|\langle A_sv,\, \tfrac{w}{\|w\|}\rangle\right|\right),$$

and we can further estimate

$$\begin{aligned}
|\langle A_sv,\, \gamma_s\rangle| &= \left|\alpha\langle A_s\gamma_s,\, \gamma_s\rangle + \langle A_sw,\, \gamma_s\rangle\right| = |\alpha\mu_s|, \\
|\langle A_sv,\, \tfrac{w}{\|w\|}\rangle| &= |\alpha\langle A_s\gamma_s,\, \tfrac{w}{\|w\|}\rangle + \langle A_sw,\, \tfrac{w}{\|w\|}\rangle| \geq \tfrac{c}{\|w\|}\|w\|^2 = c\|w\|,
\end{aligned}$$

where c is the stability constant from Assumption 2. This, together with the fact that $\|v\| \leq |\alpha| + \|w\|$ readily implies that we can set $\tilde{c} := \frac{1}{2}\min\{|\mu_s|, c\}$ and conclude that for all $v \in \dot{\mathcal{H}}^1$

$$\|A_s v\| \geq \tilde{c}\|v\|.$$

Thus, as in the case $s \in \mathcal{I}_{\text{pos}}$, (5.5.31) ensures that we can apply the ABCD lemma and deduce again that A_s is an isomorphism.

Case 3, $s = b_i$: Finally, suppose $s = b_i$ for some $i \in \{1, \dots, M\}$. Due to Assumption 2 we know that the kernel of A_s is one-dimensional at a fold point and thanks to Proposition 5.2.4 we know that it is spanned by γ_s, which means that (5.5.30) implies that $\bar{u}_s' = \gamma_s$. By Definition 5.2.2 we know that $\langle b_s, \gamma_s \rangle \neq 0$, which implies that the ABCD Lemma is again applicable.

Uniform Stability of M_s^1: We have shown so far that, for all $s \in [0,1]$, M_s^1 is an isomorphism from $\dot{\mathcal{H}}^1 \times I$ to $(\dot{\mathcal{H}}^1)^* \times \mathbb{R}$. In particular, this implies that for any $x = (u_x, k_x) \in \dot{\mathcal{H}}^1 \times I$ we have

$$\|M_s^1 x\| \geq \tilde{c}_s \|x\|,$$

where $\tilde{c}_s > 0$.

Since $s \mapsto M_s^1$ is continuous in operator-norm due to smoothness of $\mathcal{E}$ established in Theorem 5.2.1 and smoothness of $s \mapsto (\bar{u}_s, \bar{k}_s)$ established in Proposition 5.2.3, it follows that the infimum $\inf \tilde{c}_s$ is attained on $[0,1]$ and must therefore be positive. In summary, we have established the existence of $\tilde{c} > 0$ such that

$$\|M_s^1 x\| \geq \tilde{c}\|x\| \qquad \forall s \in [0,1], \quad x \in \mathcal{H}_0^R \times \mathbb{R}.$$

Uniform Stability: Next, using the definition of M_s^2 we can bound

$$\begin{aligned}\|D_y F(s, y_R(s))x\| &\geq \|M_s^1 x\| - \|M_s^2 x\| \geq \tilde{c}\|x\| - \|A_s^R - A_s\|\|u_x\| - \|b_s^R - b_s\||k_x| \\ &\geq \frac{\tilde{c}}{2}\|x\|,\end{aligned}$$

for R large enough, thus ensuring that $D_y F(s, y_R(s))$ is an isomorphism from $\mathcal{H}_0^R \times I$ to $(\mathcal{H}_0^R)^* \times \mathbb{R}$, thus satisfying condition (i) from Theorem 5.5.2, with uniform bound

$$\|D_y F(s, y_R(s))x\| \geq \frac{\tilde{c}}{2}\|x\| \qquad \forall s \in [0,1], \xi \in \mathcal{H}_0^R \times \mathbb{R},$$

that is c_0 from (5.5.1) is given by $c_0 = \frac{2}{\tilde{c}}$.

Conclusion: So far we have confirmed Condition (i) of Theorem 5.5.2. To

conclude the proof, we now need to also check conditions (ii, iii).

It can be readily checked that

$$\|D_s F(s, y_R(s))\| = |-1 + (T_R \bar{u}_s - \bar{u}_s, \bar{u}_s'')_{\dot{\mathcal{H}}^1}| \leq 2$$

for R large enough. Thus the condition (ii) in Theorem 5.5.2 is satisfied with c_1 in (5.5.2) given by $c_1 = 2$.

The condition (iii) from Theorem 5.5.2 is satisfied with

$$L_1(\xi) := \sup_{(s_*, y_*) \in S(s, y_R(s), \xi)} \|D^2 F(s_*, y_*)\|,$$

where

$$S(s, y_R(s), \xi) = \{(s_0, y_0) \in \mathbb{R} \times (\mathcal{H}_0^R \times I) : \ |s - s_0| + \|T_R \bar{u}_s - u_y\| + |\bar{k}_s - k_y| \leq \xi\}.$$

Finally, we observe that

$$\sup_{s \in [0,1]} \|F(s, y_R(s))\| = \sup_{s \in [0,1]} \left(\|\delta_u \mathcal{E}(T_R \bar{u}_s, \bar{k}_s)\| + |(T_R \bar{u}_S - \bar{u}_s, \gamma_s)| \right) \to 0,$$

as $R \to \infty$, which implies that no matter how large constants c_0, c_1 and c_2 were and how badly behaved L_1 was, we would still fall within the regime where the result of Theorem 5.5.2 was applicable for R large enough.

We can thus conclude that there exists $\mathcal{B}_R : [0,1] \to \mathcal{H}_0^R \times \mathbb{R}$ given by $\mathcal{B}_R(s) := (\bar{u}_s^R, \bar{k}_s^R)$, such that $F(s, (\bar{u}_s^R, \bar{k}_s^R)) = 0$, which in particular implies

$$\delta_u \mathcal{E}(\bar{u}_s^R, \bar{k}_s^R) = 0.$$

Furthermore, using (5.5.3) we can conclude that

$$\|\bar{u}_s^R - T_R \bar{u}_s\|_{\dot{\mathcal{H}}^1} + |\bar{k}_s^R - \bar{k}_s| \leq K_0 \|F(s, y_R(s))\| \lesssim \|T_R \bar{u}_s - \bar{u}_s\| \lesssim R^{-1/2+\beta},$$

for arbitrarily small $\beta > 0$. Crucially, K_0 depends only on c_0 and c_1, which are independent of s and the last inequality follows from Lemma 5.5.27 and the regularity estimate from Theorem 5.2.5. This concludes the result, since trivially

$$\|\bar{u}_s^R - \bar{u}_s\|_{\dot{\mathcal{H}}^1} \leq \|\bar{u}_s^R - T_R \bar{u}_s\|_{\dot{\mathcal{H}}^1} + \|T_R \bar{u}_s^R - \bar{u}_s\|_{\dot{\mathcal{H}}^1}.$$

Finally, we note that (5.3.3) follows as an immediate collorary, arguing exactly as in the proof of [33, Theorem 2.4]. □

To prove our final result, the superconvergence of critical values of the stress intensitt factor, we first need to quote two intermediate technical steps. The first lemma, which highlights the origin of this superconvergence, is taken from [27, Theorem 4.1], restated in our notation for the sake of convenience.

Lemma 5.5.6. *Let $(\bar{u}_{b_i}, \bar{k}_{b_i}) \in \mathcal{B}$ be a simple quadratic fold point. Under Assumptions 1,2 & 3, for R large enough, the approximate bifurcation diagram $\mathcal{B}_R$ has a quadratic fold point at $s = b_i^R$, where $|b_i^R - b_i| \to 0$ as $R \to \infty$. Furthermore,*

$$\begin{aligned}|\bar{k}_R(b_i^R) - \bar{k}(b_i)| \leq \big\|\bar{u}_R'(b_i) - \bar{u}'(b_i)\big\|_{\dot{\mathcal{H}}^1}^2 + \big|\bar{k}_R'(b_i) - \bar{k}'(b_i)\big|^2 \\ + \|\bar{u}_R(b_i) - \bar{u}(b_i)\|_{\dot{\mathcal{H}}^1}^2 + |\bar{k}_R(b_i) - \bar{k}(b_i)|^2 \\ + \inf_{v \in \mathcal{H}_0^R} \|v - \gamma_{b_i}\|_{\dot{\mathcal{H}}^1}^2.\end{aligned}$$

To exploit the inequality from Lemma 5.5.6, we adapt [20, Theorem 2], which is a follow-up result to Theorem 5.5.2 for derivatives.

Lemma 5.5.7. *Assume the hypotheses of Theorem 5.5.2 and in addition that*

$$\sup_{x_0 \in U} \|DF(x_0, y(x_0)\| \leq c_1.$$

Then there exists a continuous function $K : \mathbb{R}_+ \to \mathbb{R}_+$, which depends only on c_0, c_1, L_1 such that for all $x_0 \in U$ and all $x \in B(x_0, a)$ it holds that

$$\begin{aligned}\|Dg(x) - Dy(x_0)\| \leq K(\|Dy(x_0)\|)\Big(\|x - x_0\| + \|F(x_0, y(x_0)\| \\ + \|DF(x_0, y(x_0), Dy(x_0)\|\Big).\end{aligned}$$

Proof of Theorem 5.3.2. Lemma 5.5.6 implies that, for a domain radius R large enough, we have exactly M approximate fold points $b_j^R \to b_j$ as $R \to \infty$. By assumption, $b_j \in (0,1)$ and hence also $b_j^R \in (0,1)$. Arguing analogously as in the proof of Theorem 5.3.1, it is not difficult to show that F defined in (5.5.28) satisfies the conditions of Lemma 5.5.7, thus

$$\big\|\bar{u}_R'(b_i) - \bar{u}'(b_i)\big\| + \big|\bar{k}_R'(b_i) - \bar{k}'(b_i)\big| \lesssim R^{-1/2+\beta},$$

for arbitrary small $\beta > 0$. Furthermore,

$$\inf_{v \in \mathcal{H}_0^R} \|v - \gamma_{b_i}\|_{\dot{\mathcal{H}}^1} \leq \|T_R \gamma_{b_i} - \gamma_{b_i}\| \lesssim R^{-1/2+\beta},$$

with the first inequality following from the obvious fact that $T_R \gamma_{b_i} \in \mathcal{H}_0^R$ and the

second from the regularity result for γ_{b_i} in Theorem 5.2.5.

Applying Lemma 5.5.6 we therefore obtain the desired result that

$$|\bar{k}_R(b_i^R) - \bar{k}(b_i)| \lesssim R^{-1+\beta}. \qquad \square$$

5.6 Discussion

The results obtained here, in tandem with those of in Chapters 3 & 4, introduce a mathematical framework in which a rigorous formulation and study of atomistic models of cracks and their propagation is possible. In particular, we have shown how the theory of atomistic modelling of defects developed in [19, 34, 50] can be combined with classical results from bifurcation theory [20, 54] to study this problem, and a key insight is the identification of the stress intensity factor as a suitable bifurcation parameter which allows us to explore the energy landscape. Our analysis sets earlier numerical work of [59, 60] into a rigorous framework, and provides a comprehensive explanation as to why the bifurcation diagram is a snaking curve.

While further work is needed to extend our analytical results to more general models (and particularly to the case of other crack modes), from a numerical perspective several aspects of our theory are of universal applicability. We therefore conclude by pointing out a series of interesting conclusions which arise from our analysis.

Periodicity of the bifurcation diagram In an infinite lattice, shifting the crack tip by one lattice spacing results in a physically identical configuration. Therefore, it is reasonable to conjecture that $\mathcal{B}_R$ in the limit as $R \to \infty$ generates a bifurcation diagram in which the critical points exist for values of the SIF k within a fixed finite interval of admissible values. In Section 5.4 we have exploited the superconvergence result in Theorem 5.3.2 to test this hypothesis numerically and the results summarised in Figure 5.4 confirm this intuition, as the extrapolated limit values of SIF as $R \to \infty$ for every second bifurcation point are numerically identical, occuring at

$$k = 0.45903, \quad k = 0.46234, \quad k = 0.45905, \quad k = 0.46231, \quad k = 0.45905.$$

A translation invariance in the critical points further implies that, if we denote

the centre of the CLE predictor by

$$x_\lambda := (\lambda, 0) \tag{5.6.1}$$

for some $\lambda \in \mathbb{Z}$, and define $\mathcal{E}_\lambda : \dot{\mathcal{H}}^1 \times \mathbb{R} \to \mathbb{R}$ by

$$\mathcal{E}_\lambda(\bar{u}, k) = \sum_{m \in \Lambda} V(\tilde{D}\hat{u}_k(m - x_\lambda) + \tilde{D}\bar{u}(m)) - V(\tilde{D}\hat{u}_k(m - x_\lambda)),$$

then assuming $\mathcal{B}(s) = (\bar{u}_s, \bar{k}_s) \in \dot{\mathcal{H}}^1 \times \mathbb{R}$ is a parametrisation as described in Section 5.2, we naturally have

$$\delta_u \mathcal{E}_\lambda(\bar{u}_s(\cdot - x_\lambda), \bar{k}_s) = 0. \tag{5.6.2}$$

We further notice for any $s \in [0, 1]$ the total displacement $y_s = \hat{u}_{\bar{k}_s} + \bar{u}_s$ can be rewritten as $y_s(m) = \hat{u}_{\bar{k}_s}(m - x_\lambda) + w_{s,\lambda}(m)$, where $\lambda \in \mathbb{Z}$ and

$$w_{s,\lambda}(m) := \big(\hat{u}_{\bar{k}_s}(m) - \hat{u}_{\bar{k}_s}(m - x_\lambda)\big) + \bar{u}_s(m).$$

Crucially,

$$|D\hat{u}_k(l) - D\hat{u}_k(l - x_\lambda)| \lesssim |l|^{-3/2} \implies w_{s,\lambda} \in \dot{\mathcal{H}}^1 \tag{5.6.3}$$

and for any choice of $\lambda \in \mathbb{Z}$

$$\delta_u \mathcal{E}_\lambda(w_{s,\lambda}, \bar{k}_s) = \delta_u \mathcal{E}(\bar{u}_s, \bar{k}_s) = 0. \tag{5.6.4}$$

In other words, no matter which x_λ we choose to centre the crack predictor $\hat{u}_k$ at, the same configuration $y_s = \hat{u}_{\bar{k}_s} + \bar{u}_s$ always remains an equilibrium and $w_{s,\lambda}$ exactly captures the resulting changes to the atomistic correction.

To be precise, let us fix some $s \in [0, 1]$ thus giving us a pair $\mathcal{B}(s) = (\bar{u}_s, \bar{k}_s)$, let $K := \bar{k}_s$ and further consider

$$I_K := \{s \in [0, 1] \,|\, \bar{k}_s = K\}.$$

Equations (5.6.2) and (5.6.4) indicate that for any $s' \in I_K$ for which $\bar{u}_{s'}$ is a solution of the same type as $\bar{u}_s$ (either stable, or unstable or a bifurcation point), we can find a unique $\lambda \in \mathbb{Z}$ such that $\bar{u}_{s'} = w_{s,\lambda}$.

In particular we note that the above strongly suggests that in some cases one may be able to prove results about periodicity and boundedness in k of the bifurcation diagram, which we hope to achieve in future work.

Interplay between the stress intensity factor and the domain size and its effect on lattice trapping. The tilt of bifurcation diagrams seen in Figure 5.3 indicates that the size of the domain heavily impacts the shape of the corresponding solution curve. Notably, each successive bond-breaking event has a different interval of admissible values of SIF associated to it and the corresponding unstable segments are much shorter than stable ones for small domain sizes. The fact that the influence of such finite-domain effects can still be observed for a fairly large R can be explained by the very slow rate of convergence in Theorem 5.3.2.

In practice, one hopes to investigate crack propagation and associated energy barriers for a fixed value of SIF and subsequently compare it against other admissible choices of SIF to measure the strength of lattice trapping [45, 82], measured by the relative height of the energy barrier. Our work indicates that such investigations are particularly challenging due to the extent to which finite–size effects dominate, an effect we observe to be strong even in the simple model considered here. Only a very large choice of truncation radius R ensures that the resulting solution paths are close to the periodic results one expects in the full lattice case. It may be possible to overcome such difficulties by prescribing a more accurate predictor describing the far–field behaviour, in line with the idea of development of solutions introduced in [19]: this is a clear direction for future investigation.

Identification of the correct bifurcation parameter. It is interesting to note that varying the intuitively natural bifurcation parameter λ introduced in (5.6.1) to reflect the crack tip at which the continuum prediction is centred in fact fails to capture the bifurcation phenomenon. This can be seen by considering $\tilde{\mathcal{E}} : \dot{\mathcal{H}}^1 \times \mathbb{R} \to \mathbb{R}$ given by

$$\tilde{\mathcal{E}}(v, \lambda) = \sum_m V\big(\tilde{D}\hat{v}_\lambda(m) + \tilde{D}v(m)\big) - V\big(\tilde{D}\hat{v}_\lambda(m)\big),$$

where $\hat{v}_\lambda = \hat{u}_K(\cdot - x_\lambda)$ for some fixed SIF $K > 0$. This fundamentally differs from the energy defined in (2.5.1), as in that case we have linear dependence of the displacement on k, $\tilde{D}\hat{u}_k(m) = k\tilde{D}\hat{u}_1(m)$, which in turn leads to a particular form of derivatives with respect to k; in particular, this ensures we have quadratic fold points. In $\tilde{\mathcal{E}}$, however, the dependence is inside $\hat{v}_\lambda$, thus the crucial derivative with

respect λ is given by

$$\delta^2_{v\lambda}\tilde{\mathcal{E}}(v,\lambda)[w,h] = h\sum_m \delta^2 V(\tilde{D}\hat{v}_\lambda(m) + \tilde{D}v(m))\tilde{D}f_\lambda(m)\cdot\tilde{D}w(m),$$

where $f_\lambda(m) = \nabla\hat{u}_K(m_1-\lambda, m_2)\cdot e_1$. In this case, as in (5.6.3), we can conclude $f_\lambda \in \dot{\mathcal{H}}^1$. This implies that a fold point cannot occur, as that would require that there exists $\gamma \in \dot{\mathcal{H}}^1$ such that

$$\langle \delta^2_{vv}\tilde{\mathcal{E}}(v,\lambda)\gamma,\, v\rangle = \sum_m \delta^2 V\big(\tilde{D}\hat{v}_\lambda(m) + \tilde{D}v(m)\big)\tilde{D}\gamma(m)\cdot\tilde{D}w(m) = 0$$

for all $w \in \dot{\mathcal{H}}^1$, which further implies that

$$\begin{aligned}\delta^2_{v\lambda}\tilde{\mathcal{E}}(v,\lambda)[\gamma,1] &= \sum_m \delta^2 V\big(\tilde{D}\hat{v}_\lambda(m) + \tilde{D}v(m)\big)\tilde{D}f_\lambda(m)\cdot\tilde{D}\gamma(m)\\ &= \sum_m \delta^2 V\big(\tilde{D}\hat{v}_\lambda(m) + \tilde{D}v(m)\big)\tilde{D}\gamma(m)\cdot\tilde{D}f_\lambda(m) = 0,\end{aligned}$$

since $f_\lambda \in \dot{\mathcal{H}}^1$. This breaches the defining property of a fold point given in Definition 5.2.2; in fact, it is not possible to drive a bifurcation in this way precisely because of the observation made in (5.6.3) and the resulting periodicity.

Parameter-driven analysis for other models and defects: An overarching idea of this chapter is that a careful analysis of a crucial parameter involved in the model can reveal the energy landscape of the problem, and this can be particularly fruitful in the study of defect migration. In the case of a crack, using the SIF as a driving parameter naturally generalises to more complex fracture models, though in general there may be multiple SIFs.

It would be interesting to undertake future study to see whether such an analysis is applicable more widely to other defects. In the particular case of dislocations, nucleation and motion have been studied in the atomistic context in a number of recent studies, including [3, 4, 25, 41, 49]. Since these defects are the carriers of plastic deformation, the study of their mobility is important, and natural candidates for the parameters in this case are the shear modulus and externally–applied stress [56].

Chapter 6

Conclusions

We conclude by summarising the main findings of this thesis and pointing to interesting open problems that our analysis give rise to. We will also comment on an on-going collaboration with James Kermode and Punit Patel from Warwick Centre for Predictive Modelling (WCPM), in which the aim is to exploit our results in the numerical study of more advanced vectorial models.

Chapter 2 was devoted to introducing the general atomistic formulation of static crack problems. Firstly, we discussed the particularly relevant discrete kinematics setting, which in the case of the crack had to correctly take the inherent loss of interaction into account. This was shown to be achieved by either manually removing interaction bonds across the crack or encoding the loss of interaction into the interatomic potential and strain. We further introduced and emphasised the importance of the loading parameter k known as stress intensity factor.

Subsequently, in Chapter 3, we treated the small-loading regime, which refers to the manual removal of interaction bonds across the crack coupled with requiring k to be sufficiently small. In this setup we succeeded in proving existence, local uniqueness and stability of solutions. Crucially, we also proved far-field decay estimates of the resulting atomistic corrections and thus recovered a result about convergence to the thermodynamic limit. We refer to the discussion in Section 3.6 for a more detailed summary of this particular case.

The far-field decay estimate result was only possible due to the detailed study of the associated lattice Green's function in the anti-plane geometry conducted in Chapter 4. We were able to show that there exists such a function and further established its decay properties, by considering the problem as an instance of coupling between continuum and atomistic descriptions. Furthermore, we employed a technically involved argument to prove the desired decay. Among other things, it included

a construction of a locally isomorphic mapping of the problem onto a discrete manifold corresponding to the complex square root, followed by a delicate boot-strapping argument that saturates at the known rate of decay of the corresponding continuum Green's function.

We note that this result is of independent interest and in particular it gave rise to an on-going study of near-crack-tip plasticity, which in our context refers to movement of screw dislocations in the vicinity of a Mode III crack. A similar study without the crack present was conducted in [49].

Finally, in Chapter 5, we focused on capturing atomistic crack propagation. We reformulated our model by introducing interactions across the crack and encoding the possibility of them being broken into the atomistic potential, proving that the resulting model is still well-defined. However, this change put us into a setup rather common in the atomistic study of defects - due to the complex nonconvex energy landscape, we could no longer rigorously prove that a strongly stable solution exists, but under the natural assumption that there is one (interpreted as an inherent feature of the lattice and the potential in place), we employed the tools of bifurcation analysis on Banach spaces to conduct a detailed study of crack propagation.

We identified the stress intensity factor k as a particularly suitable bifurcation parameter and, motivated by the fact the continuum linearised elasticity solution depends on k linearly, we provided strong evidence that the resulting bifurcation diagram has to be a snaking curve, with the stability of solutions changing at each fold point. This observation was further motivated by the fact that the anti-plane setup naturally binds the crack to the horizontal axis. As a result we introduced some natural structural assumptions on the bifurcation diagram and subsequently studied cell size effects in finite-domain approximation to the problem on the infinite lattice. In particular, we were able to prove sharp convergence rates of finite segments of the bifurcation diagram and established an interesting superconvergence result for the critical values of k at which bifurcation points occur. We refer to Section 5.6 for a more detailed discussion about that particular part of the analysis.

The contributions of Chapters 3-5 constitute a rigorous framework in which atomistic models of fracture can be formulated and studied. At present, it is not entirely clear how to extend our results to vectorial models and cracks of different mode due to the following two major obstacles. One is the ability to estimate the lattice Green's function in the crack geometry for interactions beyond nearest-neighbours. At present we rely on a delicate construction involving a discrete manifold - this is conceptually ill-suited for more general setups. The second, potentially far more persistent problem is the phenomenon of surface effects induced by the crack surface,

with atoms near prone to assuming a different structure altogether.

However, while these complications require further fundamental work to be overcome on a rigorous level, our analysis obtained for a scalar Mode III crack model is of universal applicability on a heuristic level. In particular the insights about the decay of atomistic corrections, the crucial role of the stress intensity factor and the resulting pseudo-arclength continuation scheme all persist for vectorial models. This is the subject of the aforementioned on-going work with James Kermode and Punit Patel from WCPM, who are interested in studying energy barriers for atomistic models of Mode II (in-plane) fracture. With our numerical scheme for tracing energy landscape as one varies the stress intensity factor, we were able to find a saddle point in-between two stable solutions, which precisely corresponds to the energetic cost of propagation. In that sense, we were also able to precisely capture the phenomenon of lattice trapping, which postulates that the lattice can keep the crack trapped for a range of values of the stress intensity factor. With this tool one can carry out a rigorous qualitative analysis of energy barriers and in particular our work with regards cell-size effects also warns against the possibility of strong numerical artefacts, should one choose the computational domain not large enough. As already noted, this is substantially more challenging in vectorial models and notably has to be combined with the idea of development of solutions discussed in [19] to create a convergent numerical scheme. This is an on-going collaboration and we refer to Figures 6.1 & 6.2 for visualisation.

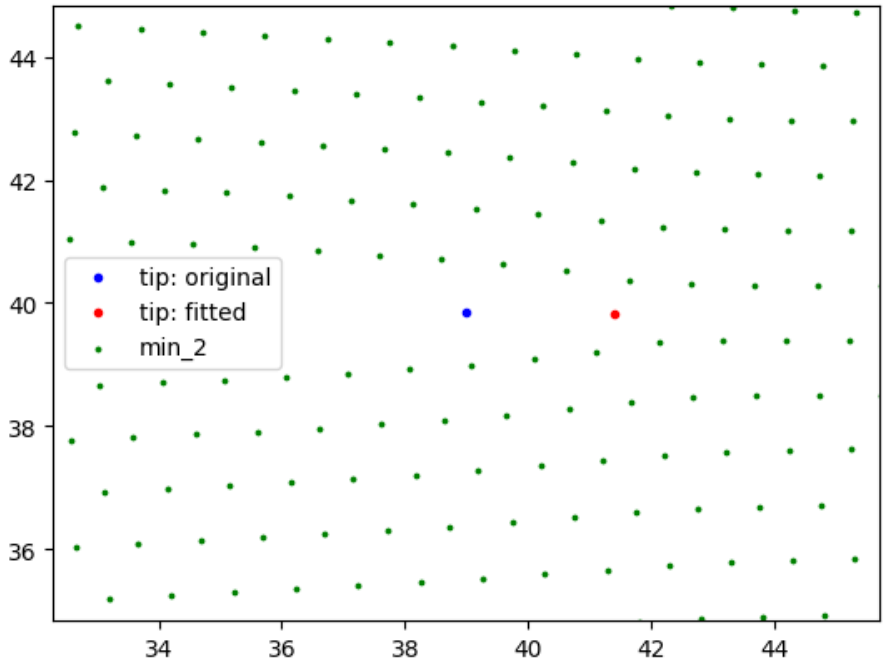

Figure 6.1: Atomistic crack propagation captured for a vectorial Mode II fracture model.

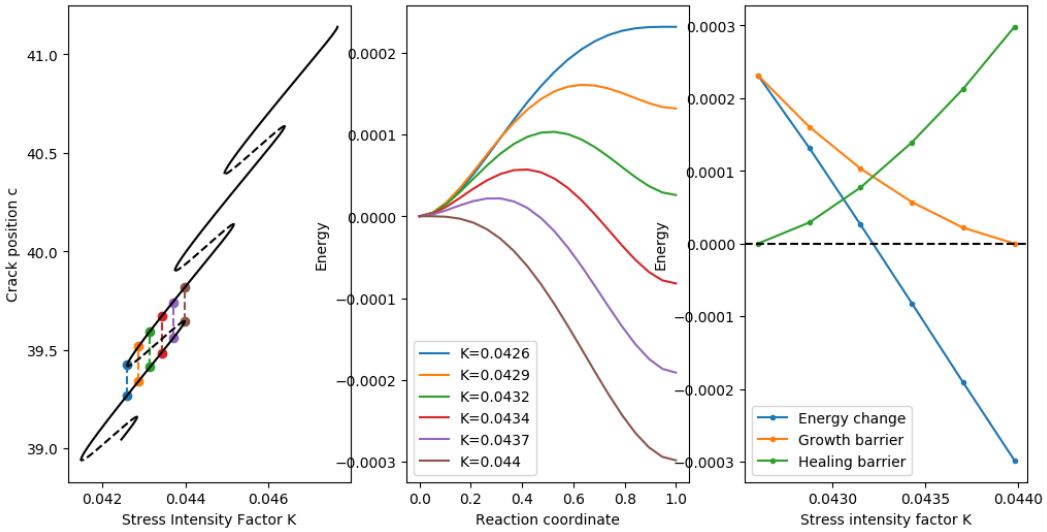

Figure 6.2: The analysis of energy barriers in a vectorial Mode II fracture model.

Bibliography

[1] M. J. Ablowitz and A. S. Fokas. *Complex Variables: Introduction and Applications*. Cambridge University Press, second edition, 2003. ISBN 9780521534291.

[2] R. Alicandro and M. Cicalese. A general integral representation result for continuum limits of discrete energies with superlinear growth. *SIAM J. Math. Anal.*, 36(1):1–37, 2004.

[3] R Alicandro, L De Luca, A Garroni, and M Ponsiglione. Metastability and dynamics of discrete topological singularities in two dimensions: a Γ-convergence approach. *Arch. Ration. Mech. Anal.*, 214(1):269–330, 2014. ISSN 0003-9527. doi:10.1007/s00205-014-0757-6.

[4] R Alicandro, L De Luca, A Garroni, and M Ponsiglione. Minimising movements for the motion of discrete screw dislocations along glide directions. *Calc. Var. Partial Differential Equations*, 56(5):Art. 148, 19, 2017. ISSN 0944-2669. doi:10.1007/s00526-017-1247-0.

[5] M.P. Ariza and M. Ortiz. Discrete crystal elasticity and discrete dislocations in crystals. *Arch. Ration. Mech. Anal.*, 178:149–226, 11 2005. doi:10.1007/s00205-005-0391-4.

[6] N. Berglund. Kramers' law: validity, derivations and generalisations. *Markov Process. Related Fields*, 19(3):459–490, 2013. ISSN 1024-2953.

[7] W.-J. Beyn, A. Champneys, E. Doedel, W. Govaerts, Y. A. Kuznetsov, and B. Sandstede. Numerical continuation, and computation of normal forms. In *Handbook of Dynamical Systems III: Towards Applications*, 2002.

[8] E. Bitzek, J. R. Kermode, and P. Gumbsch. Atomistic aspects of fracture. *International Journal of Fracture*, 191(1):13–30, Feb 2015. ISSN 1573-2673. doi:10.1007/s10704-015-9988-2.

[9] X. Blanc, C. Le Bris, and F. Legoll. Analysis of a prototypical multiscale method coupling atomistic and continuum mechanics: the convex case. *Acta Mathematicae Applicatae Sinica, English Series*, 23(2):209–216, Apr 2007. ISSN

1618-3932. doi:10.1007/s10255-007-0364-5. URL https://doi.org/10.1007/s10255-007-0364-5.

[10] A. Braides. Homogenization of some almost periodic functional. *Rend. Accad. Naz. Sci.*, XL 103(3):313–322, 1985.

[11] A. Braides and M. Cicalese. Surface energies in nonconvex discrete systems. *Mathematical Models and Methods in Applied Sciences*, 17(07):985–1037, 2007. doi:10.1142/S0218202507002182.

[12] A. Braides and V. De Cicco. Relaxation and γ-convergence of quadratic forms in $\mathrm{BV}(\mathbb{I};\mathbb{R}^n)$. *Annali dell'Università di Ferrara*, 38(1):145–175, Dec 1982. ISSN 1827-1510. doi:10.1007/BF02827089.

[13] A. Braides, G. Dal Maso, and A. Garroni. Variational formulation of softening phenomena in fracture mechanics: The one-dimensional case. *Arch. Ration. Mech. Anal.*, 146:23–58, 4 1999. doi:10.1007/s002050050135.

[14] A. Braides, A. Lew, and M. Ortiz. Effective cohesive behavior of layers of interatomic planes. *Arch. Ration. Mech. Anal.*, 176:151–182, 5 2006. doi:10.1007/s00205-005-0399-9.

[15] A. Braides, M. Solci, and E. Vitali. A derivation of linear elastic energies from pair-interaction atomistic systems. *Networks and Heterogeneous Media*, 2:551–567, 2007. ISSN 1556-1801. doi:10.3934/nhm.2007.2.551.

[16] J. Braun and C. Ortner. Sharp uniform convergence rate of the supercell approximation of a crystalline defect. *ArXiv e-prints*, 1811.08741, 2018. URL https://arxiv.org/abs/1811.08741.

[17] J. Braun and B. Schmidt. On the passage from atomistic systems to nonlinear elasticity theory for general multi-body potentials with p-growth. *Networks and Heterogeneous Media*, 8(4):879–912, 2013. doi:10.3934/nhm.2013.8.879.

[18] J. Braun, M. H. Duong, and C. Ortner. Thermodynamic limit of the transition rate of a crystalline defect. *ArXiv e-prints*, 1810.11643, 2018. URL https://arxiv.org/abs/1810.11643.

[19] J. Braun, M. Buze, and C. Ortner. The effect of crystal symmetries on the locality of screw dislocation cores. *SIAM J. Math. Anal.*, 51, 2019. doi:10.1137/17M1157520. URL http://arxiv.org/abs/1710.07708.

[20] F. Brezzi, J. Rappaz, and P.A. Raviart. Finite dimensional approximation of nonlinear problems. *P.A. Numer. Math.*, 36, 1980. doi:10.1007/BF01395985.

[21] K. B. Broberg. *Cracks and fracture*. Academic Press,San Diego, 1999.

[22] M. Buze, T. Hudson, and C. Ortner. Analysis of an atomistic model for anti-plane fracture. *ArXiv e-prints*, 1810.05501, 2018. URL `https://arxiv.org/abs/1810.05501`.

[23] M. Buze, T. Hudson, and C. Ortner. Analysis of cell size effects in atomistic crack propagation. *ArXiv e-prints*, 1905.13328, 2019. URL `https://arxiv.org/abs/1905.13328`.

[24] R. Chang. An atomistic study of fracture. *International Journal of Fracture Mechanics*, 6(2):111–125, Jun 1970. ISSN 1573-2673. doi:10.1007/BF00189819. URL `https://doi.org/10.1007/BF00189819`.

[25] J. Chaussidon, M. Fivel, and D. Rodney. The glide of screw dislocations in bcc fe: Atomistic static and dynamic simulations. *Acta Materialia*, 54(13):3407 – 3416, 2006. ISSN 1359-6454. doi:10.1016/j.actamat.2006.03.044.

[26] H. Chen and C. Ortner. QM/MM methods for crystalline defects. Part 1: Locality of the tight binding model. *Multiscale Model. Simul.*, 14(1), 2016. doi:http://dx.doi.org/10.1137/15M1022628. URL `http://arxiv.org/abs/1505.05541`.

[27] K. A. Cliffe, A. Spence, and S. J. Tavener. The numerical analysis of bifurcation problems with application to fluid mechanics. *Acta Numerica*, 9:39–131, 2000.

[28] S. Conti, G. Dolzmann, B. Kirchheim, and S. Müller. Sufficient conditions for the validity of the Cauchy-Born rule close to $SO(n)$. *J. Eur. Math. Soc. (JEMS)*, 8:515–539, 2006. doi:10.4171/JEMS/65.

[29] G. Dal Maso. *An Introduction to* Γ*-Convergence*. Birkhäuser, 1993.

[30] G. Dal Maso and R. Toader. Revisiting brittle fracture as an energy minimization problem. *Arch. Ration. Mech. Anal.*, 162:101–135, 4 2002. doi:10.1007/s002050100187.

[31] G. Dal Maso and R. Toader. Quasistatic crack growth in nonlinear elasticity. *Arch. Ration. Mech. Anal.*, 176:165–225, 5 2005. doi:10.1007/s00205-004-0351-4.

[32] W. E and P. Ming. Cauchy–born rule and the stability of crystalline solids: Static problems. *Arch. Ration. Mech. Anal.*, 183:241–297, 2007. doi:10.1007/s00205-006-0031-7.

[33] V. Ehrlacher, C. Ortner, and A. V. Shapeev. Analysis of boundary conditions for crystal defect atomistic simulations (preprint). URL `https://arxiv.org/abs/1306.5334`.

[34] V. Ehrlacher, C. Ortner, and A. V. Shapeev. Analysis of boundary conditions for crystal defect atomistic simulations. *Arch. Ration. Mech. Anal.*, 222(3): 1217–1268, 2016. ISSN 1432-0673. doi:10.1007/s00205-016-1019-6.

[35] J. L. Ericksen. On the Cauchy-Born rule. *Mathematics and Mechanics of Solids*, 13(3-4):199–220, 2008. doi:10.1177/1081286507086898.

[36] J.L Ericksen. The Cauchy and Born hypotheses for crystals. *Phase Transformations and Material Instabilities in Solids (ed. M.E. Gurtin)*, pages 61–77, 1984.

[37] H. Eyring. The activated complex in chemical reactions. *The Journal of Chemical Physics*, 3(2):107–115, 1935. doi:10.1063/1.1749604. URL `https://doi.org/10.1063/1.1749604`.

[38] G. A. Francfort and J.-J. Marigo. Revisiting brittle fracture as an energy minimization problem. *Journal of Mechanics Physics of Solids*, 46:1319–1342, 8 1998. doi:10.1016/S0022-5096(98)00034-9.

[39] L. B. Freund. *Dynamic Fracture Mechanics*. Cambridge Monographs on Mechanics. Cambridge University Press, 1990. doi:10.1017/CBO9780511546761.

[40] G. Friesecke and F. Theil. Validity and failure of the Cauchy-Born hypothesis in a two-dimensional mass-spring lattice. *J. Nonlinear Sci.*, 12:445–478, 2002. doi:10.1007/s00332-002-0495-z.

[41] A. Garg, A. Acharya, and C. E. Maloney. A study of conditions for dislocation nucleation in coarser-than-atomistic scale models. *Journal of the Mechanics and Physics of Solids*, 75:76 – 92, 2015. ISSN 0022-5096. doi:10.1016/j.jmps.2014.11.001.

[42] E. Giusti. *Direct Methods in the Calculus of Variations*. World Scientific, 2003. ISBN 9789814488297.

[43] E. H. Glaessgen, E. Saether, J. Hochhalter, and V. Yamakov. Modeling near-crack-tip plasticity from nano-to micro-scales. *Collection of Technical Papers - AIAA/ASME/ASCE/AHS/ASC Structures, Structural Dynamics and Materials Conference*, 2010.

[44] A. A. Griffith. The phenomena of rupture and flow in solids. *Philos Trans R Soc A Math Phys Eng Sci*, 221:163–198, 1921. doi:10.1098/rsta.1921.0006.

[45] P. Gumbsch and R. M. Cannon. Atomistic aspects of brittle fracture. *MRS Bulletin*, 25(5):15–20, 2000. doi:10.1557/mrs2000.68.

[46] P. Hänggi, P. Talkner, and M. Borkovec. Reaction-rate theory: fifty years after Kramers. *Rev. Mod. Phys.*, 62:251–341, Apr 1990. doi:10.1103/RevModPhys.62.251. URL `https://link.aps.org/doi/10.1103/RevModPhys.62.251`.

[47] J. Heinonen. *Poincaré Inequality*, pages 27–33. Springer New York, New York, NY, 2001. ISBN 978-1-4613-0131-8. doi:10.1007/978-1-4613-0131-8_4.

[48] J. P. Hirth and J. Lothe. *Theory of dislocations*. New York Wiley, second edition, 1982. ISBN 0471091251.

[49] T. Hudson. Upscaling a model for the thermally-driven motion of screw dislocations. *Arch. Ration. Mech. Anal.*, 224(1):291–352, February 2017. doi:10.1007/s00205-017-1076-5.

[50] T. Hudson and C. Ortner. Existence and stability of a screw dislocation under anti-plane deformation. *Arch. Ration. Mech. Anal.*, 213(3):887–929, 2014. ISSN 1432-0673. doi:10.1007/s00205-014-0746-9.

[51] F. John and L. Nirenberg. On functions of bounded mean oscillation. *Communications on Pure and Applied Mathematics*, 14(3):415–426, 1961. doi:10.1002/cpa.3160140317.

[52] C. Jordan. *Calculus of Finite Differences*. AMS Chelsea Publishing, third edition, 1965. ISBN 9780828400336.

[53] H. Kanzaki. Point defects in face-centred cubic lattice—i distortion around defects. *Journal of Physics and Chemistry of Solids*, 2(1):24 – 36, 1957. ISSN 0022-3697. doi:10.1016/0022-3697(57)90003-3.

[54] H. B. Keller. Numerical solution of bifurcation and nonlinear eigenvalue problems. *Applications of bifurcation theory: proceedings of an Advanced Seminar*

conducted by the Mathematics Research Center, the University of Wisconsin at Madison, pages 359–384, 1977.

[55] A. Kelly and K.M. Knowles. *Crystallography and Crystal Defects*. John Wiley & Sons, Ltd., second edition, 2012. doi:10.1002/9781119961468.

[56] L.D. Landau, E.M. Lifshitz, and J.B. Sykes. *Theory of Elasticity*. Course of theoretical physics. Pergamon Press, 1989. ISBN 9780029462232. URL https://books.google.co.uk/books?id=YjDiQwAACAAJ.

[57] S. Lang. *Fundamentals of Differential Geometry, Graduate Texts in Mathematics*. New York Springer, 1999. ISBN 9780387985930.

[58] B. Lawn. *Fracture of Brittle Solids*. Cambridge Solid State Science Series. Cambridge University Press, 2 edition, 1993. doi:10.1017/CBO9780511623127.

[59] X. Li. A bifurcation study of crack initiation and kinking. *The European Physical Journal B*, 86(6):258, Jun 2013. ISSN 1434-6036. doi:10.1140/epjb/e2013-40145-9. URL https://doi.org/10.1140/epjb/e2013-40145-9.

[60] X. Li. A numerical study of crack initiation in a bcc iron system based on dynamic bifurcation theory. *Journal of Applied Physics*, 116(16):164314, 2014. doi:10.1063/1.4900580. URL https://doi.org/10.1063/1.4900580.

[61] P. Lin. Theoretical and numerical analysis for the quasi-continuum approximation of a material particle model. *Mathematics of Computation*, 72(242):657–675, 2003. ISSN 00255718, 10886842. URL http://www.jstor.org/stable/4099924.

[62] M. Luskin and C. Ortner. Atomistic-to-continuum-coupling. *Acta Numerica*, 2013. URL http://journals.cambridge.org/action/displayJournal?jid=anu.

[63] M. Mullins and M. A. Dokainish. Simulation of the (001) plane crack in α-iron employing a new boundary scheme. *Philosophical Magazine A*, 46(5):771–787, 1982. doi:10.1080/01418618208236930.

[64] S. Müller. Homogenization of nonconvex integral functionals and cellular elastic materials. *Arch. Ration. Mech. Anal.*, 99(3):189–212, 1987.

[65] D. Olson and C. Ortner. Regularity and locality of point defects in multilattices. *Appl. Math. Res. Express*, 1-41, 2017. doi:10.1093/amrx/abw012. URL http://arxiv.org/abs/1608.08930.

[66] C. Ortner and A. Shapeev. Interpolants of lattice functions for the analysis of atomistic/continuum multiscale methods. *ArXiv e-prints*, 1204.3705, 2012. URL `http://arxiv.org/abs/1204.3705`.

[67] C. Ortner and E. Süli. A note on linear elliptic systems on $\mathbb{R}^d$. *ArXiv e-prints*, 1202.3970, 2012. URL `http://arxiv.org/abs/1202.3970`.

[68] C. Ortner and F. Theil. Justification of the cauchy–born approximation of elastodynamics. *Arch. Ration. Mech. Anal.*, 207, 2013. doi:10.1007/s00205-012-0592-6. URL `http://arxiv.org/abs/1202.3858`.

[69] R. Phillips. *Crystals, Defects and Microstructures: Modeling Across Scales*. Cambridge University Press, 2001. doi:10.1017/CBO9780511606236.

[70] M. Ponsiglione. Elastic energy stored in a crystal induced by screw dislocations: from discrete to continuous. *SIAM J. Math. Anal.*, 2007.

[71] J. R. Rice. Mathematical analysis in the mechanics of fracture. *Fracture: An Advanced Treatise (Vol. 2, Mathematical Fundamentals) (ed. H. Liebowitz)*, pages 191–311, 1968.

[72] L.F. Richardson. The approximate arithmetical solution by finite differences of physical problems including differential equations, with an application to the stresses in a masonry dam. *Philosophical Transactions of the Royal Society*, 210:307–357, 1911. doi:10.1098/rsta.1911.0009.

[73] R. T. Rockafellar and R. J.-B. Wets. *Variational analysis*. Springer, 1998.

[74] W. Rudin. *Real and Complex Analysis*. McGraw-Hill, 1966. ISBN 0071002766.

[75] T.O. Saposnikova and V. Maz'ya. *Sobolev Spaces*. Springer Series in Soviet Mathematics. Springer Berlin Heidelberg, 2013. ISBN 9783662099223. URL `https://books.google.co.uk/books?id=9tn6CAAAQBAJ`.

[76] B. Schmidt. On the derivation of linear elasticity from atomistic models. *Networks and Heterogeneous Media*, 4(4):789–812, 2009. doi:10.3934/nhm.2009.4.789.

[77] J. E. Sinclair. Improved atomistic model of a bcc dislocation core. *Journal of Applied Physics*, 42(13):5321–5329, 1971. doi:10.1063/1.1659943.

[78] C.T. Sun and Z.-H. Jin. *Fracture Mechanics*. Academic Press, 2012. ISBN 9780123850010. doi:10.1016/C2009-0-63512-1.

[79] E. B. Tadmor, M. Ortiz, and R. Phillips. Quasicontinuum analysis of defects in solids. *Philosophical Magazine A*, 73(6):1529–1563, 1996. doi:10.1080/01418619608243000.

[80] C. Taylor and J.H.P. Dawes. Snaking and isolas of localised states in bistable discrete lattices. *Physics Letters A*, 375(1):14 – 22, 2010. ISSN 0375-9601. doi:https://doi.org/10.1016/j.physleta.2010.10.010. URL `http://www.sciencedirect.com/science/article/pii/S0375960110013460`.

[81] Florian Theil. Surface energies in a two-dimensional mass-spring model for crystals. *ESAIM: Mathematical Modelling and Numerical Analysis*, 45:873–899, 2011. doi:10.1051/m2an/2010106.

[82] R. Thomson, C. Hsieh, and V. Rana. Lattice trapping of fracture cracks. *Journal of Applied Physics*, 42(8):3154–3160, 1971. doi:10.1063/1.1660699. URL `https://doi.org/10.1063/1.1660699`.

[83] L. Truskinovsky. Fracture as phase transition. *Contemporary Research in the Mechanics and Mathematics of Materials*, pages 322–332, 1996.

[84] E. P. Wigner. *The Transition State Method*, pages 163–175. Springer Berlin Heidelberg, Berlin, Heidelberg, 1997. ISBN 978-3-642-59033-7. doi:10.1007/978-3-642-59033-7_16. URL `https://doi.org/10.1007/978-3-642-59033-7_16`.